

A PARTIAL-WAVE ANALYSIS OF THE REACTION  
 $\pi N \rightarrow \pi\pi N$  IN THE c.m. ENERGY RANGE 1300 - 2000 MeV \*

D. J. Herndon,<sup>†</sup> R. Longacre,<sup>††</sup> L.R. Miller,  
A. H. Rosenfeld, G. Smadja,<sup>††</sup> and P. Söding,<sup>‡</sup>  
Lawrence Berkeley Laboratory, University of California  
Berkeley, California 94720

R. J. Cashmore,<sup>§</sup> and D.W.G.S. Leith  
Stanford Linear Accelerator Center, Stanford University  
Stanford, California 94305

October 1974

ABSTRACT

A partial-wave analysis of the reaction  $\pi N \rightarrow \pi\pi N$  has been carried out in the energy region 1300-2000 MeV. Two continuous solutions have been found; they are very similar in regions where data exists, but differ in the continuation of amplitudes through a gap between our low and high energy data. The second solution ("B") gives a much better fit to the data. These new partial wave amplitudes provide important information on the inelastic couplings of the nucleon resonances to the  $N\rho$ ,  $N\epsilon$ , and  $\Delta\pi$  channels. A new resonance,  $D_{13}(1700)$ , long predicted by the quark model, has been observed coupling to two inelastic channels --  $\epsilon N$  and  $\Delta\pi$ , and the existence of a  $P_{13}(1700)$  state is corroborated. Our preferred solution indicates a second new resonance,  $P_{33}(1700)$ , coupled strongly to the  $\Delta\pi$  channel.

---

\* Work supported by the U. S. Atomic Energy Commission.

<sup>†</sup> Present address, Lawrence Livermore Laboratory, Livermore, California 94550.

<sup>††</sup> Present address, CEN, Saclay, (France).

<sup>‡</sup> Present address, DESY, Notkestieg 1, 2000 Hamburg-52.

<sup>§</sup> Present address, Nuclear Physics Laboratory, Oxford, OX1 - 3RH.

A PARTIAL-WAVE ANALYSIS OF THE REACTION  
 $\pi N \rightarrow \pi \pi N$  IN THE c.m. ENERGY RANGE 1300-2000 MeV\*

	<u>Page</u>
I. Introduction . . . . .	1
II. The Data . . . . .	3
III. Extended Isobar Model. . . . .	4
A. Ingredients of Isobar Model . . . . .	5
B. The Final State Interaction . . . . .	8
C. The Centrifugal Barrier, $b_L$ . . . . .	9
D. The Partial Waves Used in Our Fits . . . . .	9
IV. The Fitting Program . . . . .	10
A. Choice of Method . . . . .	10
B. Likelihood Formulation. . . . .	11
C. Unitarity, Agreement with Elastic Phase Shifts Predictions . . . . .	14
D. Stepping to a Maximum . . . . .	15
E. Errors in Amplitudes on Argand Plots . . . . .	17
F. Relative Likelihood of Competing Solutions . . . . .	18
G. Program Tests . . . . .	20
H. Limits for the Observation of Partial Waves. . . . .	21
V. Fitting Procedure, Tests, Quality of Final Solutions . . . . .	22
A. The 1972 24-wave Solution A. . . . .	22
B. The 1973 28-wave Solution B. . . . .	24
C. Tests and Quality of our Fits. . . . .	25
1. Four Dimensional $\chi^2$ . . . . .	25
2. Agreement with Inelastic Cross Sections . . . . .	25
3. Removing Waves, Monte Carlo Checks . . . . .	26
4. 60 X 60 Errors . . . . .	27
D. Comparison of Solutions A and B . . . . .	28
E. Summary . . . . .	29

	<u>Page</u>
VI. The Partial-Wave Amplitudes, Description and Discussion . . . . .	30
VII. Conclusions . . . . .	36
VIII. Acknowledgments . . . . .	37
Appendices . . . . .	38
A. Maximizing the Scale Parameter in the Likelihood Fit . . . . .	38
B. Example of Stepping Procedure when $\nabla\nabla^T f$ Matrix is Singular. . . . .	41
C. Choice of Angular Momentum Barrier Factors and of the $N^*$ Radius . . . . .	43

Supplement

Tables of Partial Wave Amplitudes. Tables and punched cards, for Solution B, including  $28 \times 28$  and  $60 \times 60$  error matrices, are available on request.

The Data-Summary Tape of the actual  $\pi^-$  events is also available from LBL, SLAC, or Saclay. The  $\pi^+$  events for  $\sqrt{s} = 1810$  MeV and above may be requested from the UCR-LBL Collaboration (see Table I).

## I. INTRODUCTION

Elastic phase shift analyses have provided us with an impressive list of resonances, which is both the essence of our understanding of baryon spectroscopy and also the main testing ground for many of the ideas on the dynamics of hadronic processes. The agreement among the many independent groups is very impressive,<sup>1-3</sup> and gives confidence in the resulting scattering amplitudes.

Corresponding investigation of the inelastic scattering reactions has not kept pace with that of elastic reactions. This derives not only from the lack of data (with high statistics, and systematically spread in energy), but also from the complexity of the phenomenological analysis. However, the study merits the effort. As can be seen from Fig. 1, the inelastic cross section represents a very substantial fraction of the total  $\pi N$  cross section, even at 1.0 GeV/c, and it is therefore intrinsically interesting to understand the scattering process. In addition, the inelastic decays of  $N^*$  are a very specific signature of the state and its properties, and therefore an important study in their own right. Finally, for resonances with very small coupling to the elastic channel [e.g.  $D_{13}(1700)$ ] these studies are the only effective means of investigating the resonance in a formation experiment.

In the resonance region the principle inelastic reaction is

$$\pi N \rightarrow \pi \pi N. \quad (1.1)$$

We have therefore made a detailed study of this channel in the c.m. energy range 1300-2000 MeV. In a previous analysis of this data in the range 1640-1760 MeV we attempted to isolate the reaction

$$\pi^- p \rightarrow \pi^+ \Delta^- \quad (1.2)$$

from  $\pi^- p \rightarrow \pi^+ \pi^- n$

by selecting only events with  $1.14 < M(\pi^- n) < 1.320$ .<sup>4</sup> This study enabled us to extract values for the  $F_{15}$  and  $D_{15}$  coupling constants to the  $\pi\Delta$  channel. Another group has used a similar technique to analyze<sup>5</sup> the reaction

$$\pi^+ p \rightarrow \pi^0 \Delta^{++} \quad (1.3)$$

to obtain the isospin-3/2 amplitudes in the c.m. energy range 1820-2090 MeV. (They have also contributed their data to the present study.)

In reactions of type (1.1) there is the possibility of producing many resonances which overlap strongly in the final states, particularly at lower c.m. energies. The interference effects associated with these overlaps are not removed by the  $\Delta$ -selection techniques described above, and hence are an inherent limitation of such analyses. At higher energies the increased phase space and the possibility of using the mass conjugation technique<sup>6</sup> improve the situation. Nevertheless, the interference effects are still a problem. These effects led to fitting the reactions in their entirety using the isobar model and its extension;<sup>7</sup> these take into account the effects associated with the many strong final-state interactions present. These methods have only been used currently at c.m. energies below 1560 MeV.<sup>8-10</sup>

We have extended this latter approach by including many more intermediate final states (and partial waves) and using the maximum likelihood technique in confronting the data with theory. These

extensions have allowed us to successfully apply this method throughout the energy range considered, 1300-2000 MeV. The data covers the regions 1300-1540 MeV and 1640-2000 MeV with a 100-MeV gap between the two regions. We presented one solution at the 1972 Batavia Conference.<sup>11</sup> The energy-independent partial wave analysis now yields two continuous solutions over the whole energy range. The solutions are very similar in the two regions where we have data, but have different continuations through the 100-MeV gap in the data. We favor Solution B, but no fundamental ambiguity exists in the partial wave analysis--when data in the gap region (1540-1640) become available, a clear choice between our two solutions will emerge. We include plots of our earlier Solution A for historical reasons and also to demonstrate the stability of many of our conclusions concerning the partial wave amplitudes. This analysis provides for the first time information on 50 inelastic couplings of the nucleon isobars and essentially accounts for all of the  $\pi N \rightarrow \pi\pi N$  cross section in this energy range.

## II. THE DATA

In the energy range we consider, single pion production reactions can be unambiguously identified in the bubble chamber, resulting in effectively bias-free data. We have gathered data from several large bubble chamber experiments<sup>8-10, 12, 13</sup> leading to a total sample of 200,000 events covering the reactions

$$\pi^- p \rightarrow \pi^- \pi^0 p, \quad (2.1)$$

$$\pi^- p \rightarrow \pi^+ \pi^- n, \quad (2.2)$$

$$\pi^+ p \rightarrow \pi^+ \pi^0 p, \quad (2.3)$$

$$\pi^+ p \rightarrow \pi^+ \pi^+ n, \quad (2.4)$$

at energies 1300-2000 MeV. These experiments are listed in Table I.

The major features of Reactions (2.1)-(2.3) can be observed in Figs. 2 and 3. The Dalitz plots of Fig. 2 demonstrate the presence of  $\Delta(1236)$  production in all cases although its contribution decreases at the higher energies. Indeed, at these higher energies the major final state interaction is due to the  $\rho$  meson and its effects clearly should not be ignored even at the lower energies. The presence of these obvious resonance bands was the motivation for the quasi-two-body analyses of Refs. 4 and 5, but while the present solutions contain their qualitative features, they differ by many standard deviations from the earlier quantitative conclusions.

The variations in the structure of the production angle,  $\theta$ , of the nucleon (see Fig. 3) are indicative of the presence of rapidly varying transition amplitudes. We can therefore anticipate that many partial waves will be necessary and that these will change rapidly with energy as expected from the presence of the structure in the inelastic cross sections of Fig. 1.

### III. THE EXTENDED ISOBAR MODEL

In this section we summarize the ingredients of our extended isobar model and give the final formulae and partial waves we use in our fits. A detailed discussion and derivation of all

formulae may be found in Herndon, Söding, and Cashmore.<sup>14</sup>

### A. Ingredients of Isobar Model

(i) We assume that the reaction proceeds through three quasi-two-body channels



where  $\epsilon$  represents the strong  $s$ -wave  $\pi\pi$  final state interaction at around 650 MeV.

(ii) The reaction can proceed through a large number of partial waves. We then have a transition amplitude for each angular momentum and isospin state which we write as  $T_{\alpha\mu}^c(\omega)$ , where

- $c$  represents the charge channel, e.g.  $\pi^+\pi^-n$ ,  $\pi^-\pi^0p$ , etc.;
- $\alpha$  is the group of quantum numbers  $(F, L, L', I, J)$  describing the reaction. These are summarized in Fig. 4, and the notation is spelled out below Eq. (3.2);
- $\mu$  represents  $\mu_i, \mu_f$ , the initial and final nucleon helicities;
- $\omega$  describes the four kinematical quantities necessary to describe an event: we choose these to be  $\omega_1^2, \omega_2^2$ —the Dalitz plot variables—and

$\cos\theta, \phi$ —where  $\theta, \phi$  are the angles of the incident  $\pi$  in our final-state coordinate system.<sup>14</sup> Our  $z$ -axis lies along the direction of the outgoing nucleon, and the  $y$ -axis is perpendicular to the production plane.

We note at this point that different charge channels differ only in isospin Clebsch-Gordan coefficients.



(iii) We can now explicitly develop some of the factors contained in  $T_{a\mu}^c(\omega)$ ;

$$T_{a\mu}^c(\omega) = A_a D_{a\mu}(\omega) B_a(\omega) W_F(\omega) C_a^c \equiv A_a X_{a\mu}^c, \quad (3.2)$$

where  $D_{a\mu}(\omega)$  contains all spherical harmonic factors (D-functions) associated with the angular momentum decomposition;

$B_a(\omega)$  contains the centrifugal barrier factor  $b_L$ , associated with the decay of the intermediate  $J^P$  state;

$W_F(\omega)$  represents the Watson factor for the final state interaction;

$A_a$  represents the amplitude for the particular wave and is assumed to be only dependent on the total mass of the system and not on any of the submasses. It is these complex parameters  $A_a$  which we vary during a fit;

$C_a^c$  the appropriate isospin Clebsch-Gordan coefficients for channel  $c$ .

(iv) The final transition amplitude to a given final state is then obtained by making a coherent sum of these individual amplitudes,

$$T_{\mu}^c(\omega) = \sum_a T_{a\mu}^c(\omega). \quad (3.3)$$

This summation implies some double counting of the amplitudes, which had been thought to be a small effect.<sup>15</sup> However, prompted by Aaron and Amado and others,<sup>16</sup> the Illinois group<sup>17</sup> and we are both estimating corrections to the amplitudes.<sup>18</sup>

(v) The differential cross section is then given by

$$d\sigma^c(\omega) = \lambda^2 \sum_{\mu} |T_{\mu}^c(\omega)|^2, \quad (3.4)$$

where we sum over initial and final nucleon helicities as we are neither working with polarized targets nor observing the final polarization.

This construction of the final state amplitude and cross section allows easy fitting to all single-pion production channels and hence allows the partial-wave decomposition of the scattering amplitude.

(vi) Cross sections are expressed in terms of the conventional T-matrix elements  $T_{\alpha}$  (called  $T_{\pi N}$  for elastic scattering,  $T_{\Delta\pi}$  for  $\Delta$  production, etc.). The unitary circle has unit diameter, and if there were only a single channel present, the total cross section would be

$$\sigma_{\alpha} = 4\pi \lambda^2 (J + \frac{1}{2}) |T_{\alpha}|^2. \quad (3.5)$$

Note that by convention T carries no subscript  $\mu$  as in Eq. (3.4); i. e.,

$$|T_{\alpha}|^2 = \int \sum_{\mu} |T_{\alpha\mu}|^2 d\Omega. \quad (3.6)$$

The nucleon helicity states are uniquely related by Clebsch-Gordan coefficients, i. e.  $T_{\alpha\mu} \propto C(J, L', \mu) T_{\alpha}$  and so the actual amplitude  $T_{\alpha}$  is well defined.

In practice however a single incoming partial wave can feed several values of  $\alpha$  (i. e. several channels, like  $\pi\Delta$ ,  $\rho N$ ,  $\epsilon N$ ). This may result in substantial interference effects which are observable in the integrated cross section [ see Eq. (3.7) ]. The cross section is

written as in (3.4),

$$\sigma_{\text{in}}^{(J^P)} = \lambda^2 \int d\Omega \sum_{\mu} \left\{ \sum_{\alpha} |T_{\alpha\mu}|^2 + \text{interference terms} \right\},$$

which in the spirit of Eqs. (3.5) and (3.6) we define as

$$\sigma_{\text{in}}^{(J^P)} = 4 \pi \lambda^{2(J+\frac{1}{2})} \left\{ \sum_{\alpha} |T_{\alpha}|^2 + \text{overlap integrals} \right\}. \quad (3.7)$$

Equation (3.7) defines the normalization of the Argand plots. The overlap integrals are important and are taken into account at all stages of the program.

Different incoming partial waves never interfere, so we can write

$$\sigma = \sum_{J^P} \sigma^{(J^P)}. \quad (3.8)$$

### B. The Final State Interaction, $W_F$

This could be parametrized as a Breit-Wigner factor. However, rather than attempting to represent the  $\Delta$ ,  $\rho$  or  $\epsilon$  by Breit-Wigner forms we chose to use the Watson Final State Interaction to describe the effects of these strong interactions by a factor

$$W_F = \frac{e^{i\delta_F} \sin\delta_F}{q^{l+1}}.$$

Here  $\delta_F$  is the appropriate elastic phase for the strongly interacting particles, and  $q$  is the momentum of each particle in the isobar rest frame.

The actual values of  $\delta_F$  are summarized in Fig. 5. The only uncertain phase shift was for the  $\epsilon$  ( $I=0$ ,  $J=0$   $\pi\pi$ ) but our parametrization is in close agreement with recent analyses<sup>19</sup> except near 1000 MeV

which fortunately is at the extreme limit of phase space for our highest beam energy. For more discussion, see Herndon.<sup>20</sup>

### C. The Centrifugal Barrier, $b_{L'}$

We should include centrifugal barriers in both the incident state and the quasi-two-body intermediate state. However, the first of these is constant for a given partial wave at a given energy and hence we have ignored it. (It's inclusion would just result in a rescaling of  $A_d$ , which is unimportant--see below).

The barrier factor in the intermediate state has been introduced as

$$b_{L'} = Q^{L'} \quad (3.10)$$

where  $Q$  is the isobar momentum in the c. m. and  $L'$  the orbital angular momentum.

Equation (3.10) is only the low-QR limit of the standard Blatt-Weisskopf factor,<sup>21</sup> which we meant to use. We inadvertently started with (3.10) and caught the mistake only after it was inconvenient to change. In Appendix C we show that (3.10) is adequate for our purpose, but urge the use of the correct form for all future partial-wave analyses.

### D. The Partial Waves Used in Our Fits

As discussed above we only considered three final state interactions in our analysis

- (i) the  $\Delta(1236)$  - intermediate state  $\pi\Delta$
- (ii) the  $\rho(760)$  - intermediate state  $N\rho$
- (iii) the  $I=J=0$   $\pi\pi$  interaction - intermediate state  $N\epsilon$ .

Since our decomposition of the amplitude is essentially an LS representation [where  $\underline{S} = \underline{S}$  (diparticle spin) +  $\underline{S}$  (bachelor spin)], in the case of the  $\rho$  meson we have two transition amplitudes. These are obtained because

$$\underline{S}_\rho + \underline{S}_N = 1/2 \text{ or } 3/2, \quad (3.12)$$

and are denoted as  $\rho_1$  or  $\rho_3$  waves.

In order to make the fitting problem tractable we have limited ourselves to orbital angular momenta in the incident and final states,  $l \leq 3$  and total angular momentum to  $j \leq 7/2$ . In Table II we list the 60 waves with which we began the analysis. As described in the later sections the actual number of waves required increased with c.m. energy, the maximum being 28 at our higher energies.

#### IV. THE FITTING PROGRAMS

##### A. Choice of Method

The choice of fitting procedure is clearly dictated by the number of events available in a given experiment. To exploit the correlations that exist in the data in the case of limited statistics the most powerful approach is that of the maximum likelihood technique.<sup>22</sup>

At the time we began our analysis, none of the existing maximum-likelihood fitting programs could handle either the amount of data or the number of parameters (up to 120) in a reasonable amount of computer time, so we developed a new program (RUMBLE)<sup>23</sup> which handles any problem in which the parameters appear bilinearly in the probability density (see below). It took the equivalent of 400 hours on the CDC 7600 to perform the analysis described in this paper, including random starts, studies of uniqueness, etc.

## B. Likelihood Formulation

### 1. Likelihood in Each Charge Channel

The full expression of  $\frac{d\sigma^c}{d^4\omega}$  (in charge channel c) in terms of the search parameters,  $A_a$ , is given by (3.2) through (3.4) as

$$\frac{d\sigma^c}{d^4\omega}(\omega_i) = \lambda^2 \sum_a |T_{a\mu}|^2$$

$$\frac{d\sigma^c}{d^4\omega}(\omega_i) = \lambda^2 \sum_\mu \left| \sum_a A_a X_{a\mu}^c(\omega_i) \right|^2. \quad (4.1)$$

For this formulation we rewrite  $\frac{d\sigma}{d^4\omega}$  as  $p(A_a)$  to emphasize that it is a cross section predicted by the  $A_a$ , i.e.,

$$p^c(\omega_i, A_a) = \lambda^2 \sum_\mu \left| \sum_a A_a X_{a\mu}^c(\omega_i) \right|^2. \quad (4.2)$$

We write the predicted total cross sections as

$$R^c(A_a) = \int d^4\omega p^c(\omega_i). \quad (4.3)$$

The normalized probability for each event is then

$$P(\omega_i, A_a) = \frac{p^c(\omega_i, A_a)}{R^c(A_a)}, \quad (4.4)$$

and the likelihood  $L^c$  describing the shape of the distribution is

$$L_{\text{shape}}^c(\omega_i, A_a) = \prod_{i=1}^{N^c} p^c = \frac{1}{(R^c)^{N^c}} \prod_{i=1}^{N^c} p^c(\omega_i, A_a). \quad (4.5)$$

If we dealt with only one charge channel, common sense would tell us to adjust the scale of the  $A_a$  by setting  $R^c(A_a)$  equal to the measured channel cross section  $\sigma^c$ , but for several channels the correct

scaling is more complicated. Hence we must next formulate the generalized likelihood  $L^c$  more precisely.

The path length  $l^c$  may differ from channel to channel. If each experiment reports  $N^c$  events and a cross section  $\sigma^c$ , then

$$l^c = \frac{N^c}{\sigma^c} \text{ (events}/\mu\text{b)} \quad (4.6)$$

and the predicted number of events  $\nu^c$  is given by

$$\nu^c = l^c R^c(A_a) = \frac{N^c}{\sigma^c} R^c(A_a). \quad (4.7)$$

The Poisson probability of observing  $\nu$  events when  $N$  are expected is

$$P(\nu, N) = \frac{N^N e^{-\nu}}{N!}. \quad (4.8)$$

Using (4.7) this becomes  $P(\nu, N) = \frac{1}{N!} \left(\frac{N}{\sigma}\right)^N R^N e^{-\frac{NR}{\sigma}}$ , i.e., inserting the superscript  $c$ ,

$$P(\nu^c, N^c) = \frac{1}{N^c!} \left(\frac{N^c}{\sigma^c}\right)^{N^c} (R^c)^{N^c} e^{-\frac{N^c R^c}{\sigma^c}}. \quad (4.9)$$

We now form the generalized channel likelihood,<sup>24</sup>

$L^c = P(\nu^c, N^c) L^c_{\text{shape}}$  where  $P$  is given by (4.9) and  $L^c_{\text{shape}}$  by (4.5).

The  $R^c$  factors cancel, to give

$$L^c = \frac{(N^c/\sigma^c)^{N^c}}{N^c!} \cdot \exp\left\{-\frac{N^c R^c}{\sigma^c}\right\} \cdot \prod_1^{N^c} p^c(\omega_i, A_a). \quad (4.10)$$

Finally the multichannel likelihood  $L$  is the product of each  $L^c$

$$L = \prod_c \left[ \frac{(N^c/\sigma^c)^{N^c}}{N^c!} \right] \exp\left\{-\frac{N^c R^c}{\sigma^c}\right\} \prod_1^{N^c} p^c(\omega_i, A_a). \quad (4.11)$$

## 2. Analytic Scaling of the $A_a$

We have already said that if we had only one charge channel we could set  $R^c = \sigma^c$ . Let us check this for single channel Eq.(4.10) by introducing a scale factor,  $s$ , e. g.

$$A_a = s A_a^0. \quad (4.12)$$

Dropping factors which do not contain  $s$ , Eq. (4.10) becomes

$$L^c(s A_a^0) = \exp\left\{-\frac{N^c s^2 R^c(A_a^0)}{\sigma^c}\right\} (s^2)^{N^c} \prod_1^{N^c} p^c(\omega_i, A_a^0) \quad (4.13)$$

$$\ln L^c(s A_a^0) = -\frac{N^c s^2 R^c(A_a^0)}{\sigma^c} + N^c \ln s^2 + \text{constant} \quad (4.14)$$

$$\frac{\partial \ln L^c(s A_a^0)}{\partial s} = -\frac{2N^c s R^c(A_a^0)}{\sigma^c} + 2N^c \frac{1}{s}. \quad (4.15)$$

Setting this to zero gives

$$\frac{1}{s^2} = \frac{R^c(A_a^0)}{\sigma^c}, \quad (4.16)$$

which as we guessed earlier indeed gives

$$R^c(A_a) = s^2 R^c(A_a^0) = \sigma^c$$

$$\text{and } L^c(s^{\max} A_a^0) = e^{-N^c} \left[\frac{\sigma^c}{R^c(A_a^0)}\right]^{N^c} \prod_1^{N^c} p^c(\omega_i, A_a^0). \quad (4.17)$$

This expression is manifestly independent of the magnitude of the vector  $A_a^0$ .

Next we can apply the same procedure to the multichannel  $L$  of Eq. (4.11). Details are given in Appendix A. This time the equivalent of (4.16) is easily found to be



$$s^2 \Big|_{L_{\max}} \equiv s^2 = \frac{\sum N^c \equiv N}{\sum \frac{R^c N^c}{\sigma^c}} . \quad (4.18)$$

It is also shown in Appendix A that inserting this into (4.11) yields a multichannel likelihood

$$L(s_{\max} A_a) = B e^{-N} N^N \left[ \frac{\sum \frac{N^c R^c(A_a)}{\sigma^c}}{\sigma^c} \right]^{-N} \prod_{c=1}^{N^c} \prod_{i=1}^{N^c} p^c(\omega_i, A_a). \quad (4.19)$$

The quantity which we actually maximize is the average log of (4.19) premaximized with respect to the scale of  $A_a$ ,

$$F = \frac{1}{N} \ln L = \text{constant} - \ln \left[ \sum_c \frac{N^c R^c(A_a)}{\sigma^c} \right] + \frac{1}{N} \sum_c \sum_{i=1}^{N^c} \ln p(\omega_i, A_a). \quad (4.20)$$

### C. Unitarity and the Agreement with Elastic Phase-Shift Predictions

Using unitarity and the elastic amplitude from elastic partial-wave ("phase shift") analysis (EPSA), one gets upper bounds for  $\sigma(N\pi\pi, IJ^P)$ . The partial waves used were those available in 1970, when we started this analysis.<sup>20</sup> For most of our fits we did not need (or impose) these constraints. Even in those cases in which we predicted more cross section than allowed, we were within two standard deviations of the upper bound. To correct this, we added to  $F(A_a)$  the  $\chi^2$ -like terms  $F_{\text{EPSA}}$

$$F_{\text{EPSA}} = - \frac{1}{N} \sum_{IJ^P} \alpha_{IJ^P} \left[ \frac{\sigma^{IJ^P} - \sigma_{\text{EPSA}}^{IJ^P}}{\delta \sigma_{\text{EPSA}}^{IJ^P}} \right]^2 \theta(\sigma^{IJ^P} - \sigma_{\text{EPSA}}^{IJ^P}), \quad (4.21)$$

where  $\sigma^{IJ^P}$  is defined by (3.7) and  $\sigma_{\text{EPSA}}^{IJ^P}$  is an average over the different EPSA, and  $\delta \sigma_{\text{EPSA}}^{IJ^P}$  are the external errors on  $\sigma_{\text{EPSA}}^{IJ^P}$ .

By using the step function,  $\theta$ ,  $F_{\text{EPISA}}$  only affected the likelihood when the fitting parameters predicted more cross section than allowed. These additional terms had very little effect on the fitted parameters. Of those amplitudes affected, the modulus was slightly reduced but the phases never changed.

#### D. Stepping to a Maximum

Maximizing procedures are of three general categories. At each step they evaluate

- (i) only the function  $F$ , or
- (ii)  $F$  and the first derivative vector  $\nabla F$  or
- (iii)  $F$ ,  $\nabla F$ , and the second derivative matrix,<sup>\*</sup>  $\nabla\nabla^T F$ . For convenience we define the variance matrix  $\underline{V} = (\nabla\nabla^T F)^{-1}$ .

We have found the most efficient fitting technique is a combination of types (ii) and (iii).

In both types of fitting programs, one "step" in the parameters is given by  $\Delta \vec{A} = -\underline{V}' \cdot \nabla F$  where  $\underline{V}'$  is a negative definite approximation to  $\underline{V}$  (for some cases  $\underline{V}' = \underline{V}$ ). We use two methods of updating  $\underline{V}'$ , the Davidon method<sup>25</sup> and a modified form of the Newton-Raphson method.<sup>26</sup>

#### 1. The Davidon Method

The Davidon method belongs to category (ii). The initial  $\underline{V}' = \underline{V}'_1$  is chosen to be diagonal, and at each subsequent step  $\underline{V}'_1$  is modified by the addition of a rank-one matrix. A rank-one matrix is one having just one eigenvector with a nonzero eigenvalue. A typical example is the outer product of a vector with itself,  $M_{ij} = v_i v_j$  or in matrix notation  $\underline{M} = \vec{v}\vec{v}^T$ . If  $\vec{v}$  has unit magnitude, then  $\underline{M}$  is called a projector.

<sup>\*</sup>The superscript T means transpose.

Davidon showed that at the  $i^{\text{th}}$  step  $\underline{v}'$  should be modified by

$$\underline{V}'_{i+1} = \underline{V}'_i + \lambda [\underline{V}'_i \cdot \nabla F_i] [\underline{V}'_i \cdot \nabla F_i]^T. \quad (4.22)$$

The number  $\lambda$  is calculated from  $\underline{V}'_i, \nabla F_i$ , and  $\nabla F_{i-1}$ . To ensure that the step is towards a maximum, rather than a minimum or saddle-point,  $\lambda$  is adjusted if necessary to keep  $\underline{V}'_i$  negative definite. This adjustment to  $\underline{V}'_i$  reflects the additional knowledge about the curvature of  $F$  gained from knowing the new first derivative  $\nabla F_i$ . If the  $2n$ -dimensional  $\vec{A}$  space is quadratic, Davidon showed that after  $2n$  steps  $\underline{V}'_{2n} = \underline{V}'$ .

## 2. The Original Newton-Raphson Method

This method chooses  $\underline{V}' = \underline{V}$  and recalculates the entire matrix at each step. The modified method, which we use, calculates a negative definite approximation to  $\nabla \nabla^T F$  and takes  $\underline{V}'$  to be the inverse of this approximate matrix. The approximation is such that if our model exactly predicts the event distribution for some vector  $\vec{A}'$ , then  $\underline{V}' = \underline{V}$  at  $\vec{A}'$ .

## 3. Our Procedure

Our fitting procedure was to calculate and invert the approximate second derivative matrix every twenty steps. In between these steps we used the Davidon technique to update the matrix. We also found it more efficient to take a few (in our case 5) Davidon-type steps initially before inverting the second derivative matrix.

## 4. Redundant Parameters

Since  $F$  is invariant to scale changes in  $\vec{A}$  and to an overall phase change in  $\vec{A}$ , there are two redundant parameters, and the second derivative matrix is singular. These singularities are usually

eliminated in problems similar to ours by permanently freezing the phase and modulus of one  $A_\alpha$  and reducing by two the dimension of  $\nabla\nabla^T F$ . We find, however, that the maximizing procedure takes less than one-third the number of steps to reach a maximum if all the  $A_\alpha$  are permitted to vary. In this case, the second derivative matrix has two eigenvectors with zero eigenvalues. The desired  $V'$  is the inverse of  $\nabla\nabla^T F$ , restricted to the space spanned by the set of eigenvectors with nonzero eigenvalues. For details on how the fitting program calculates the proper  $V'$ , see Ref. 23. A two-dimensional example is given in Appendix B.

#### E. Errors in Amplitudes on Argand Plots

The error matrix  $E$  is given by

$$E = \langle \delta \vec{A} \cdot \delta \vec{A}^T \rangle = \frac{1}{N} \cdot V' \quad (4.23)$$

where  $V' \approx \nabla\nabla^T F$  as described above, and the factor  $\frac{1}{N}$  arises because  $\ln L = NF$ .

In the neighborhood of any local maximum at  $A^{\max}$  with likelihood  $L^{\max}$ , we can expand  $L$  as

$$L = L^{\max} \exp \left\{ -\frac{1}{2} \chi^2 \right\} \quad (4.24)$$

and an error hyperellipsoid may be defined by a hypersurface in  $A$  space labelled by  $\Delta\chi^2 = 1$ , i.e. by  $L = L^{\max} e^{-1/2}$ .

To plot error ellipses on our Argand plots we project this hypersurface on the complex plane representing a single  $T_\alpha$  (or  $A_\alpha$ ). However, the probability that a result will be within this ellipse is only 40%. In order to increase this probability we have conservatively doubled our estimated error, thereby raising the  $\chi^2$  contour

to 4, and enclosing 87% of the probability. In summary, all the errors plotted or tabulated in this paper and in our previous publications are twice those calculated by the program RUMBLE which uses (4.23).

#### F. Relative Likelihood of Competing Solutions

We were bound to encounter two different sorts of competing solutions:

- i) The number of parameters (waves) is the same for both solutions, as in the case where two starting values lead to competing maxima
- ii) The number of parameters differs, as when we have cast out a wave from solution A with likelihood  $L_A$ , found a new maximum B, and wonder if the new  $L_B$  is significantly worse than  $L_A$ .

For the discussion below, assume that hypothesis A is the right one and that after a fit we find a likelihood ratio  $L_A/L_B$  which we call  $L_{AB}$ . A standard approach is then to say that solution B is ruled out to  $3\sigma$  if  $\ln L_{AB} = NF_{AB}$  is greater than 4.5 (or  $2\sigma$  of  $NF_{AB} > 2$ ). We now carry this test one step further and take into account the error  $\delta F_{AB}$  in  $F_{AB}$ . Specifically we wish not to eliminate solution B unless  $F_{AB}/\delta F_{AB}$  is safely larger than unity. (More sophisticated versions of this test are discussed by P. H. Eberhard, A. H. Rosenfeld, and M. Tabak).<sup>27</sup> We apply the same numerical test to both sorts of competing solutions i) and ii) mentioned above.

Of course without generating Monte Carlo events we do not know  $\delta NF_{AB}$  but we can estimate it from the 10,000 events in hand at each energy. For each event  $i$  we form  $F_{AB}^i$  and can then evaluate.

$$(\delta' F_{AB})^2 = \frac{\sum (F_{AB}^i)^2}{N} - \left(\frac{\sum F_{AB}^i}{N}\right)^2. \quad (4.25)$$

Figure 6 is a scatter plot of typical values of  $\delta' F_{AB}$  vs.  $F_{AB}$ . The ln-likelihood-ratios are of course  $NF_{AB}$ , not  $F_{AB}$ , but we plot  $F_{AB}$  so that we can show that all points scatter about the dashed line, even though the number of events differs from energy to energy.

For easy interpretation we label the scale as  $10,000 \delta F_{AB}$  and  $10,000 F_{AB}$ , corresponding to ln-likelihood-ratios for typical 10,000-event samples. The points seem to scatter around the dashed line independently of:

- i) the number of events (as just mentioned),
- ii) the number of parameters,
- iii) whether the events are real or Monte Carlo.

We have erected a vertical line at a ln-likelihood ratio of 3, and the standard test would say that to the right of this line solution B would begin to be ruled out. But consider the "X" plotted as far right as 4.5; its error  $10,000 \delta' F_{AB}$  is estimated to be 8.5, so that the value 4.5 is not an adequate reason for eliminating one hypothesis.

Our extra test agrees well with our studies (in Section V.C.) of actually casting out waves and refitting. Thus on Table V we show the results of removing a wave ( $PP_{13}$ ) whose amplitude  $|T|$  appeared to be only 2 to 3 standards deviations from zero. After refitting,  $\chi^2$  went up only 11 (for Monte Carlo events) or 14 (for real events) but ln-L decreased by 30 for both sets of events. We do not believe that the solution with the  $PP_{13}$  wave is  $e^{30}$  more likely than the solution without. But Fig. 6 shows that when  $\Delta \ln L$  is 30, its error is about 10, and the significance test  $F_{AB} / \delta' F_{AB} = 30/10 = 3$  seems quite reasonable.

In any case this extra test ( $\delta'F_{AB} < F_{AB}$ ) offers a convenient numerical way to relate the result of several studies to the frequently-occurring question "can we throw out this solution?" and it is sufficiently conservative that we use it with considerable faith.

Finally we should point out the large circles plotted higher on Fig. 6. They are not  $\delta'F_{AB}$ , but just  $\delta'F_A$  or  $\delta'F_B$ . These fluctuations in the ln-likelihood are of course much larger than the fluctuations in its ratio, but it is reassuring to note that as hypotheses A and B become significantly different,  $\delta'F$  approach  $\delta'F_{AB}$ . We plot these  $\delta'F$  dots for two reasons:

i) We know that some older programs have used  $\delta'F$  rather than  $\delta'F_{AB}$  to compare competing solutions, and we want to warn that  $\delta'F$  is too coarse.<sup>28</sup>

ii) Sometimes one knows that the two competing solutions are really very different, and it is of course easier to calculate  $\delta'F$  rather than  $\delta'F_{AB}$  since a program does not need to know about both hypotheses at the same time. In this case it is convenient to know that  $\delta'F$  is an upper limit to  $\delta'F_{AB}$ .

#### G. Program Tests

We made several checks on our programs:

1) To insure we were calculating that  $X_{\alpha\mu}^c$  correctly in Eq.(3.2), we obtained the programs from three other analyses.<sup>7, 9, 10</sup> In all cases we got agreement<sup>29</sup> among the different programs.

2) To test the fitting program itself, we generated artificial data from eleven "known" amplitudes and then fit for the amplitudes. We generated 7583 events (4733  $N\pi^+\pi^-$  and 2850  $p\pi^-\pi^0$ ) at  $\sqrt{s} = 1690$  MeV. To obtain a set of reasonable starting values, we generated

2000 sets of random amplitudes and kept the 20 sets with the highest likelihood. These 20 sets coalesced to five distinct solutions after fitting. Any wave among the 60 for which the modulus was within one standard deviation of zero in at least three solutions, was considered statistically insignificant and eliminated. After elimination, we refit with fewer waves and again eliminated waves. This was repeated a total of four times until no further waves could be removed. All five solutions coalesced into one solution and the number of waves dropped from 60 to 24. These 24 waves consisted of the original 11 waves and another 13 waves, each of which had  $|T| < 0.05$ . Figure 7 shows the initial 11 waves (as dots) and the corresponding 11 fitted amplitudes. The agreement is very reassuring, and gives us confidence that we can select the important waves for an original 60-wave hypothesis. However, in the case of real data, we are concerned with the extra uncertainties of fitting with an imperfect model, so we prefer to quote a "sensitivity" of  $T = 0.1$ .

We also tried to break up the 7583 events into smaller samples of the order of 1000 events, but we found we needed all the events generated to get a good 60-wave fit. From this we decided to work with at least 10,000 events at each energy in order to make fits to 60 waves.

This completes our discussion of program tests made before we started fitting real events. More tests of realistic amplitudes (from fitting real events) are described in Sec. VC.

#### H. Limits for the Observation of Partial Waves

From the tests above, and from our experience to be described in Sec. V, we estimate that we are sensitive to any inelastic partial wave for which



$$T_{\alpha} > 0.1, \quad (4.26)$$

or, in terms of branching fractions  $X_{\alpha} = \Gamma_{\alpha}/\Gamma$ ,

$$T_{\alpha} = \sqrt{X_{e1} X_{\alpha}} > 0.1.$$

## V. FITTING PROCEDURES, TESTS, AND QUALITY OF THE FINAL SOLUTIONS

### A. Obtaining The 1972 24-Wave Solution "A"

The number and distribution of the events used in the analysis are given in Table III. The continuous distribution of events was binned into c.m. energy intervals of 30 or 40 MeV, except between 1560 and 1630 MeV, where no data were available. In this section, we give an outline of the procedure used in obtaining our final solution. This procedure involved several distinct stages.

The data were fitted in three parts: below 1560 MeV, 1630-1830 MeV, and above 1830 MeV.

#### i) 1310-1560 MeV

In this region (9 bins) we reduced our 60 waves to 36 by removing all waves with  $J \geq 5/2$ . In each of the six bins between 1380 and 1560 MeV, we generated 2000 random sets of amplitudes to use as starting values to the fitting program and kept the top ten.

Any wave within two standard deviations of zero was considered statistically insignificant and removed. In this manner we were able, at each energy, to reduce to one solution. To look for continuity in energy we used each solution as a starting value for the neighboring energy bins. This new starting value always converged to the existing solution at that energy. Moreover our  $\vec{A}(E)$  varied

smoothly with energy providing a continuous solution. Below 1380 MeV, there were too few events for the fitting program to be able to distinguish between different solutions. In this region we propagated the solution from the bin above, removing all unnecessary waves.

ii) 1630-1830 MeV

In each of these five energy bins, we again generated 2000 random sets of amplitudes and this time kept the 20 with the highest likelihoods. From these twenty sets, we fit with as many sets (10-15) as necessary to generate five distinct 60-wave solutions. We then made a list of all waves whose modulus was within 2.0 standard deviations of zero in three of the five solutions. These waves were removed and the solutions were refit. This continued until no further waves could be removed. At this point, the five original solutions at each energy had reduced to two or three at that energy. However, the removed waves were different at each energy!

We then returned to the 60-wave solution and removed all those waves which had been eliminated in at least three energy bins. Then we remaximized. We continued to remove waves that were unnecessary in at least three bins. In this way we reduced from 60 to 30 waves, but still had several competing solutions at each energy.

iii) 1830-1990 MeV

Instead of using the full 60 waves, we started with the 30 waves from the lower energies together with the eight  $F_{35}$  and  $F_{37}$  waves which had been removed at lower energy. We generated 2000 random starts in this 38-wave set and kept only enough of the highest sets to give four separate solutions after fitting. Where possible we again removed the unnecessary waves.

iv) Continuity in Energy Above 1630 MeV

To look for continuity, we now used each solution as a starting value in the energy bin above and below its own. In more than half the cases, these starting values led to already existing solutions. If a new solution had a comparable likelihood ( $\Delta F/\delta\Delta F < 1$ ), we not only kept it, but also used it as a starting value above and below its energy; and of course we checked that waves needed at  $\sqrt{s} = 1540$  were present above the energy gap. In looking for smooth energy behavior, we found that some waves had discontinuous (almost random) behavior. We removed these waves even though the fitting program felt they were necessary. In 1972 we found only one chain of solutions over the entire energy range 1620-1999 MeV. This chain consisted of 20 waves from 1620 to 1710 MeV, 23 waves from 1710 to 1750 MeV, and 24 waves from 1750 to 1990 MeV. Figure 8 gives the waves needed at each energy. This is the point at which our analysis stood at the end of 1972 and this solution will be referred to as solution A.

B. The 1973 28-Wave Solution B

As we will discuss in Sec. VI C, the 1972 solution had some 'undesirable' theoretical properties. In an effort to see if this solution was completely stable to the inclusion of new partial waves, we added some further amplitudes to our 1972 set (those marked "\*" in Fig. 8), and repeated the fitting process. We found a new continuous solution in each energy range which differed dramatically from our previous solution only in the  $P_{11}$  waves and the new waves. However, as we shall see this has allowed us a further degree of flexibility in relating the partial-wave amplitudes in our two regions of analysis. In this case the final set contained 28 waves and we will refer to this

as solution B.

### C. Tests and Quality of our Fits

#### 1. Four-dimensional $\chi^2$

To compare our fits with the data, we consider four-dimensional (or less) binning of our data. A theoretical bin population can be calculated by binning Monte Carlo events weighted by  $p(\omega_1, \vec{A})$ . The solid lines in Fig. 9 were generated for Solution A in this manner. From these theoretical bin populations we can also calculate various  $\chi^2$  for the fit. Results are given in Table IV; 24 Dalitz plots corresponding to Fig. 9 are given in Ref. 20.

The purpose of using the maximum likelihood technique is to take advantage of the many correlations that exist in the data and thus the real test of our solutions lie in the ability to account for such correlations. As can be seen from Fig. 9 and the  $\chi^2$  values, we observe excellent reproduction of those correlations. This constitutes a major justification for our solutions.

#### 2. Agreement with Total and Partial-Wave Inelastic Cross Sections

In Fig. 10 we demonstrate that the single-pion production cross sections in the channels we fit are well reproduced. However, we can compare our prediction for

$$\begin{aligned} \pi^- p &\rightarrow n \pi^0 \pi^0 \\ \pi^+ p &\rightarrow n \pi^+ \pi^+ \end{aligned}$$

which are not included in our analysis. This is done in Fig. 11 where we observe excellent agreement for  $\sigma(n \pi^0 \pi^0)$  but a large discrepancy for  $\sigma(n \pi^+ \pi^+)$ . This latter fact may well have a simple physical interpretation and we return to this point in Sec. VII.

We can make even more stringent tests by comparing our inelastic partial-wave cross sections with the predictions from EPSA. At the lower energies where single-pion production is the major inelastic channel we find excellent agreement as demonstrated in the next section. However, at high energies, other inelastic channels begin to appear and the prediction from EPSA only becomes an upper bound on the single-pion production cross section and this bound is satisfied at all energies.

### 3. Removing Waves, Monte-Carlo Checks

At 1530 MeV we tested the final fit to see if our model was adequately describing the data. From the final amplitudes ( $T_R$  for "Real") we generated an equivalent number of Monte Carlo events. By fitting these Monte Carlo events, we determined a set of amplitudes  $T_{MC}$  which gave the best fit (within the errors we indeed found  $T_{MC} = T_R$ ). From both fits  $T_R$  and  $T_{MC}$  we then removed a wave, refit, and compared the changes in the likelihoods and in  $\chi^2$ . The  $\chi^2$  was calculated by binning each variable into four bins ( $4^4 = 256$  bins total). We did this for the four waves shown in Table V. The top wave listed,  $DS_{13}(\rho_3 N)$  is a "large" wave having  $|T|/\delta|T| \approx 10$  and its removal caused the other fitted  $T_a$  to move by many standard deviations. The  $PP_{33}(\Delta\pi)$  and  $PP_{13}(\rho_1 N)$  are medium waves with  $|T|/\delta|T| \approx 6$  and 3 respectively. The  $DS_{33}(\rho_3 N)$  is a "small" wave with  $|T|/\delta|T| \approx 1/2$ . Table V shows the results of these changes, which seem reasonable, and suggests that our program behaves properly. Since the results are the same for both the real and Monte Carlo events we believe our model fits the data adequately.

We also removed waves at higher energies: the  $DD_{15}(\Delta\pi)$  wave at 1650 and the  $FP_{15}(\Delta\pi)$  wave at 1690. The  $DD_{15}(\Delta\pi)$  is the only  $D_{15}$  at 1650 and is quite large. Indeed  $\ln L$  dropped by 584 when it was removed. The  $FP_{15}(\Delta\pi)$  wave however, is one of three  $F_{15}$  waves at 1690 and is only "medium" in size. Here  $\Delta \ln L$  was 186. So again the program seems adequately sensitive to "medium" waves.

#### 4. Checks with a $60 \times 60$ Error Matrix

After finding a best fit at each energy, we found it useful to calculate the full  $60 \times 60$  error matrix, even though a satisfactory fit had been obtained with only, say, 20 waves.

The idea behind inspection of the full error matrix is as follows: Suppose some untried wave, e. g. No. 59, is highly correlated with a wave used in the fit, e. g. No. 19. Then we had better try No. 59: we will probably find a new maximum with No. 59 as large as No. 19, and with No. 19 considerably changed. The clue that some wave is highly correlated with No. 19 can already be found in the diagonal elements of the error matrices, i. e., by comparing the error in a 19 as computed in the  $60 \times 60$  error matrix and in the  $20 \times 20$  matrix. If the  $60 \times 60$  error is, say, twice as big as the  $20 \times 20$  one, we should look among the off-diagonal elements for large correlation coefficients like  $\langle \delta x \delta y \rangle_{19, 59}$ , where  $x$  and  $y$  can each be either amplitude or phase. A geometrical interpretation of the relation between the off-diagonal correlation and the increase in the diagonal error can be found in Fig. A1 of Appendix 1 of Ref. 20.

A  $60 \times 60$  error matrix is too large to reproduce here (it is available in the supplement), however, the diagonal elements only,

for both  $20 \times 20$  and  $60 \times 60$  matrices, are compared in Table VI. We see that the  $60 \times 60$  errors are only 30% larger than their  $20 \times 20$  counterparts, reassuring us that no highly correlated waves have been omitted.

Another use for the  $60 \times 60$  error matrix is in making the transformation from partial-wave amplitudes, e. g.  $\rho_1 N(\text{FF}_{15})$ ,  $\rho_3 N(\text{FP}_{15})$ , to helicity amplitudes, i. e.,  $\rho N(F_{15})$ ,  $\lambda = 1/2$ , and  $3/2$ . One or two of the  $\rho N$  partial waves may not have been needed in the fit, but clearly in making the transformation, the errors in these untried waves must be propagated along with the errors in the waves actually used.

#### D. Comparison of Solutions A and B

In the above sections we have discussed the origin of Solutions A and B and demonstrated that either corresponds to a good representation of the data available to date. We now make a quantitative comparison of the two solutions.

In Table VII a summary of the differences in likelihoods of Solutions A and B is given at nine energies between (1640-2000) MeV (evaluated for a standard sample of 9000 events). For each energy, Solution B gives the higher likelihood, and the difference is around 100. Since Solution B involves four additional partial waves compared to Solution A, we must determine whether this increase of 25 per wave in the likelihood function is significant. Reference to Table V, where we discuss the sensitivity of our solutions to the removal of waves, indicates that such a change in likelihood corresponds to that expected for the inclusion of three or four waves with  $|T|/\delta T \sim 3.0$  (i. e., quite significant, moderately large waves). Thus we conclude that the

four new waves are really required and that Solution B provides a substantially better representation of the data than the original solution A.

#### E. Summary

We find two solutions which possess all the following properties:

- (i) At each energy the solution parameters correspond to a maximum in the likelihood function and have a high likelihood (usually the highest of the competing solutions).
- (ii) The solution at each energy propagates to the solution at the adjacent energies above and below.
- (iii) Qualitatively it has no discontinuous motion between adjacent energies.
- (iv) It possesses good agreement with the EPSA predictions for the inelastic cross sections.

The crucial step was the selection of a good subset of waves. Our two final subsets were the only ones we found that had solutions satisfying all the above requirements. Due to cost of computer time we cannot be certain that we have found the only two subsets. But we believe that the larger waves are uniquely determined. We cannot be as certain in the case of the smaller waves, the amplitudes of which are never more than two or three standard deviations from zero. Furthermore, with 30-40 MeV energy bins, our emphasis on continuity clearly biases us against very narrow resonances.



## VI. THE PARTIAL WAVE AMPLITUDES--DESCRIPTION AND DISCUSSION

At each energy the solution of any fits to inelastic data are only defined up to an overall phase. Thus, in order to give Argand diagrams of the partial-wave amplitudes we must determine this phase. Of the variety of methods by which this can be achieved, we have linked the inelastic amplitudes to published elastic amplitudes (which have known phase) via a K-matrix fit at energies where both elastic and inelastic amplitudes are large,<sup>30</sup> -- this turns out to be in the region of a prominent resonance. This has been done for both Solutions A and B.

In Figs. 12 and 13 we present summary Argand diagrams for Solutions A and B and, in Fig. 14 both Argand diagrams and partial-wave cross sections for Solution B. The equivalent complete figures for Solution A are contained in Ref. 11. A summary of the major characteristics of each partial wave is given in Table VIII, together with comments on resonance interpretations.

Next we discuss the unambiguous results in our two solutions and contrast the differences between them. Before entering into too great detail we should note that the major difference between the two solutions lies in the relative orientation of the low-energy (1300-1540 MeV) and high-energy (1630-2000 MeV) amplitudes. This flexibility is due solely to the fact that we have not been able to analyze data in the "gap", and clearly the correct solution will be identified when this is done reliably. It is important to point out that within each energy regime, Solutions A and B are essentially identical, except in the  $P_{11}$  waves and the new waves added. All of the major features remain the same providing one does not try to link the two energy regions.

A.  $I = \frac{1}{2}$  States

The considerable amount of motion in these plots is not surprising since most of the structure observed may be associated with the existence of already established resonant states.

1.  $P_{11}$

In both solutions, the  $P_{11}(1470)$  is clearly observed decaying strongly into  $\pi\Delta$  and  $N\epsilon$ . A higher-mass  $P_{11}$  is also present in both solutions although there are distinct differences in shape in this case.

2.  $N\rho$  Couplings

We observe strong  $N\rho$  couplings of the  $P_{13}(1700)$ ,  $D_{13}(1520)$  and  $F_{15}(1680)$  resonances. This is not surprising, as the last two resonances are strongly seen in photoproduction and application of the Vector Dominance Model would imply this result. In the case of the new  $P_{13}(1700)$ ,  $N\rho$  is the major decay channel.

3.  $D_{13}(1700)$

This state is observed in our solutions. Its presence is predicted<sup>31</sup> by the L excitation quark model and is the last remaining  $N^*$  or  $\Delta$  state of the  $(70, 1^-)$  supermultiplet of negative parity baryon states to be identified. It decays into the  $\pi\Delta(DS_{13})$  and  $N\epsilon(DP_{13})$  channels, but its mass and width are difficult to estimate and probably differ between our Solutions A and B.

4.  $D_{15}$  and  $F_{15}$

These two resonances are strongly observed in our analysis. This verifies our previous result that the  $D_{15}$  couples exclusively (within errors) to the  $\pi N$  and  $\pi\Delta$  channels. Moreover, we have now determined unambiguously the relative sign of the  $F_{15}$  and  $D_{15}$   $\Delta\pi$  couplings and accounted for all the  $F_{15}$  inelasticity. Thus we have made a

significant improvement over our previous analysis.<sup>4</sup>

### 5. N $\epsilon$ Decay Modes

In our analysis the  $\epsilon$  is a slowly varying effect over the Dalitz plot. Hence N $\epsilon$  decays may also be interpreted as direct three-body  $\pi\pi N$  decays of a given J<sup>P</sup>.

#### B. I = 3/2 States

1. For  $E < 1540$ , all of the I = 3/2 amplitudes are small, whereas for  $E \geq 1650$  MeV (where we again have data) the S<sub>31</sub>, D<sub>33</sub> and P<sub>33</sub> amplitudes are already large. This means that we cannot observe the complete anti-clockwise motion in these channels.

2. The presence of two low-energy P<sub>11</sub> states ( $\sim 1410$  and  $\sim 1730$  MeV) implies the need for two P<sub>33</sub> states in most schemes, while the (56, L = 2<sup>+</sup>) supermultiplet requires yet a third. In terms of partial-wave analyses, the situation is confused--the two EPSA's disagree; likewise our Solution A and B. We compare the CERN and Saclay parameters:

	Mass (MeV)	$\Gamma$ (MeV)	$\gamma$	Author's own "Crude" estimate of resonance quality
CERN <sup>1</sup>	1680	220	0.1	"D"
Saclay <sup>2</sup>	1900	204	0.19	"***"

Our Solution A does not show these resonances, but our preferred Solution B is consistent with the existences of both.

#### 3. F<sub>35</sub>

In both Solutions A and B we have evidence for an F-wave  $\pi\Delta$  system, as do Mehtani et al.,<sup>5</sup> although one might expect, on kinematical barrier-factor arguments, the P-wave would dominate. In our solution the decay into N $\rho$  dominates, and this final state allows us to saturate the EPSA inelastic cross section prediction.

4. F<sub>37</sub>

This resonance is observed both in the  $\pi\Delta$  and  $N\rho$  channels. However, these two channels do not saturate the predicted inelastic cross section (only  $\sim 60\%$  is accounted for). The strong  $N\rho$  decay might well be expected again as this resonance is a dominant feature of photoproduction.

5. P<sub>31</sub>, D<sub>35</sub>

These waves fall short of the EPSA predictions. In particular we find no need for any  $D_{35}$  interactions i.e.,

$$\sigma_{\text{in}}(D_{35}) = 0.$$

Thus, if there are any low-lying  $D_{35}$  resonances they do not couple to the  $\pi\Delta$  or  $N\rho$  channels. However, EPSA does predict a large inelastic cross section from the wave ( $\sim 4$  mb) and this is a shortcoming of our results, although it probably has a simple interpretation. [ See E(i) below. ]

C. The Origin of Solution B and the New Waves Added

We were motivated to study the stability of Solution A by the observation that some of the relative coupling signs between resonances in our lower energy region and resonances in our upper energy region (in Solution A) conflicted with the predictions of broken  $SU(6)_W$ <sup>32</sup> and Melosh transformations,<sup>33</sup> although within each energy region there was consistency with theory. Thus we studied several ways in which another continuation of the partial-wave amplitudes across the energy gap might be achieved. A second solution--our

Solution B--was found in the following manner. We added many new waves (admittedly suggested by theory) and re-performed our whole fitting process. This led to the new solutions in the two energy regions which allow a different continuation through the energy gap and hence the new Solution B. This solution is an even better fit to the data than Solution A, and furthermore the signs of the  $DD_{13}(1520)$  and  $DD_{15}(1660)$  are now in good agreement with the theoretical expectations.

The four new waves are:  $SD_{11}$  in  $\pi\Delta$ ,  $DD_{33}$  in  $\pi\Delta$ ,  $FF_{15}$  in  $\pi\Delta$ ,  $PP_{11}$  in  $N\rho_1$ .

From the previous discussion of this section it is clear that within the energy regions in which we have data there is little difference between these solutions. The important test lies in the "gap" through which we have to make a K-matrix extrapolation. Thus this result emphasizes the need for the free availability of complete data sets or at least a reliable partial-wave analysis in the energy region 1540-1630 MeV.

#### D. Resonance Parameters

We have resisted the temptation to quote any resonance parameters in the paper. The problem of extracting these quantities is difficult and is the subject of the companion papers.<sup>30, 34-37</sup>

#### E. Further Comments

We would like to call attention to some conclusions we may draw from the absence of certain waves ( $D_{35}$ ), the failure to reach EPSA predictions ( $P_{31}$ ,  $F_{37}$ ), the poor fits to the  $\pi^+\pi^+n$  state, and the general deterioration of the fits at the higher energies.

1.  $\pi^+\pi^+n$  and  $N_{1/2}^*$  final state interactions

Our predictions for  $\sigma(\pi^+\pi^+n)$  are a factor of 2 too small ( $\sim 2-3$  mb unaccounted) at the higher energies. This is not surprising as only the  $\pi\Delta$  intermediate states of our isobar model connect with this final state and from inspection of the  $\pi^+n$  mass spectra it is clear that  $N_{1/2}^*$  isobars ( $P_{11}$ ,  $D_{13}$ ,  $F_{15}$ ,  $D_{15}$ ) may be present. Furthermore, if one considers low angular momenta in the  $\pi N_{1/2}^*$  system one finds:

$$\left. \begin{array}{l} \pi N^*(D_{13}) \text{ in a P wave} \\ \pi N^*(F_{15}) \text{ in an S wave} \end{array} \right\} \text{ are derived from } D_{35}$$

$$\pi N^*(P_{11}) \text{ in an S wave would be derived from } P_{31}$$

which suggests that our previously-noted failure to reach the  $P_{31}$  and  $D_{35}$  predictions is associated with not including  $N^*$  final-state interactions. This suggestion can be further substantiated if we note the

$$\sigma_{\text{missing}}(P_{31} + D_{35} + F_{37}) \simeq \sigma_{\text{missing}}(\pi^+\pi^+n) + \sigma(\pi\pi\pi N).$$

Finally, the inclusion of these waves would have an appreciable effect in the  $\pi^+\pi^+n$  final state whereas Clebsch-Gordan coefficients reduce their effect in the other single-pion production reactions so that our analysis of those channels would probably show little change.

2. Peripheral nucleon

The deterioration of the fits at higher energies is generally associated with being unable to entirely account for the onset of peripheral processes. This probably indicates the necessity for inclusion of  $\pi$  exchange in the production of the  $N\rho$  final state, so that higher partial waves are generated.

## VII. CONCLUSIONS

Elastic phase-shift analyses only relate to one aspect of the  $\pi N$  interaction, and the analysis described here represents a substantial progress in providing complimentary information on the inelastic channels.

This analysis has demonstrated that isobar-model partial-wave analyses of inelastic final states can reproduce the detailed nature of the data. This then allows the observation of resonances in inelastic channels.

We have evidence for the existence of a  $D_{13}(1700)$ , long predicted by the quark model. The existence of a  $P_{13}(1700)$  is corroborated through a strong  $\rho N$  coupling. Our preferred solution, B indicates a  $P_{33}(1700)$  resonance. Furthermore we have strengthened the interpretation of many resonances due to our observation of them in the inelastic channels  $N\rho$ ,  $N\epsilon$ , and  $\pi\Delta$ .

Earlier analyses have produced limited  $\pi\Delta$  Argand plots, but this analysis presents the first full Argand plots for all three channels,  $N\rho$ ,  $N\epsilon$ , and  $\pi\Delta$ . These begin to allow a complete picture of the  $\pi N$  interaction accounting for almost all of the inelastic cross section.

Finally, we are at present using these amplitudes to study resonance parameters and couplings and their relations to other theories of hadron interactions. 30, 34-37

### VIII. ACKNOWLEDGMENTS

We wish to thank the Oxford, UCR-LBL, and Saclay groups, especially A. Jones, D. Saxon (Oxford), S-Y Fung, G. Kalmus, A. Kernan, W. Michael (UCR-LBL), B. Deler, Nguyen Thuc Diem, J. Dolbeau (Saclay), for use of their data in this analysis. We also thank J. P. Berge, A. D. Brody, B. Deler, A. Kernan, B. Levi, L. R. Price, and B. Shen for their contributions to the early phase of the experiment.

We further wish to thank D. Faiman and F. Gilman and M. Kugler for their interest and suggestions.



APPENDIX A  
 MAXIMIZING THE SCALE PARAMETER IN THE LIKELIHOOD FIT

In Eq. (4.11) remember that  $N^C R^C / \sigma^C$  is the number of events  $\nu^C$  predicted by the parameters  $\vec{A}$ , so write

$$\Sigma \frac{N^C R^C}{\sigma^C} = \Sigma \nu^C(\vec{A}) \equiv \nu(\vec{A}) .$$

For this discussion the first product in Eq. (11) is only a constant  $B$  which does not depend on  $\vec{A}$ , so Eq. (4.11) becomes

$$L = B e^{-\nu(\vec{A})} \prod_{i=1}^N p_i(\vec{A}) . \quad (A1)$$

Introducing the scale factor of Eq. (4.12),

$$\vec{A} = s \vec{A}^0 \quad (A2)$$

we have

$$\nu(s\vec{A}^0) = s^2 \nu(\vec{A}^0) \equiv s^2 \nu^0$$

and

$$\prod p_i(s\vec{A}^0) = s^{2N} \prod p_i(\vec{A}^0) .$$

Equation (A1) becomes

$$L(s\vec{A}^0) = B e^{-s^2 \nu^0} s^{2N} \prod p_i(\vec{A}^0) , \quad (A3)$$

and the last factor  $\prod p_i$  is independent of  $s$ . Combining it with  $B$ ,

we have

$$L(s\vec{A}^0) = B' e^{-s^2 \nu^0} s^{2N} . \quad (A4)$$

Then

$$\ln L(s\vec{A}_0) = \ln B' - s^2 \nu^0 + 2N \ln s$$

and

$$\frac{\partial}{\partial s} \ln L(s\vec{A}_0) = -2s\nu^0 + \frac{2N}{s} \quad (A5)$$

To find  $s^2|_{L \max} \equiv s_m^2$ , set (A5) = 0, and we get Eq. (4.18), i.e.,

$$s_m^2 = \frac{N}{\nu_0} = \frac{N}{\sum \frac{N^c R^c(\vec{A}_0)}{\sigma^c}} \quad (A6), (4.18)$$

Equation (A6) is derived in Miller's thesis,<sup>23</sup> but then  $s^2$  is written by mistake as  $s$ . We now insert our result (A6) into (A4),

$$L(s_m \vec{A}^0) = B' e^{-N} \left( \frac{N}{\nu_0} \right)^N, \quad (A4_m)$$

and this in turn into (A3)

$$L(s_m \vec{A}^0) = B e^{-N} \left( \frac{N}{\nu^0(\vec{A}_0)} \right)^N \prod_{i=1}^N p_i(\vec{A}^0). \quad (A3_m)$$

Now that  $s$  is maximized, we see that (A3<sub>m</sub>) is independent of the overall magnitude of  $\vec{A}^0$ , and we can drop its superscript zero and call it  $\vec{A}$ . For the purpose of hunting in  $\vec{A}$  space for  $L_{\max}$  we emphasize factors containing  $\vec{A}$ :

$$L(s_m \vec{A}) = B e^{-N} N^N \left[ \sum \frac{N^c R^c(\vec{A})}{\sigma^c} \right]^{-N} \prod_{i=1}^N p_i(\vec{A}) \quad (A5)$$

$$\ln L(s_m \vec{A}) = \text{const.} - N \ln \left[ \sum \frac{N^c R^c(\vec{A})}{\sigma^c} \right] + \sum_{i=1}^N \ln p_i(\vec{A})$$

We actually work with the average of this premaximized  $L$ , which we call  $F(\vec{A})$

$$F(\vec{A}) = \frac{1}{N} \ln L(s_m, \vec{A}), \quad (\text{A6})$$

$$F(\vec{A}) = \text{const.} - \ln \left[ \sum_c \frac{N^c R^c(\vec{A})}{\sigma^c} \right] + \frac{1}{N} \sum_{i=1}^N \ln p_i(\vec{A}) \quad (\text{A7})$$

The factor  $1/N$  in (A6) makes  $F$  roughly independent of  $N$ , so it is easier to compare fits at different energies where there are different numbers of events. Equation (A7) is the same as Eq. (4.20) of the text.

APPENDIX B

EXAMPLE OF STEPPING PROCEDURE WHEN  
 $\nabla \nabla^T f$  MATRIX IS SINGULAR

As an example of the method discussed in Section IV.D.4, consider the function  $f(z) = -z^2 + 2z + 1$ , but let  $z = x + y$ , i.e.,

$$f(x, y) = -(x+y)^2 + 2(x+y) + 1, \quad (B1)$$

where  $f$  has a maximum at  $z = x + y = +1$ . In this case, we clearly have a redundant parameter. Now

$$\begin{aligned} \nabla f &= 2 \left[ 1 - (x+y) \right] \begin{pmatrix} 1 \\ 1 \end{pmatrix} \quad \text{and} \\ \nabla \nabla^T f &= \begin{pmatrix} -2 & -2 \\ -2 & -2 \end{pmatrix}. \end{aligned} \quad (B2)$$

The two normalized eigenvectors of  $\nabla \nabla^T f$  are  $\vec{v}_1 = \begin{pmatrix} 1/\sqrt{2} \\ 1/\sqrt{2} \end{pmatrix}$  and  $\vec{v}_2 = \begin{pmatrix} 1/\sqrt{2} \\ -1/\sqrt{2} \end{pmatrix}$ , with eigenvalues  $-4$  and  $0$ . Note that  $\nabla f$  (hence  $\nabla \nabla^T f$ )  $= 0$  along  $\vec{v}_2$ . Now

$$\nabla \nabla^T f = -4 \vec{v}_1 \vec{v}_1^T + 0 \vec{v}_2 \vec{v}_2^T. \quad (B3)$$

Let

$$\underline{M} = \nabla \nabla^T f - \vec{v}_2 \vec{v}_2^T = -4 \vec{v}_1 \vec{v}_1^T - \vec{v}_2 \vec{v}_2^T. \quad (B4)$$

Clearly

$$\underline{M}^{-1} = -\frac{1}{4} \vec{v}_1 \vec{v}_1^T - \vec{v}_2 \vec{v}_2^T. \quad (B5)$$

Now let

$$\underline{V} = \underline{M}^{-1} + \vec{v}_2 \vec{v}_2^T = -\frac{1}{4} \vec{v}_1 \vec{v}_1^T,$$

$$= -\frac{1}{4} \begin{pmatrix} 1/2 & 1/2 \\ 1/2 & 1/2 \end{pmatrix} = -\frac{1}{8} \begin{pmatrix} 1 & 1 \\ 1 & 1 \end{pmatrix} \quad (\text{B6})$$

Assume a starting value  $x_0, y_0$ . Then the first step is

$$\begin{aligned} -\underline{V} \cdot \nabla F_0 &= +\frac{1}{8} \begin{pmatrix} 1 & 1 \\ 1 & 1 \end{pmatrix} \cdot 2[1 - (x_0 + y_0)] \begin{pmatrix} 1 \\ 1 \end{pmatrix} \\ &= \frac{1}{2} \begin{bmatrix} 1 - (x_0 + y_0) \\ 1 - (x_0 + y_0) \end{bmatrix} . \end{aligned}$$

Thus

$$\begin{pmatrix} x_1 \\ y_1 \end{pmatrix} = \begin{pmatrix} x_0 \\ y_0 \end{pmatrix} - \underline{V} \cdot \nabla F_0 \quad (\text{B7})$$

$$= \begin{pmatrix} 1/2 \\ 1/2 \end{pmatrix} + \begin{pmatrix} \frac{x_0 - y_0}{2} \\ \frac{y_0 - x_0}{2} \end{pmatrix} , \quad (\text{B8})$$

and  $x_1 + y_1 = \frac{1}{2} + \frac{x_0 - y_0}{2} + \frac{1}{2} - \frac{x_0 - y_0}{2} = 1$  and we are at the minimum in one step, as we should be since  $F$  is quadratic.

Thus the problem in a multidimensional case reduces to finding the eigenvectors with zero eigenvalues, subtracting the rank-one matrices generated by these eigenvectors, inverting the resulting matrix, and finally adding back the rank-one subtractions.

In the case of likelihood problems such as ours, the eigenvector for scale changes is  $\underline{A}$  and the eigenvector for phase changes is  $i\vec{A}$ . Thus for us, we automatically had the necessary two eigenvectors.

APPENDIX C

CHOICE OF ANGULAR MOMENTUM BARRIER FACTORS  
AND OF THE  $N^*$  RADIUS

Unfortunately three different forms of barrier-penetration factors  $B_L(QR)$  are now common in partial-wave analyses. This appendix compares them in Fig. C1, points out that for  $L \geq 2$  they may differ, and makes a plea for using the standard Blatt-Weisskopf factors, which have recently been given considerable support by von Hippel and Quigg.

In the text, Eq. (3.10), we used the notation  $b_L$ , for the barrier factor for the amplitude  $T$ ; here we use the more standard notation  $B_L (= |b_L|^2)$  for the barrier factor for the intensity  $|T|^2$ . The "industry standard" for  $B_L$  is taken from Eq. 5-8, page 361, of Blatt and Weisskopf<sup>21</sup> (where they are called  $v_l$ )

$$B_0 = 1, B_1 = \frac{x^2}{1+x^2}, B_2 = \frac{x^4}{9+3x^2+x^4}, \dots \quad (C1)$$

where  $x = QR$ . These  $B_L$  have the property that their inflection point is at about  $QR = L$ . For  $x \ll L$ , they start off as

$$B_L \xrightarrow{x \rightarrow 0} \frac{x^{2L}}{[(2L-1)!!]^2} \quad (C2)$$

and for  $x \gg L$ ,  $B_L \rightarrow 1$ . Figure C1 gives  $B_L$  vs  $QR$  for  $L = 1$  to 7.

There is general agreement that the  $B_L$  should start out as  $x^{2L}$  and should approach unity for large  $L$ ; but before the 1972 paper of von Hippel and Quigg,<sup>39</sup> the detailed form C1 was regarded with some skepticism by particle physicists because it was derived by assuming that the region of interaction was a square well. This is

reasonable when the intermediate state is a nucleus, which is what Blatt and Weisskopf had in mind, but less convincing when it is an  $N^*$ . Accordingly many physicists just used the low-QR form (C2), or perhaps a form somewhat like that for  $L=1$ , which has the correct limiting properties at both ends

$$B_L \approx \frac{x^{2L}}{\text{Const} + x^{2L}}, \quad (\text{C3})$$

but in general does not have its inflection point near  $QR = L$ .

Von Hippel and Quigg have now shown that form C1 can be re-derived using only the properties of the radial wave function  $U_L(x) \propto x h_L(x)$  where  $h_L$  is a Hankel function. For more discussion and an approximate form, see Ref. 40.

Figure C1 shows not only the Blatt-Weisskopf form of  $B_L$ , but the small-QR approximation for  $L=1$  to 3. As one expects, both approximations fail badly by  $QR = L$ . This brings us to our plea. Now that the Blatt-Weisskopf form has been well justified, why not use it? Then, once most analyses use the same barrier, we can go on to gather experience on the best value for the radius  $R$ .

Next we take up the question of what value to choose for the radius parameter  $R$ . Barbaro-Galtieri<sup>41</sup> has done a thorough analysis of the  $\Delta(1336)$  peak and finds that  $R$  should be about  $1F$ . Yet when  $R$  is used in a far more indirect way to do  $SU(3)$  fits, it turns out that values of  $0.2F$ ,<sup>41</sup> or even zero,<sup>42</sup> work best.

The radius question, specifically as it applies to our reaction  $\pi N \rightarrow \pi\pi N$ , has recently been studied at Saclay by J. Dolbeau<sup>43</sup> in his isobar analysis in the  $\sqrt{s}$  range 1390-1740 MeV. These fits are very sensitive to the radius, particularly near  $\rho$  threshold around 1700 MeV. Dolbeau finds a best radius of  $\sim 1/4 F$ , i. e., in between the large value

avored by the  $\Delta(1236)$  and the small value favored by SU(3). Specifically he finds that  $1/R$  should be  $750 \pm 250$  MeV/c.

Finally a comment on what we ourselves did. Because of a programming mistake, we started our fits using the small-QR approximation C2, and did not catch the mistake until so late that it was expensive to refit. But now Dolbeau's finding that the best value of R is only  $1/4 F$  keeps QR so low that it does not pay for us to refit. Specifically, consider the kinematics of our reaction <sup>even</sup> at our highest energy  $\sqrt{s} = 1970$  MeV, and set  $R = 1/750$  MeV/c. Then for

$$\pi N \rightarrow \Delta(1236)\pi, Q_{\Delta} = Q_{\pi} \equiv Q = 393 \text{ MeV/c}, QR = 0.52$$

$$\rightarrow \rho(770)N, Q_{\rho} = Q_N \equiv Q = 500 \text{ MeV/c}, QR = 0.67.$$

This means that near the resonance bands of our Dalitz plots, where we find most of our data, the small-QR approximation is quite good, and we have decided not to refit. In our K-matrix programs for energy-dependent fits we have always used the standard Blatt-Weisskopf form C1.



FOOTNOTES AND REFERENCES

\*Work supported by the U. S. Atomic Energy Commission.

†Present address, Lawrence Livermore Laboratory, Livermore, California 94550.

††Present address, CEN, Saclay, (France).

‡Present address, DESY, Notkestieg 1, 2000 Hamburg-52.

§Present address, Nuclear Physics Laboratory, Oxford, OX1-3RH.

1. S. Almehed and C. Lovelace, Nucl. Phys. B40, 157 (1972). For earlier references, see our Ref. 3.
2. R. Ayed and P. Bareyre, paper presented at the Second Aix-en-Provence International Conference on Elementary Particles (1973).
3. Particle Data Group, Rev. Mod. Phys. 45, (April 1973, Part II).
4. A. D. Brody et al., Phys. Lett. 34B, 665 (1971).
5. a. U. Mehtani et al., Phys. Rev. Lett. 29, 1634 (1972);  
b. Y. Williamson et al., Phys. Rev. Lett. 29, 1353 (1972);  
c. A. Kernan et al., LBL Report No. LBL-2017, or Proc. Baryon Resonance Conference, (Purdue, 1973), p. 113.
6. P. Eberhard and M. Pripstein, Phys. Rev. Lett. 10, 8 (1963).
7. B. Deler et al., Nuovo Cimento 45A, 559 (1966).
8. M. DeBeer et al., Nuclear. Phys. B12, 599, 617 (1969). Further analyses may be found in the theses of B. Deler (CEA-R-3579, 1969), G. Smadja (Orsay Series A, No. 556, 1969), M. P. Chavannon (D. Ph. P. E. Saclay, 1971), Nguyen Thuc Diem (CEA-N-1602, 1973); and in the recent papers by J. Dolbeau and F. Triantis, submitted to the 1973 Aix-en-Provence Conference;<sup>2</sup> and P. Chavannon, J. Dolbeau, and G. Smadja, Nucl. Phys. B75, 157 (1974).
9. M. G. Bowler and R. J. Cashmore, Nucl. Phys. B17, 331 (1970).
10. W. Chinowsky, J. M. Mulvey, and D. H. Saxon, Phys. Rev. D 2, 1790 (1970).

11. D. J. Herndon et al., LBL Report No. LBL-1065/SLAC-PUB-1108, presented to the XVI International Conference on High Energy Physics, Chicago-Batavia, Ill. (1972).
12. A.D. Brody et al., Phys. Rev. D 4, 2693 (1971).
13. U.C. Riverside-LBL collaboration, see Ref. 5a and b.
14. D.J. Herndon, P. Söding, and R.J. Cashmore, SLAC-PUB-1385, LBL Report No. LBL-543 (1973), submitted to Phys. Rev. D.
15. G. Smadja, "Resonances that Overlap", LBL Report No. LBL-382, 1974 (unpublished). We have found a mistake in this paper which greatly underestimates the problem.
16. R. Aaron and R.D. Amado, Phys. Rev. Lett. 31, 1157 (1973); G. Gustafson, Nucl. Phys. B63, 325 (1973).
17. The preliminary conclusions of R. Ascoli (private communication, February 1974) are that the corrections will not be very significant.
18. Y.N. Goradia, T.A. Lasinski, G. Smadja, M. Tabak, LBL Report No. LBL-3011 (1974).
19. S.D. Protopopescu et al., Phys. Rev. D 7, 1279 (1973); B. Hyams et al., Max-Planck preprint MPI-PAE/Exp. 28 (1973); P. Baillon et al., Phys. Lett. 38B, 555 (1972).
20. D.J. Herndon, Ph.D. Thesis, (University of California, Berkeley, 1972), LBL Report No. LBL-544, 1972 (unpublished).
21. J. Blatt and V. F. Weisskopf, Theoretical Nuclear Physics (John Wiley, 1952).
22. In our case, four kinematic variables are needed for each event: two Dalitz plot variables, and two angles,  $\theta$  and  $\phi$ . The Dalitz plots of Fig. 2 require 10-100 bins. The  $\cos\theta$  distributions of Fig. 3 need  $\sim 20$  bins and the  $\phi$  distribution needs another 10 bins. The total number of bins is then  $\sim 2,000-20,000$ , while the

experiment has only  $\sim 10,000$  events at each momentum. Under these circumstances, the event population in each bin would be too small to allow the assumption of a Gaussian distribution. It follows that the maximum likelihood technique would be the most appropriate fitting method to apply in our experiment.

23. L.R. Miller, Ph.D. Thesis (University of California, Berkeley), LBL Report No. LBL-38, 1974 (unpublished).
24. F.T. Solmitz, Ann.Rev. Nucl. Sci. 14, 379 (1964), Eq. 36.
25. W.C. Davidon, Computer J., 10, 406 (1967).
26. P.Eberhard and W.O.Koellner, "Optime System for Fitting Theoretical Expression," LBL Report No. UCRL-20159, 1970, (unpublished).
27. P.H.Eberhard, A.H.Rosenfeld, and M.Tabak, Group A Memo. Private communication, 1974.
28. Some of the numbers and conclusions in this paragraph differ from those of Miller's thesis (Ref.22), which we now think are wrong.
29. Eventually!
30. R.Longacre, Ph.D. Thesis (University of California, Berkeley, 1973), LBL Report No. LBL-948, 1974; R.Longacre et al., LBL Report No. LBL-2636/SLAC-PUB-1389, (to be submitted for publication).
31. R.H.Dalitz, " $\pi$ N Scattering", Proc. of 1967 Irvine Conference, edited by G. L. Shaw and D. L. Wong (Wiley, N.Y., 1969), p. 187.
32. D. Faiman and J. Rosner, Phys. Lett. 45B, 357 (1973).
33. F.J. Gilman, M.Kugler, S.Meskov, Phys. Lett. 45B, 481 (1973) and SLAC-PUB-1286, Phys. Rev. D (Jan. 1974, in press).

34. R.J. Cashmore, in Proc. Conf. on Baryon Resonances, edited by Earl Fowler (Purdue, 1973), p. 53.
35. A.H. Rosenfeld, Lectures at International School of Subnuclear Physics, Erice, Sicily (1973) and LBL Report No. LBL-2098 (unpublished).
36. R.J. Cashmore, D.W.G.S. Leith, R.S. Longacre, and A.H. Rosenfeld, LBL Report No. LBL-2635/SLAC-PUB-1388, 1974, (to be submitted for publication).
37. R.S. Longacre et al., LBL Report No. LBL-2637/SLAC-PUB-1390, submitted for publication.
38. E. Flaminio, J.D. Hansen, D.R.O. Morrison, N. Tovey, CERN-HERA Report Nos. 70-4 and 70-7, 1970 (unpublished).
39. F. von Hippel and C. Quigg, Phys. Rev. D5, 624 (1972).
40. A. H. Rosenfeld, in Proc. of the 1971 Irvine Conference (AIP Conf. Proc. No. 6, Particles and Fields subseries No. 2).
41. A. Barbaro-Galtieri, in Proc. of the 1971 Enrice Summer School and LBL Report No. LBL-555. See particularly Table V.
42. D. E. Plane et al., Nucl. Phys. B22, 93 (1970).
43. J. Dolbeau, Ph. D. Thesis, 1974, D. Ph. P. E., Saclay.

TABLE I: Experiments used in this analysis.<sup>a</sup>

Beam particle	Laboratory (reference)	c. m. Energy range (GeV)		Number of events	
		Low	High	$\pi^+\pi^-n$	$\pi^-\pi^0p$
$\pi^-$	SLAC-LBL (12)	1.47	1.50	1010	648
		1.64	1.97	41175	27946
	Oxford (10)	1.31	1.54	18502	5892
	Saclay (8)	1.39	1.53	13340	7314
Total		1.31	1.97	74027	41800
				$\pi^+\pi^0p$	$\pi^+\pi^+n$
$\pi^+$	Oxford (9)	1.43	1.56	7262	1374
	Riverside-LBL (13)	1.82	2.09	41412	17255
	Saclay (8)	1.64	1.97	11522	3382
	Total	1.43	2.09	60196	22011

<sup>a</sup>The events in this Table, in the form of 16 full BCD Data Summary Tapes, are available on request. The  $\pi^+$  events at or above  $\sqrt{s} = 1820$  MeV must be requested from the UCR-LBL collaboration, care of Prof. Anne Kernan, U. C. Riverside; the remainder from LBL, SLAC, or Saclay.

TABLE II: The 60 waves with angular momenta  $L, L', \ell$  each  $\leq 3$ . There are two nucleon-rho terms in the isobar model, indicated by  $\rho_3$  and  $\rho_1$ , where the subscript indicates the coupling between the spin of the  $\rho(\ell = 1)$  and the spin of the outgoing nucleon. See Fig. 4 for more complete explanation of the notation. We never used more than 28 of these 60 waves.

Isospin	Incident wave	$\pi\Delta$	$N\rho_3$	$N\rho_1$	$N\epsilon$
I = 1/2	$S_{11}$	$SD_{11}$	$SD_{11}$	$SS_{11}$	$SP_{11}$
	$P_{11}$	$PP_{11}$	$PP_{11}$	$PP_{11}$	$PS_{11}$
	$D_{13}$	$DS_{13}$ $DD_{13}$	$DS_{13}$ $DD_{13}$	$DD_{13}$	$DP_{13}$
	$P_{13}$	$PP_{13}$ $PF_{13}$	$PP_{13}$ $PF_{13}$	$PP_{13}$	$PD_{13}$
	$D_{15}$	$DD_{15}$	$DD_{15}$	$DD_{15}$	$DF_{15}$
	$F_{15}$	$FP_{15}$ $FF_{15}$	$FP_{15}$ $FF_{15}$	$FF_{15}$	$FD_{15}$
	$F_{17}$	$FF_{17}$	$FF_{17}$	$FF_{17}$	
I = 3/2	$S_{13}$	$SD_{31}$	$SD_{31}$	$SS_{31}$	
	$P_{31}$	$PP_{31}$	$PP_{31}$	$PP_{31}$	
	$D_{33}$	$DS_{33}$ $DD_{33}$	$DS_{33}$ $DD_{33}$	$DD_{33}$	
	$P_{33}$	$PP_{33}$ $PF_{33}$	$PP_{33}$ $PF_{33}$	$PP_{33}$	
	$D_{35}$	$DD_{35}$	$DD_{35}$	$DD_{35}$	
	$F_{35}$	$FP_{35}$ $FF_{35}$	$FP_{35}$ $FF_{35}$	$FF_{35}$	
	$F_{37}$	$FF_{37}$	$FF_{37}$	$FF_{37}$	

TABLE III: Number of events for the energy bins used in the fits. For availability of these events, see note at bottom of Table I.

c. m. energy	Range (MeV)	$\pi^- p \rightarrow \pi^+ \pi^- n$	$\pi^- p \rightarrow \pi^- \pi^0 p$	$\pi^+ p \rightarrow \pi^+ \pi^0 p$
i 1310	1300-1330	1069	151	
1340	1330-1360	1664	11	
1370	1360-1380	2471	2	
1400	1380-1410	5049	964	78
1440	1430-1460	4918	1802	359
1470	1460-1480	3252	1629	175
1490	1480-1510	5555	3197	1523
1520	1510-1530	3241	2588	795
1540	1530-1560	3905	3285	1114
ii 1650	1630-1670	6061	3757	2467
1690	1670-1710	5901	3689	1139
1730	1710-1750	3455	2630	4061
1770	1750-1790	3214	2352	2853
1810	1790-1830	2447	1541	3855
iii 1850	1380-1870	3931	3183	6372
1890	1870-1910	5072	3170	12690
1930	1910-1950	5817	4080	4298
1970	1950-1990	5277	3544	7744
Total	1300-1990	72299	41575	49523

TABLE IV:  $\chi^2$  at each energy based on four-dimensional bins. The four-dimensional space is subdivided into  $4^4 = 256$  bins, but some have no population, hence the number tabulated below is  $< 250$ .

$\sqrt{s}(\text{MeV})$	$\chi^2_{n\pi^+\pi^-}$	Bins	$\chi^2_{p\pi^-\pi^0}$	Bins	$\chi^2_{p\pi^+\pi^0}$	Bins
1370	279	228				
1440	243	235	216	233	90	160
1530	328	229	253	236	209	216
1690	526	237	378	236	182	208
1970	864	236	601	233	907	235



TABLE V: Effect of removing waves of varying importance at  $\sqrt{s} = 1530$  MeV, 9000 events. Each box is arranged [ $\Delta \ln L$  for real events/ $\Delta \ln L$  for Monte-Carlo], and the same format holds for  $\Delta \chi^2$ .

Original 18-wave fit	Real	$\frac{\ln L}{0.2817}$	$\frac{\chi^2/D.F.}{790/681}$
	Monte Carlo	0.3198	624/788
	$ T /\delta T$	$\Delta \ln L$	$\Delta \chi^2$
18 waves minus DS <sub>13</sub> ( $\rho_3 N$ )	11	-320	173
	10	-390	215
18 waves minus PP <sub>33</sub> ( $\Delta\pi$ )	6	-60	53
	6	-80	102
18 waves minus PP <sub>13</sub> ( $\rho_1 N$ )	2	-30	11
	3	-30	14
18 waves minus DS <sub>33</sub> ( $\rho_3 \pi$ )	1	-1	3
	1/2	-1	2

TABLE VI: Square roots of diagonal elements of a 60×60 and a 20×20 (Solution A) error matrix at 1690 MeV.

$\Delta\pi$			$\rho_3N$			$\rho_1N$			$\epsilon N$		
Wave	Error 20	Error 60	Wave	Error 20	Error 60	Wave	Error 20	Error 60	Wave	Error 20	Error 60
$\Delta SD_{11}$	----	.083	$\rho_3 SD_{11}$	----	.079	$\rho_1 SS_{11}$	.054	.069	$\epsilon SP_{11}$	.066	.087
$\Delta PP_{11}$	.061	.076	$\rho_3 PP_{11}$	----	.077	$\rho_1 PP_{11}$	----	.080	$\epsilon PS_{11}$	.067	.084
$\Delta PP_{13}$	----	.083	$\rho_3 PP_{13}$	----	.056	$\rho_1 PP_{13}$	.038	.053	$\epsilon PD_{13}$	----	.064
$\Delta PF_{13}$	----	.053	$\rho_3 PF_{13}$	----	.048	$\rho_1 DD_{13}$	----	.057	$\epsilon DP_{13}$	.042	.054
$\Delta DS_{13}$	.045	.063	$\rho_3 DS_{13}$	.040	.053	$\rho_1 DD_{15}$	----	.041	$\epsilon DF_{15}$	----	.047
$\Delta DD_{13}$	.044	.058	$\rho_3 DD_{13}$	----	.056	$\rho_1 FF_{15}$	----	.040	$\epsilon FD_{15}$	.027	.032
$\Delta DD_{15}$	.052	.068	$\rho_3 DD_{15}$	----	.050	$\rho_1 FF_{17}$	----	.033			
$\Delta FP_{15}$	.042	.054	$\rho_3 FP_{15}$	.033	.042	$\rho_1 SS_{31}$	.067	.081			
$\Delta FF_{15}$	----	.052	$\rho_3 FF_{15}$	----	.043	$\rho_1 PP_{31}$	----	.090			
$\Delta FF_{17}$	----	.052	$\rho_3 FF_{17}$	----	.041	$\rho_1 PP_{33}$	----	.060			
$\Delta SD_{31}$	.062	.075	$\rho_3 D_{31}$	----	.075	$\rho_1 DD_{33}$	----	.057			
$\Delta PP_{31}$	.063	.086	$\rho_3 PP_{31}$	----	.083	$\rho_1 DD_{35}$	----	.045			
$\Delta PP_{33}$	.062	.096	$\rho_3 PP_{33}$	----	.069	$\rho_1 FF_{35}$	----	.040			
$\Delta PF_{33}$	----	.052	$\rho_3 PF_{33}$	----	.047	$\rho_1 FF_{37}$	----	.038			
$\Delta DS_{33}$	.049	.075	$\rho_3 DS_{33}$	.042	.057						
$\Delta DD_{33}$	----	.052	$\rho_3 DD_{33}$	----	.060						
$\Delta DD_{35}$	----	.065	$\rho_3 DD_{35}$	----	.053						
$\Delta FP_{35}$	----	.048	$\rho_3 FP_{35}$	----	.041						
$\Delta FF_{35}$	----	.050	$\rho_3 FF_{35}$	----	.046						
$\Delta FF_{37}$	----	.053	$\rho_3 FF_{37}$	----	.046						

TABLE VII: Difference in likelihood,  $L(\text{Solution B}) - L(\text{Solution A})$  for a standard sample of 9000 events. Solution B is always better.

$s$ (MeV)	$\Delta \ln L$ (9000 events)
1650	113
1690	122
1730	139
1770	107
1810	84
1850	57
1890	15
1930	153
1970	19

	$M \sim 1710$ $\chi_{inel} \sim 0.9$	Clear resonant motion in $\epsilon N$ and $\pi \Delta$ , but distinctly broader than EPISA width of 100 MeV	$\pi N, \epsilon N, \pi \Delta$ First unambiguous observation of resonant behavior in this region
$D_{15}$	$M = 1660$ $\chi_{inel} \sim 0.6$	The $\pi \Delta$ channels show strong resonant behavior, saturating the unitary bound near the accepted resonant mass	$\pi N, \pi \Delta$
$F_{15}$	$M = 1680$ $\chi_{inel} \sim 0.4$	This resonance is observed in $\epsilon N$ , $\rho N$ , and $\pi \Delta$ with comparable strength	$\pi N, \epsilon N, \rho N, \pi \Delta$
$S_{31}$	$M = 1620$ $\chi_{inel} \sim 0.70$	We lack the experimental data which would reveal the behavior of this wave in the resonance region. The present points above 1650 show a smooth behavior which is compatible with the accepted resonance mass	$\pi N, \pi \Delta, \rho N$
$P_{31}$	$M = 1790$ $\chi_{inel} \sim 0.85$	No evidence for resonant behavior	$\pi N$
$P_{33}$	Suggestion of resonance with $M \sim 1900$ $\chi_{inel} \sim 0.8$	Fast $\Delta\pi$ motion across gap suggests resonance near 1700, i. e., below EPISA value of 1900. (See discussion under B(2) below.)	$\pi N, \pi \Delta$
$D_{33}$	$M \sim 1720$ $\chi_{inel} \sim 0.85$	Our analysis is consistent with a resonance interpretation for $\pi \Delta$ and $\rho N$ .	$\pi N, \pi \Delta, \rho N$
$F_{35}$	$M \sim 1870$ $\chi_{inel} \sim 0.85$	Strong resonance behavior seen in $\rho N$ channel smaller coupling to $\pi \Delta$	$\pi N, \rho N, \pi \Delta$
$F_{37}$	$M = 1930$ $\chi_{inel} \sim 0.6$	Clear resonance behavior is apparent in $\rho N$ and $\pi \Delta$ channels	$\pi N, \rho N, \pi \Delta$

FIGURE CAPTIONS

Fig. 1. Total and inelastic  $\pi^-p$  cross section vs energy. The  $\sigma$  (inelastic) curve comes from Ref. 2 ("EPSA") as in Eq. 4.21; the  $\sigma$  (tot) data comes from Lovelace et al., LBL Report No. 63.

Fig. 2.(a) Dalitz plots for the state  $n\pi^-\pi^+$  at four c.m. energies: 1490, 1650, 1770, 1930 MeV. The side of the little squares is proportional to the predicted density of our fits. On the projected distributions, the dotted line is the experimental data, while the solid histogram is the result of the fit. The scales are linear in  $(\text{mass})^2$ , but the tiny numbers are actually in MeV.

Fig. 2.(b) Dalitz plot for the state  $p\pi^-\pi^0$ . For details see caption to Fig. 2.(a).

Fig. 2.(c) Dalitz plot for the state  $p\pi^+\pi^0$ . For details see caption to Fig. 2.(a).

Fig. 3. Distribution of the angle of the final nucleon with respect to the incident pion in the center of mass. The histograms are given at four c.m. energies: 1490, 1650, 1770, 1930 MeV for the same channels as in Fig. 2. The dotted line is the data, the solid histogram the result of the fit.

Fig. 4. Schematic representation of the isobar model and definition of the partial-wave notation. F describes the final-state particles,  $\Delta\pi$ , etc.

Fig. 5. Phase shifts and modulus of Watson factor  $|W| = \sin \delta / q^{\ell+1}$  for  $\Delta$ ,  $\rho$ , and  $\epsilon$  diparticles. Dashed line on the  $\epsilon$  plot corresponds to the later analysis of Protopopescu;<sup>19</sup> all phase shifts used are given in Herndon's thesis.<sup>20</sup>

Fig. 6. Scatter plot of  $\delta'F_{AB}$  vs  $F_{AB}$  used when trying to reject one of two competing local maxima A or B.  $F_{AB}$  is the average log likelihood ratio;  $\delta'F_{AB}$  is its error. More precisely,  $F_{AB} = (1/N) \ln[L(A)/L(B)]$ , and  $\delta'F_{AB}$  is calculated using Eq. (4.25). Key to symbols:

+, competing 18-wave fits to the 9000 Monte-Carlo events of Table V;

X, 60-wave fits to 21,000 real events at 1890 MeV;

dots, 20-wave fits to 10,700 events at 1690 MeV. For comparison, we have also plotted, as symbols with circles, the errors in the  $\ln$ -likelihoods themselves,  $\delta F$ .

Fig. 7. Results of a fit to 7583 Monte Carlo events generated at 1690 MeV to test TRIANGLE/RUMBLE. The small square covers the area where we indeed reconstructed the four smallest waves, but also 13 "noise" waves. So we are insensitive to the area inside the square.

Fig. 8. Waves used in 1973 Solution B. In Solution A waves not used are indicated with an \*, and  $D_{15}$  started later (at  $\sqrt{s} = 1650$  MeV).

- Fig. 9. Solution A fits to the reaction  $\pi^- p \rightarrow \pi^+ \pi^- n$  at a c.m. energy of 1690 MeV. The figure contains  $\cos \theta$  vs  $\phi$  plots for individual regions of the Dalitz plot where  $\cos \theta$  and  $\phi$  are the angles of the incident pion in a coordinate system defined by the final state. The z axis lies along  $\vec{p}_N$  and the y axis lies along  $p_{\pi^-} \times p_{\pi^+}$ . The plots outside the Dalitz plot are the sums of the corresponding plots within the boundary.
- Fig. 10. Solution B cross sections for the fitted channels  $n\pi^-\pi^+$ ,  $p\pi^-\pi^0$ , and  $p\pi^+\pi^0$ . Crosses correspond to our fits; tiny dots with vertical error bars are experimental, from Ref. 38.
- Fig. 11. Solution B cross sections predicted for the channels  $n\pi^0\pi^0$  and  $n\pi^+\pi^+$ . Crosses are predicted from our fits to the other channels of Fig. 10; dots with vertical bars are from Ref. 38.
- Fig. 12. Summary  $N\pi\pi$  Argand plots for Solution A (1972). Nominal resonance energies come from the CERN 1972 EPSA (Ref. 1). For more details see caption to Fig. 14.
- Fig. 13. Summary  $N\pi\pi$  Argand plots for Solution B (1973). Nominal resonance energies come from the Saclay 1973 EPSA (Ref. 2). For more details see caption to Fig. 14.
- Fig. 14(a-e). Argand diagrams and partial-wave cross sections for the elastic and inelastic channels. The elastic solutions are from CERN 1972 (Ref. 1). The inelastic channels are our 1973 solution B.

On the Argand plots the nominal resonance energies come from Saclay 1973 (Ref. 2). Arrowheads are spaced every

20 MeV, with a wider arrowhead at integral hundreds of MeV. Lower- $l$  waves are plotted starting at  $\sqrt{s} = 1400$  MeV, higher- $l$  start where introduced into the fit. Last arrowhead is always at 1940 MeV. To show the gap in our data the straight line joining the five arrows in the gap has been deleted.

The + or - signs at the upper left of each circle show how to transform from our sign conventions to the "Baryon-first" convention. "New" indicates one of the four waves used in solution B only. Nine  $\rho_1$  and  $\epsilon$  signs were changed 5 July 1974.

Facing each inelastic Argand diagram of  $T_\alpha$ , we plot  $|T_\alpha|^2$  vs  $\sqrt{s}$ . Facing the top (elastic) Argand plot, the total  $\sigma_{\text{inelastic}} (\propto 1-\eta^2)$ , derived from EPSA, is compared with the sum of the  $\sigma_{\text{in}}$  from each isobar-model channel plotted below. The small interference terms between channels are taken into account, see Eq. (3.7). Note that  $\sigma$ , as plotted, are labelled by I-spin, not charge, so to get  $\sigma(\pi^- p \rightarrow N\pi\pi)$  one must use  $2/3 \sigma(I=1/2) + 1/3 \sigma(I=3/2)$ .

Fig. C1. Blatt-Weisskopf barriers (Eq. C1) for  $L=1$  through 7, compared with their approximate forms (Eq. C2) for low QR.



# $\pi^-p$ total cross section

$E_{C.M.}$  (GeV)

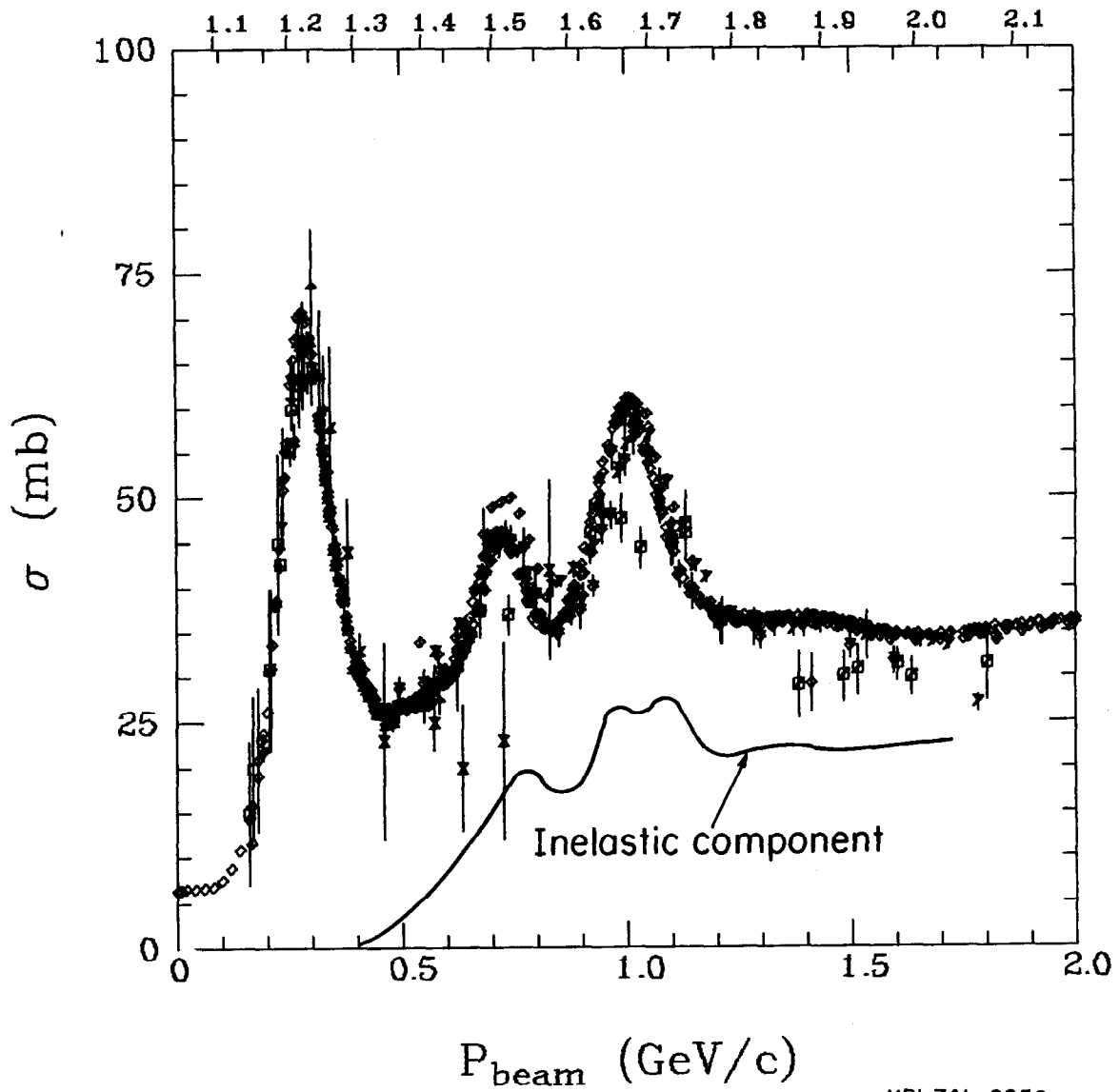
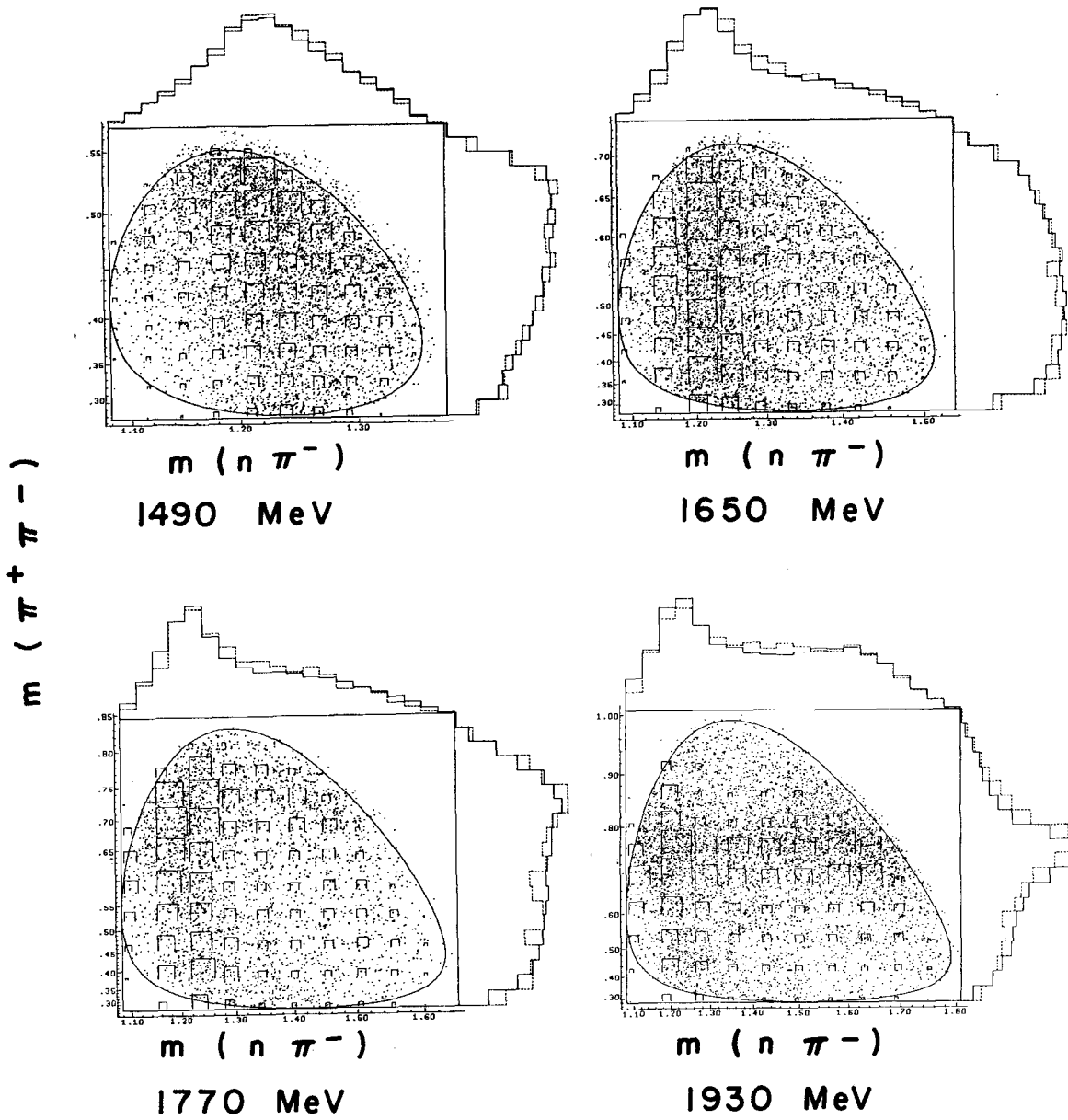
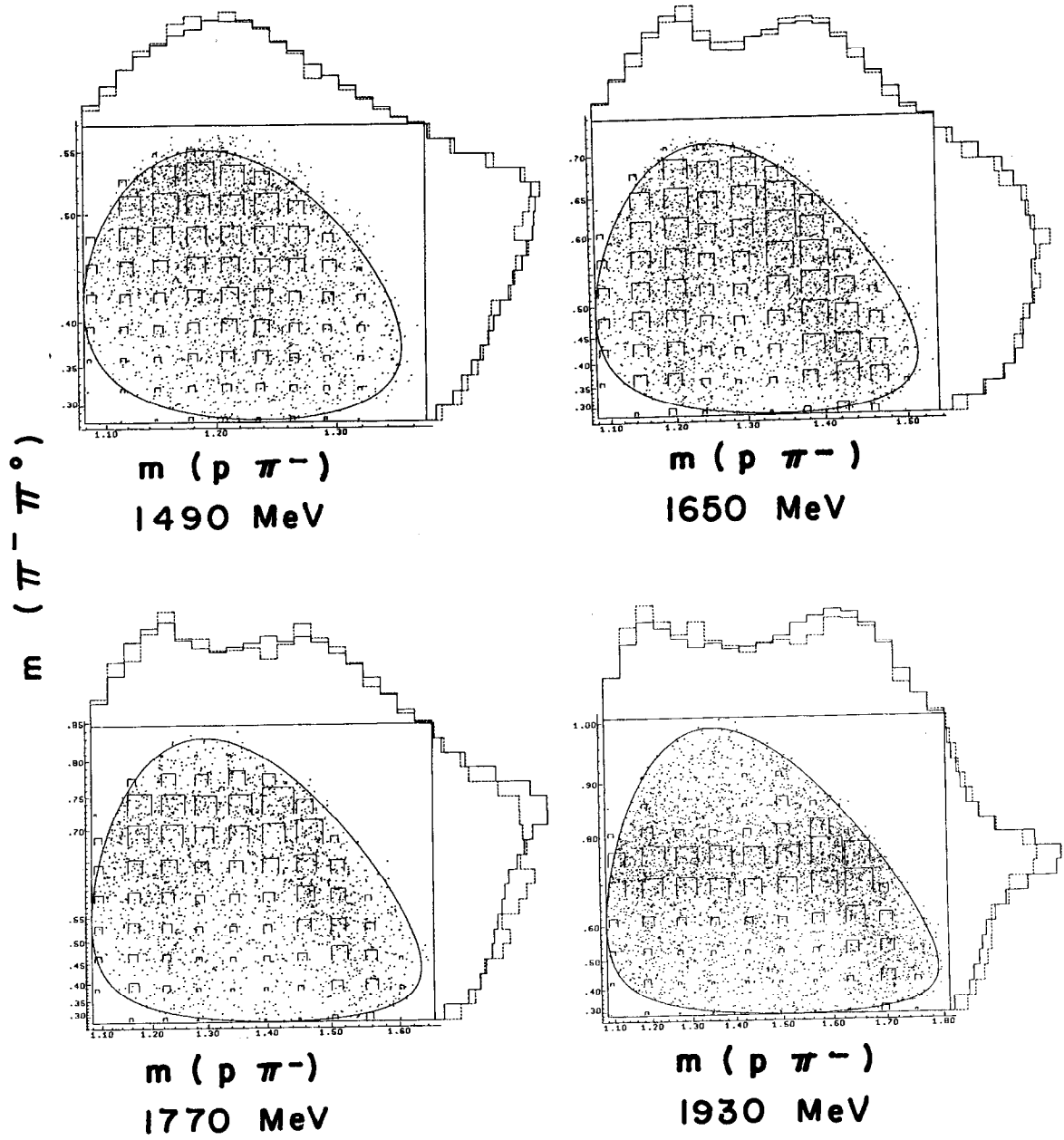


FIG. 1



XBL742-2331

FIG. 2a



XBL742 - 2332

FIG. 2b

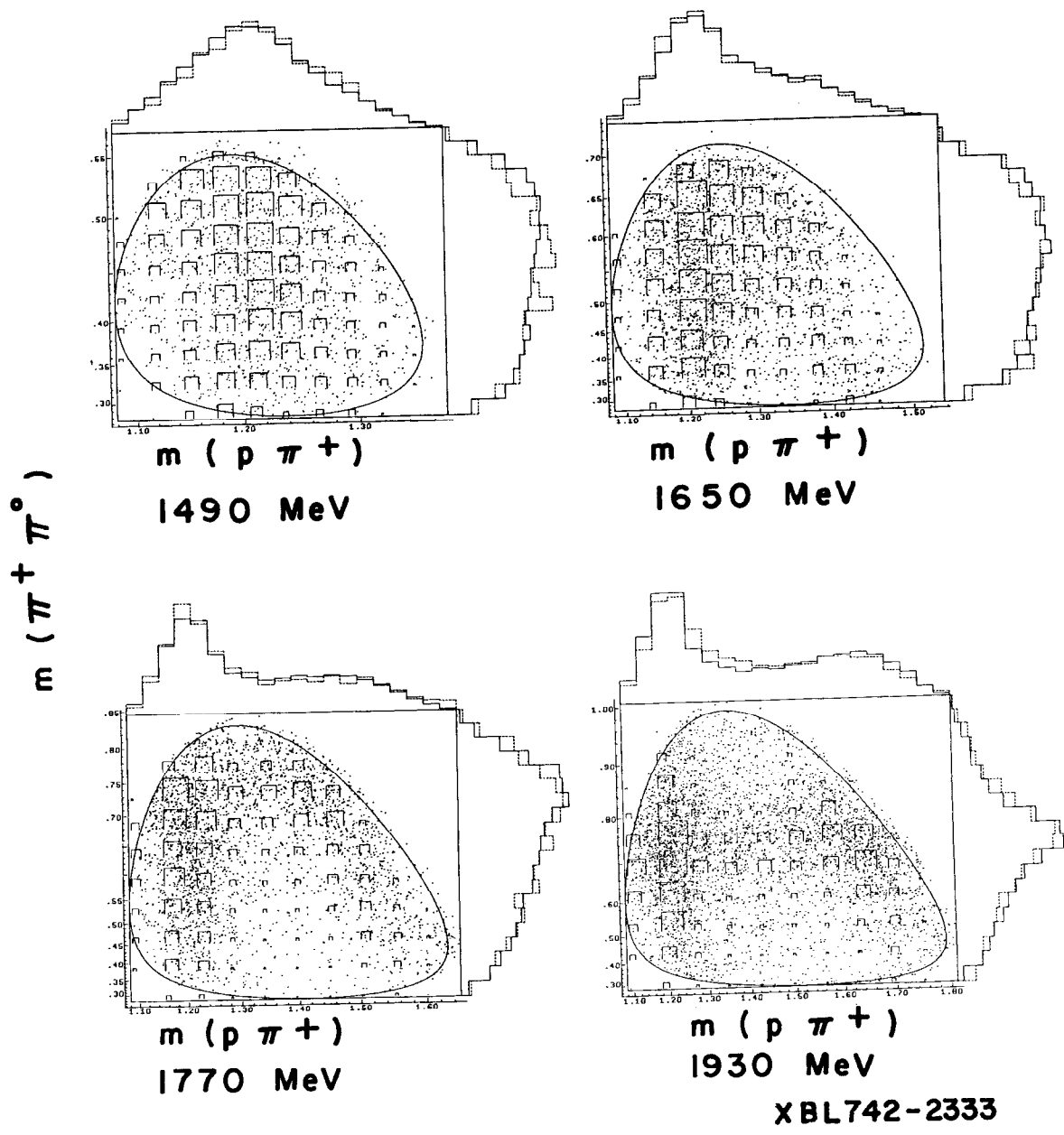
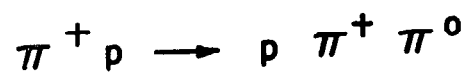
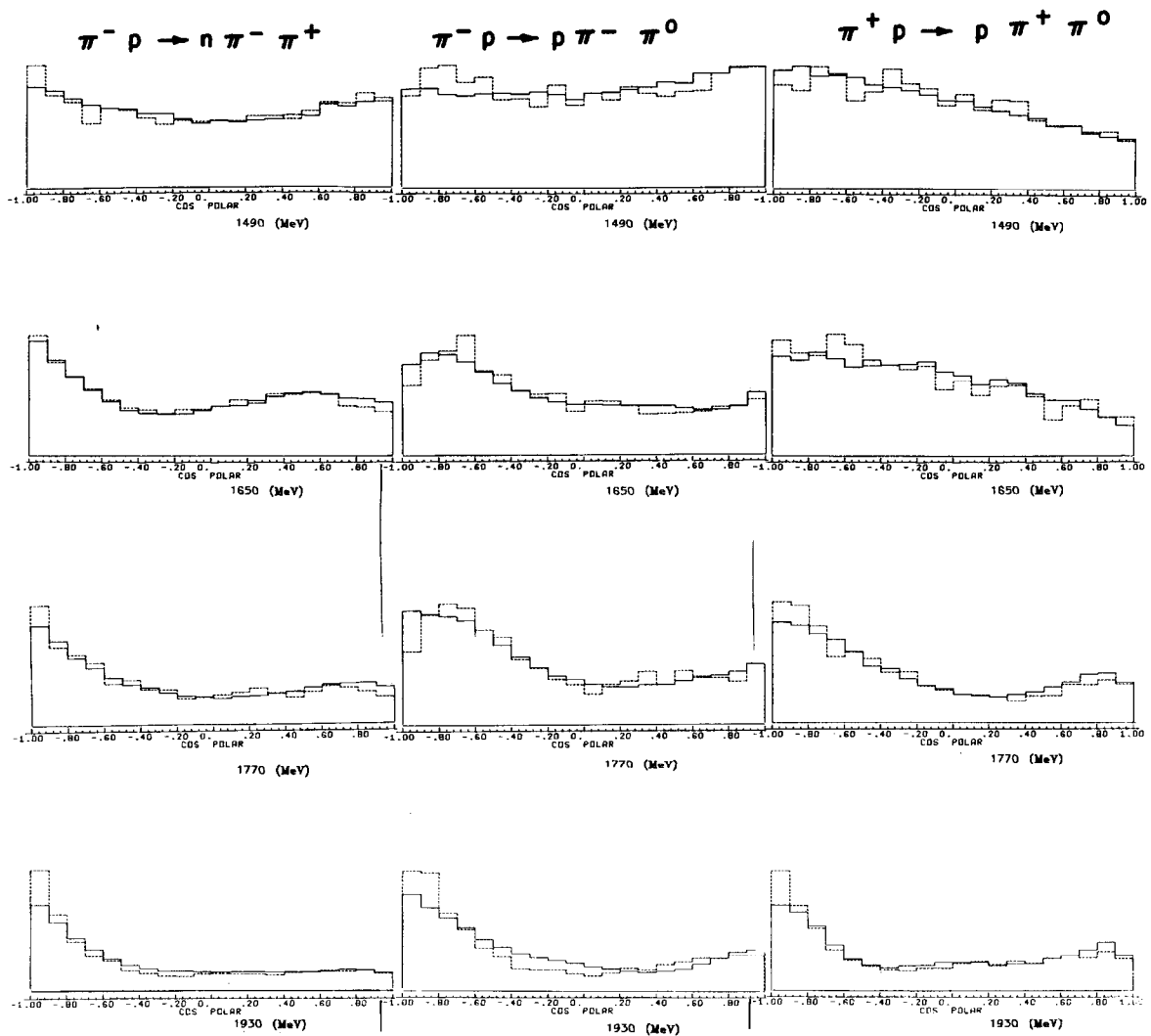


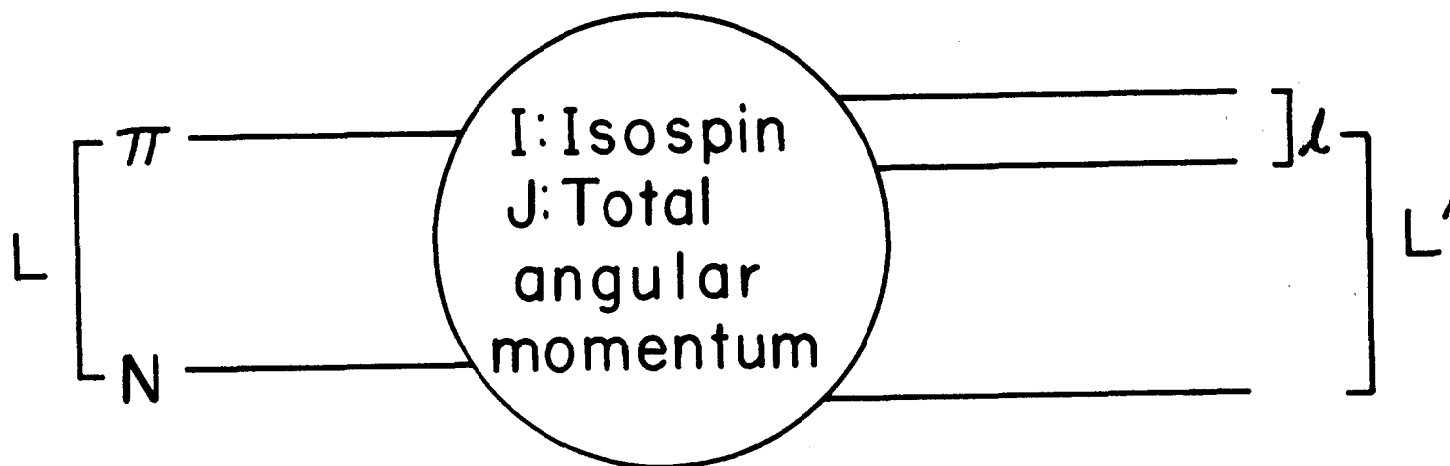
FIG. 2c



XBL742-2335

FIG. 3

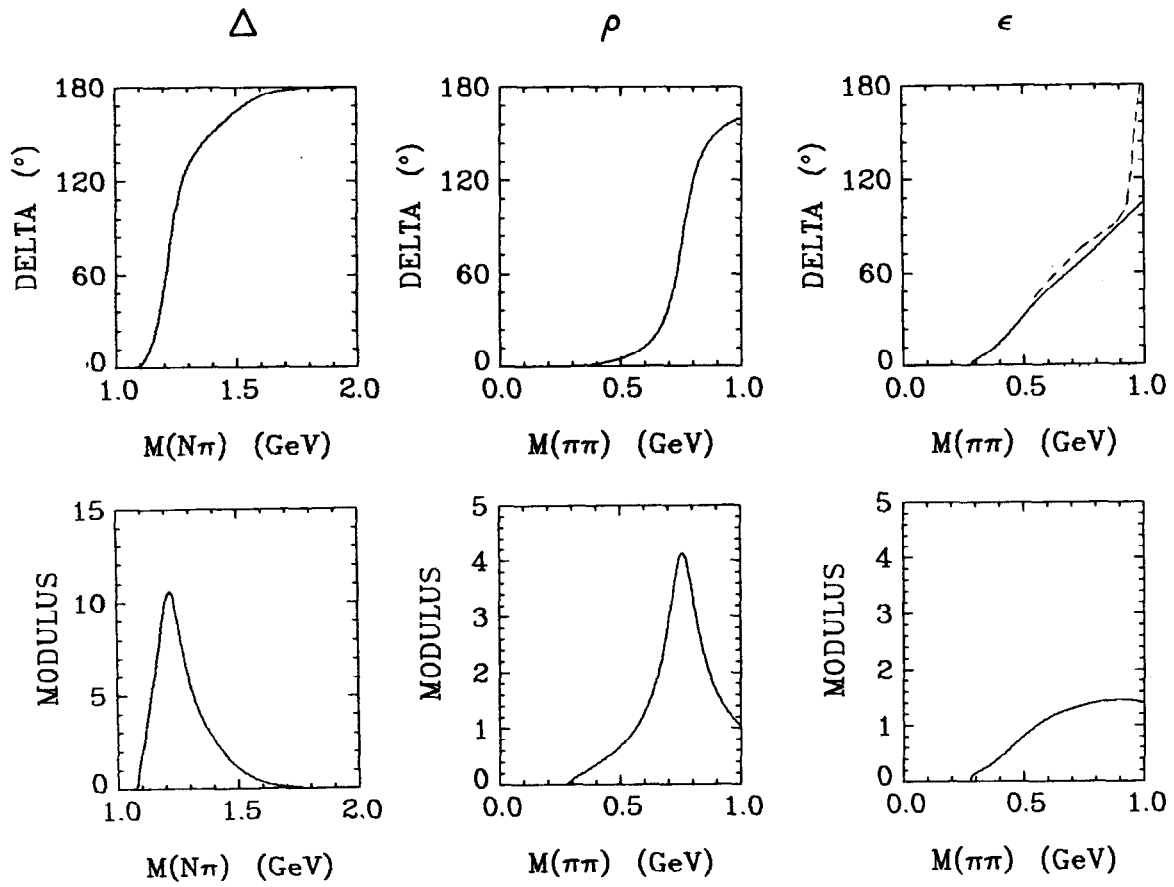
$$F = \Delta\pi, \rho_{\frac{3}{2}} N, \rho_{\frac{1}{2}} N, \text{ or } \epsilon N.$$



Notation for wave  $\alpha$ :  $F, LL' IJ$

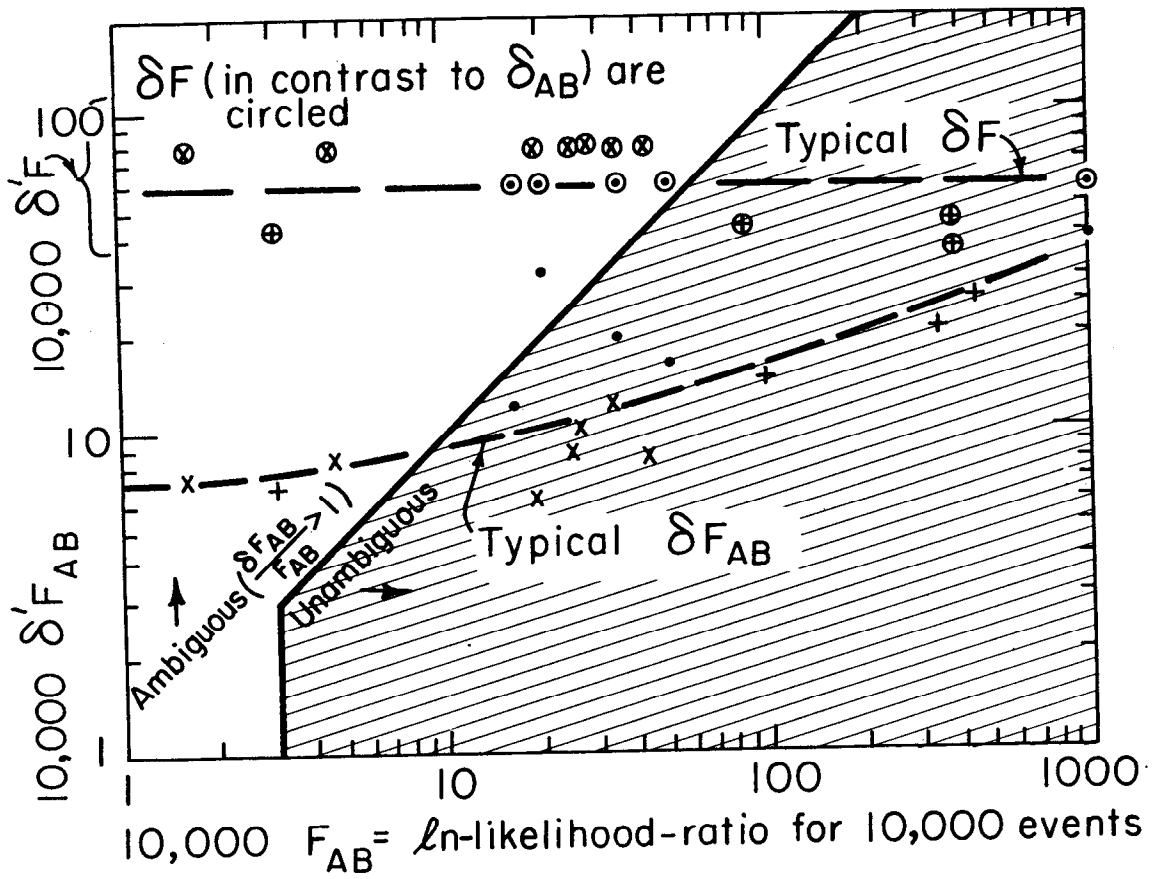
XBL 741-2301

FIG. 4



XBL 742-354

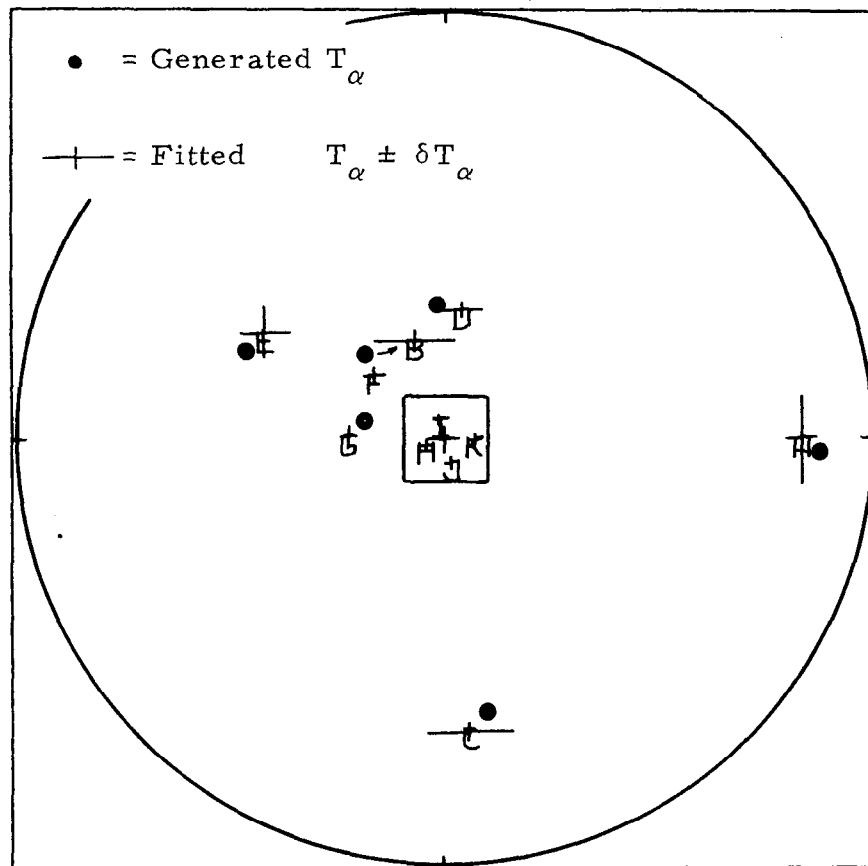
FIG. 5



XBL745-3270

FIG. 6





FITTED AMPLITUDES

XBL 726-934

FIG. 7

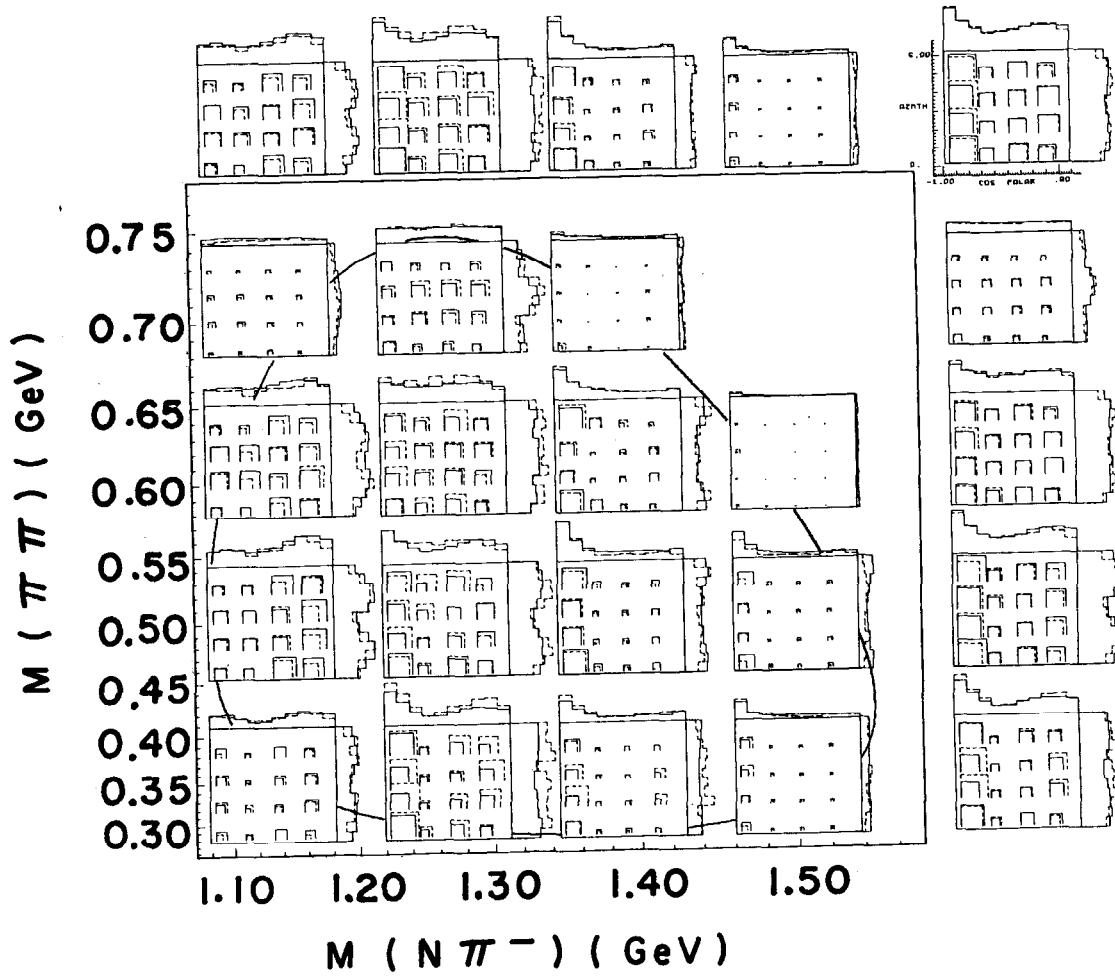
<u>Isospin 1/2</u>	Count of waves $\sqrt{S}$ (MeV)	<u>Isospin 3/2</u>
		FF37( $\rho_{3/2}N$ )
* FF15( $\Delta\pi$ )	1770(28)	FF37( $\Delta\pi$ )
FD15( $\epsilon N$ )		FP35( $\rho_{3/2}N$ )
FP15( $\rho_{3/2}N$ )	1730(27)	FF35( $\Delta\pi$ )
FP15( $\Delta\pi$ )		
*SD11( $\Delta\pi$ )	1650(24)	DS33( $\rho_{3/2}N$ )
		PP33( $\Delta\pi$ )
PP13( $\rho_{1/2}N$ )	1520(18)	*DD33( $\Delta\pi$ )
DD15( $\Delta\pi$ )	1490(16)	SD31( $\Delta\pi$ )
SS11( $\rho_{1/2}N$ )	1440(13)	SS31( $\rho_{1/2}N$ )
	1310(11)	
*SP11( $\epsilon N$ ), PP11( $\Delta\pi$ ) PP11( $\rho_{1/2}N$ ), PS11( $\epsilon N$ ) DS13( $\rho_{3/2}N$ ), DS13( $\Delta\pi$ ) DP( $\epsilon N$ ), DD13( $\Delta\pi$ )		PP31( $\Delta\pi$ ), PP31( $\rho_{1/2}N$ ) DS33( $\Delta\pi$ )

XBL741-2141A

FIG. 8

▤ Data

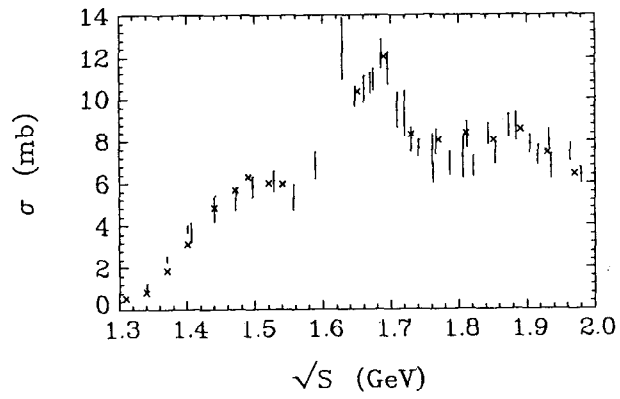
▣ Predicted



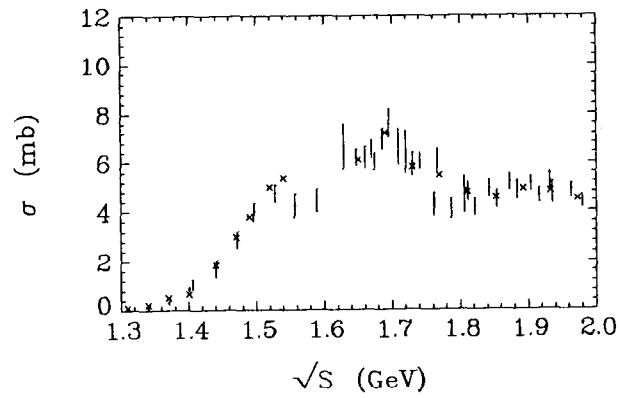
XBL742-2334

FIG. 9

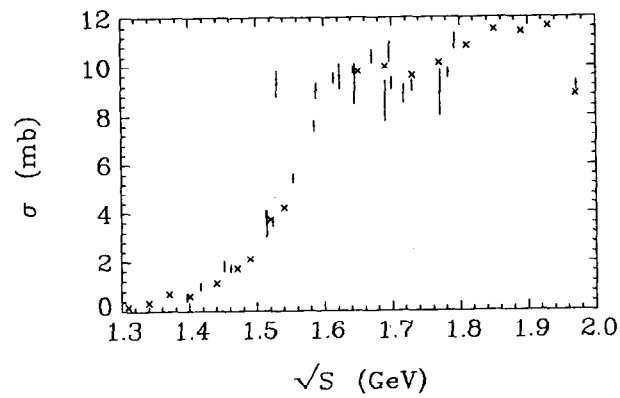
$\pi^-p \rightarrow n\pi^-\pi^+$  CROSS-SECTION



$\pi^-p \rightarrow p\pi^-\pi^0$  CROSS-SECTION

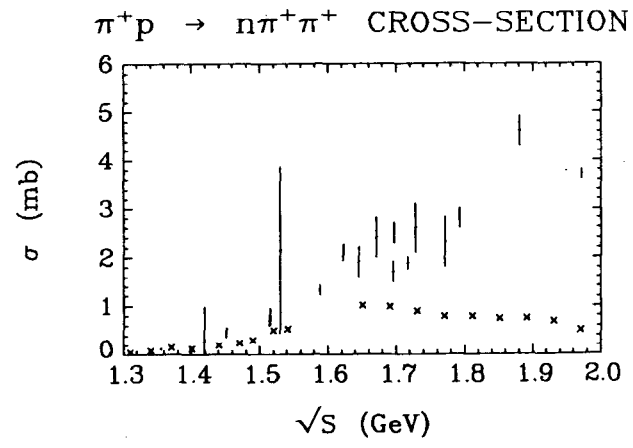
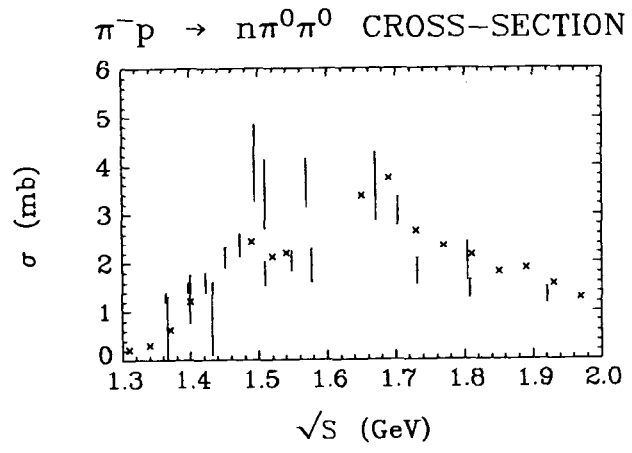


$\pi^+p \rightarrow p\pi^+\pi^0$  CROSS-SECTION



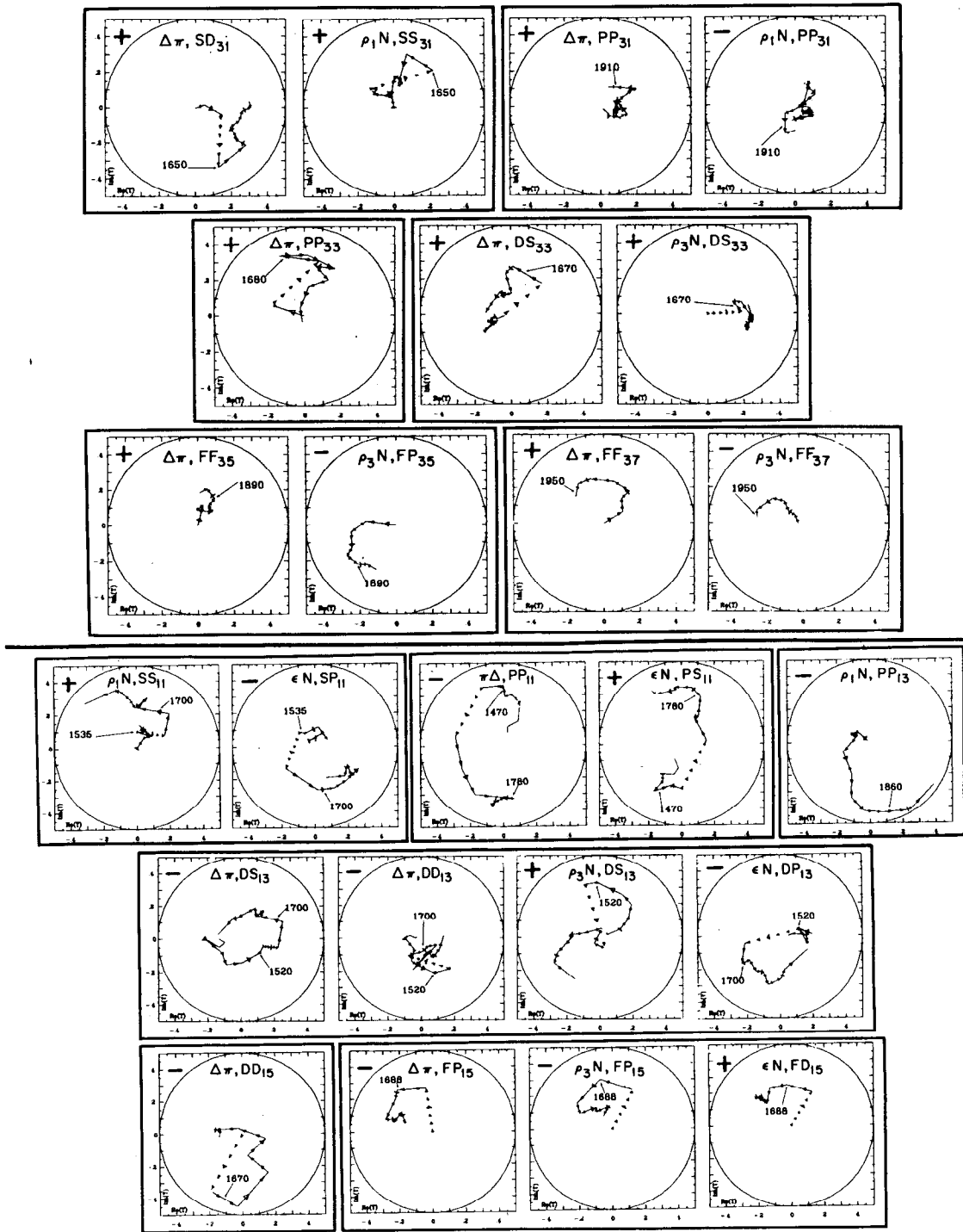
XBL 741-2080

FIG. 10



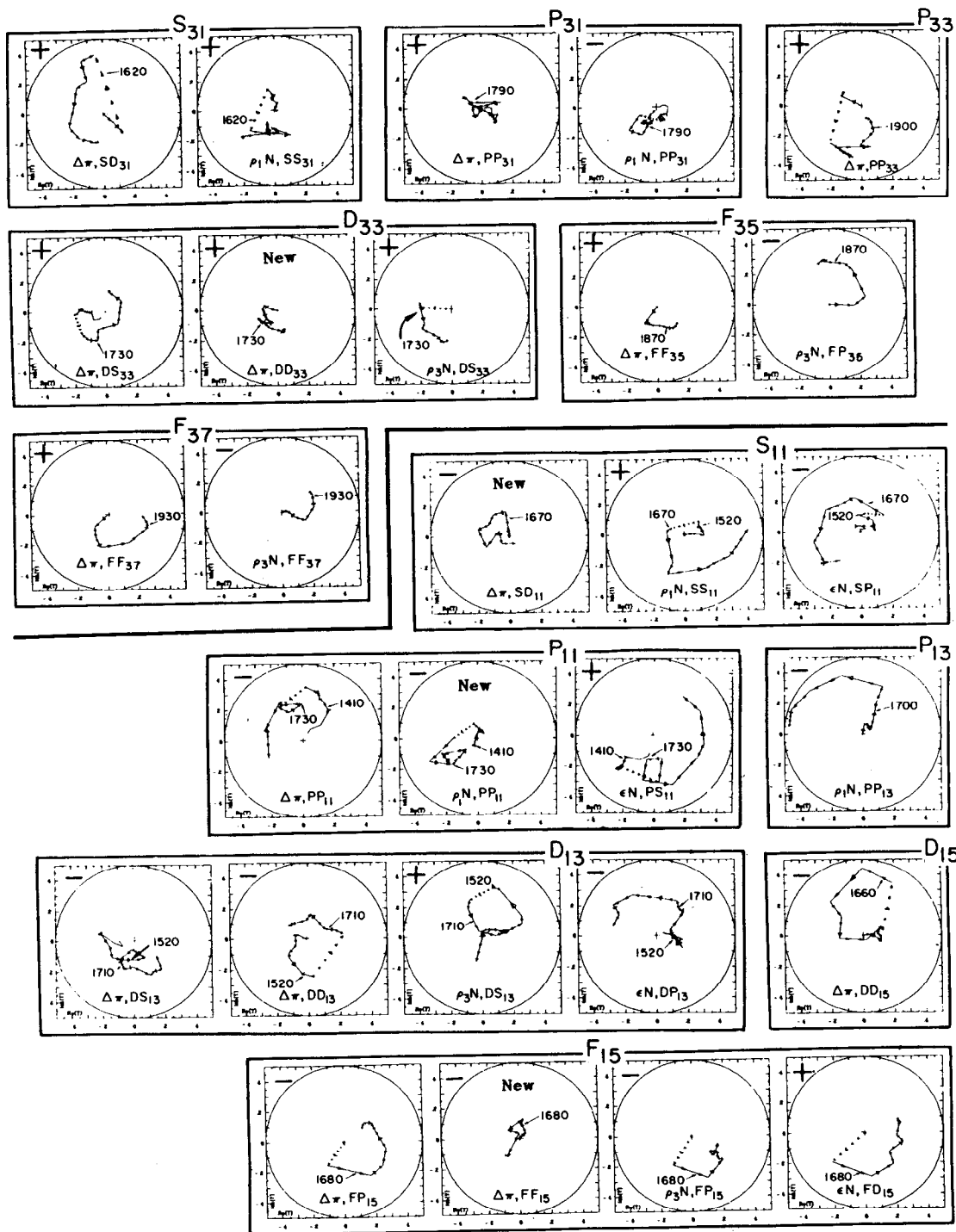
XBL 741-2079

FIG. 11



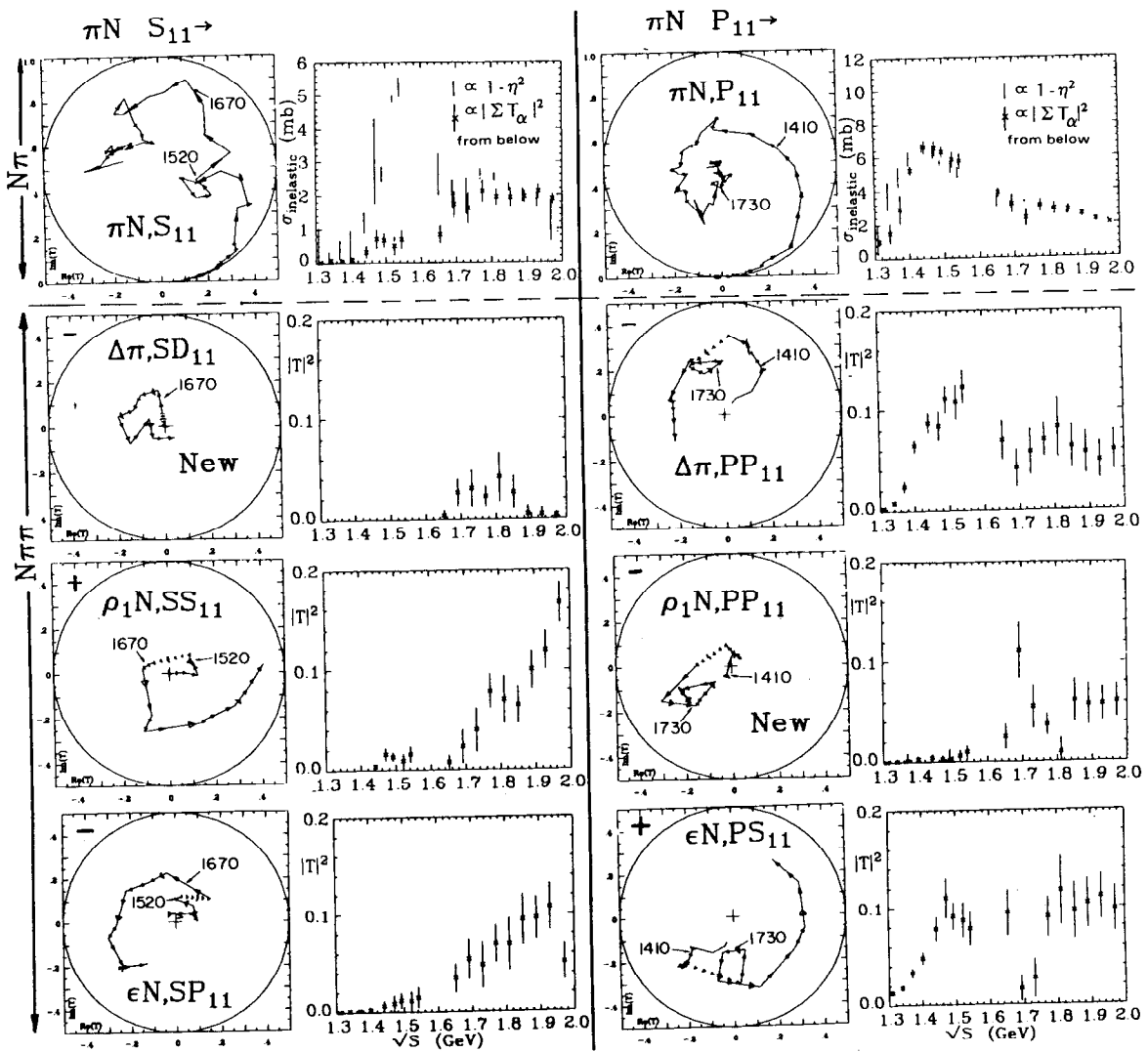
XBL 745-778A

FIG. 12



XBL 745-777A

FIG. 13



XBL 745-944 A

FIG. 14a



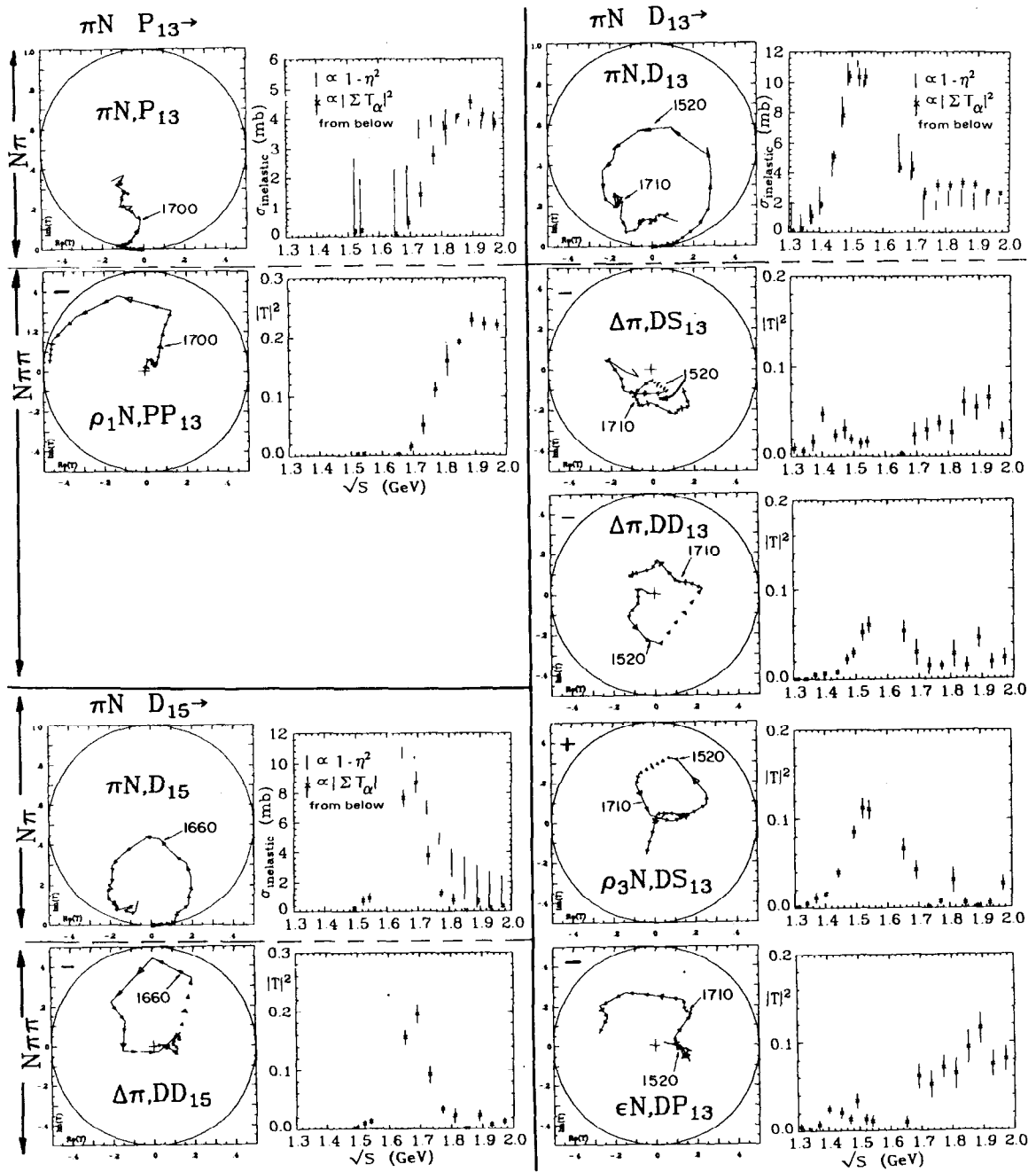
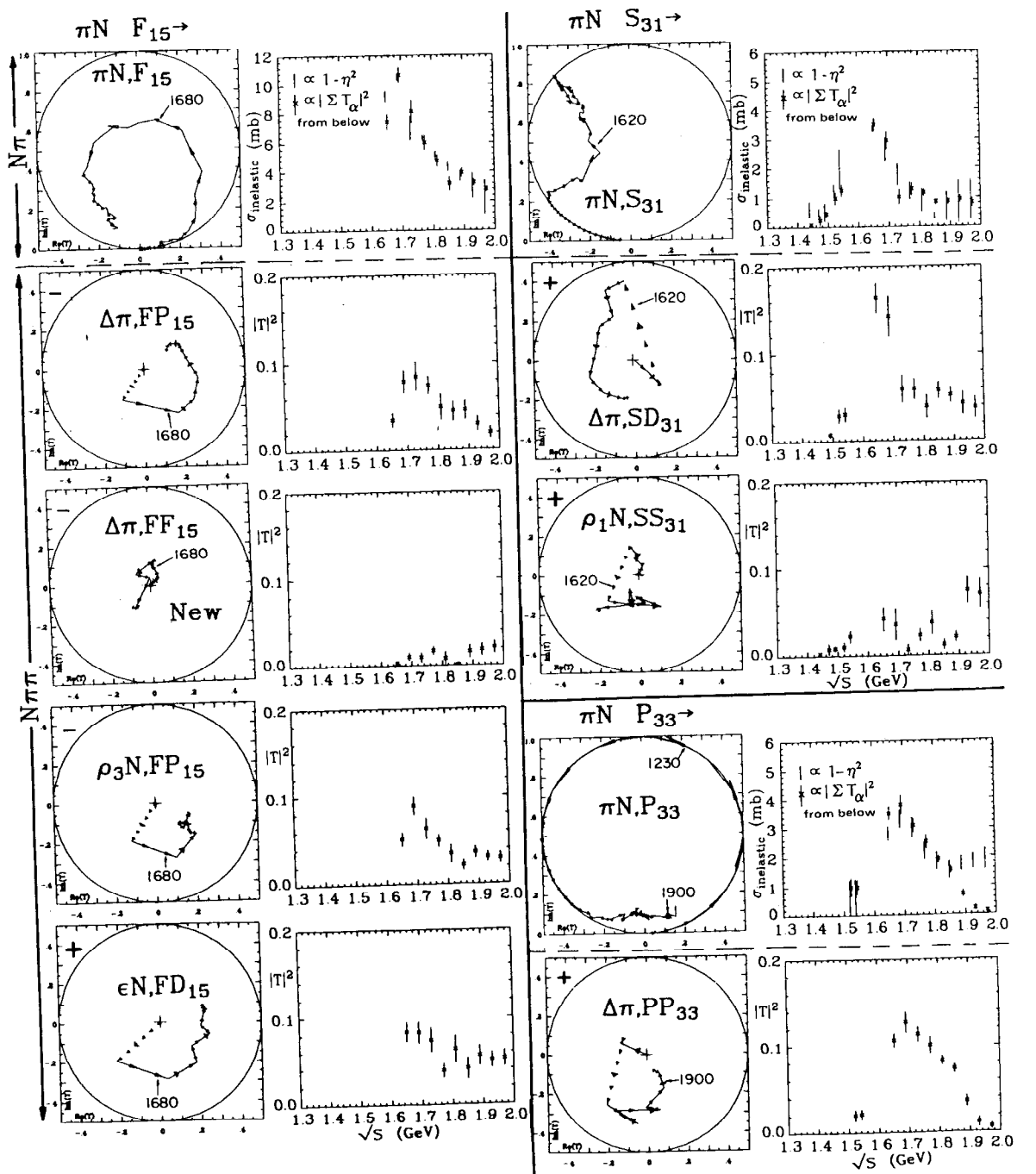
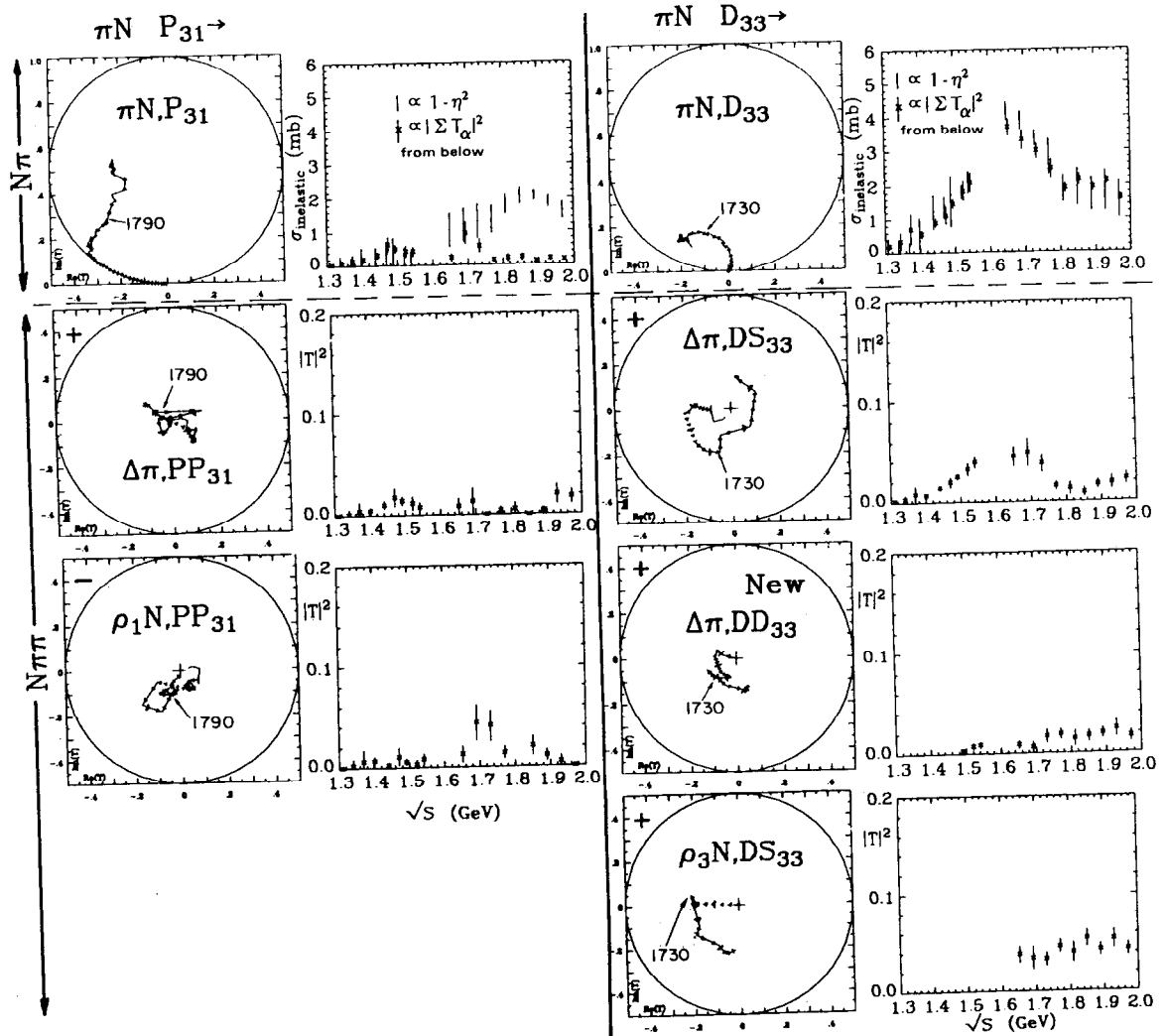


FIG. 14b



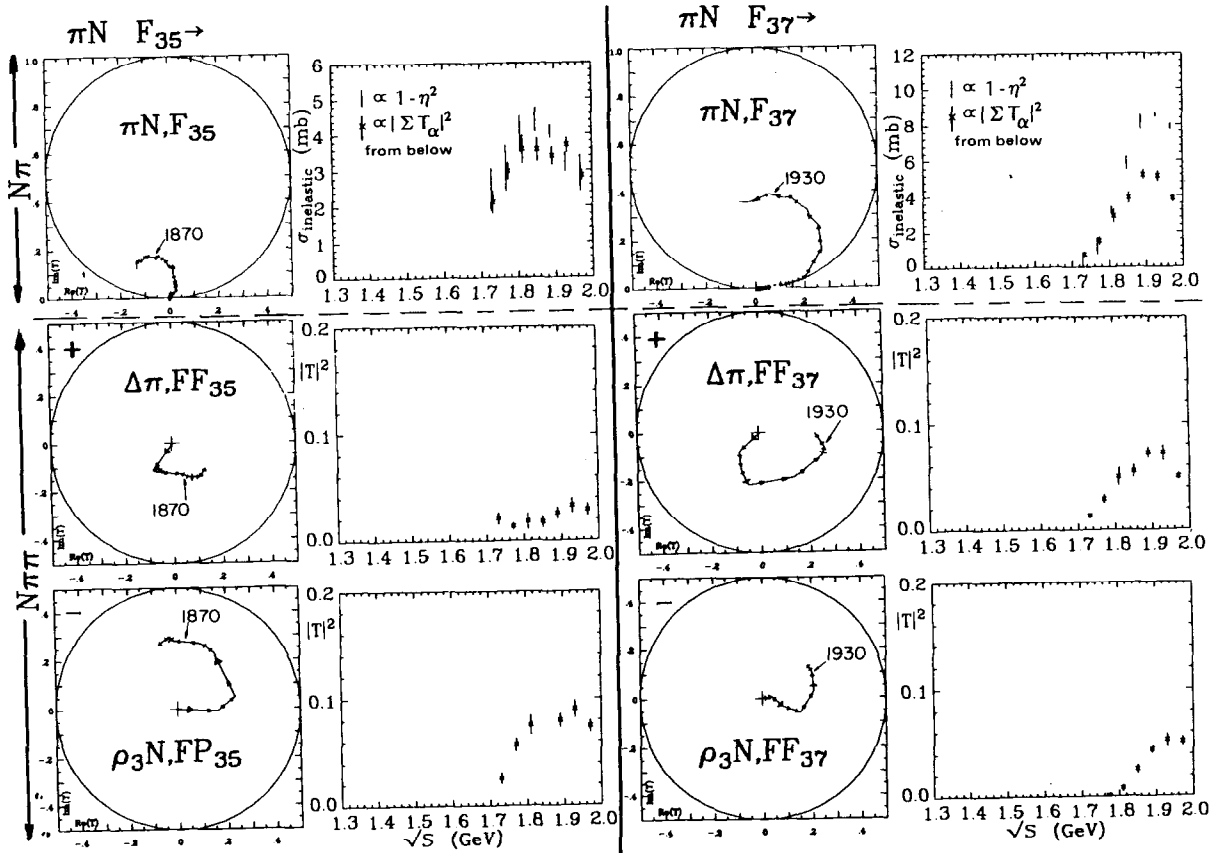
XBL 745-942 A

FIG. 14c



XBL 745-943A

FIG. 14d



XBL 745-945

FIG. 14e

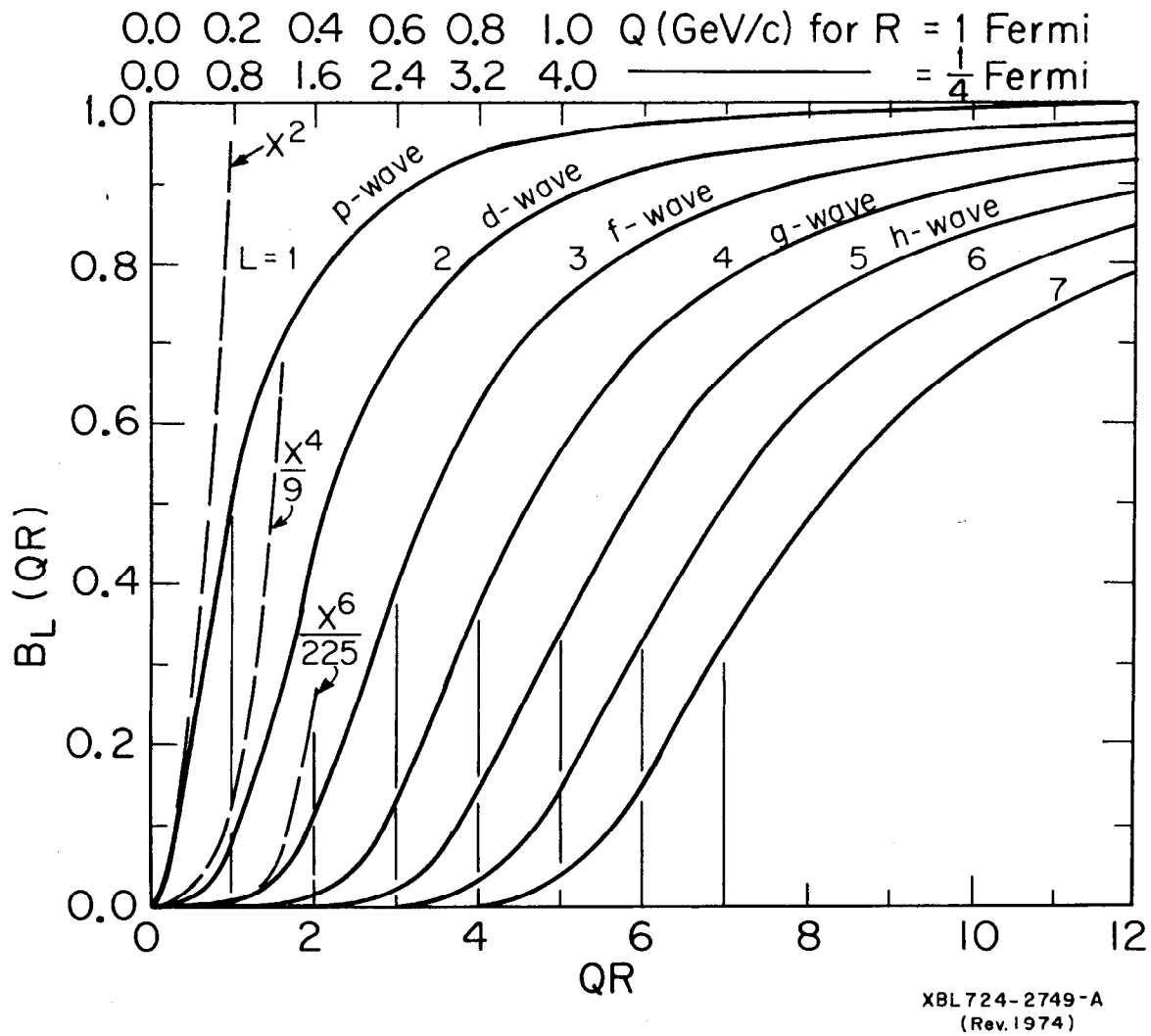


FIG. C1

Tables of Partial Wave Amplitudes\*

D. J. Herndon,<sup>†</sup> R. Longacre,<sup>††</sup> L. R. Miller,  
A. H. Rosenfeld, G. Smadja,<sup>††</sup> and P. Söding<sup>‡</sup>  
Lawrence Berkeley Laboratory, University of California  
Berkeley, California 94720

R. J. Cashmore<sup>§</sup> and D.W.S.G. Leith  
Stanford Linear Accelerator Center, Stanford University  
Stanford, California 94305

October 1974

CONTENTS

I.	Listing of Argand Amplitudes from Punched Cards . . . . .	2
II.	Solution at Four Energies: (Computer Printout) <u>1490</u> , <u>1520</u> , <u>1690</u> , and <u>1890</u> MeV . . .	10
	A. Amplitudes and Errors . . . . .	11 15 19 24
	B. Small Error Matrix ( $\leq 28 \times \leq 28$ ) . . . . .	11 15 20 25
	C. $60 \times 60$ Error Matrix . . . . .	13 17 22 27
III.	Documentations of Data Tapes of 160,000 $N\pi\pi$ . . . . .	33

---

\* Work supported by the U. S. Atomic Energy Commission.

<sup>†</sup> Present address, Lawrence Livermore Laboratory, Livermore, California 94550.

<sup>††</sup> Present address, CEN, Saclay, (France).

<sup>‡</sup> Present address, DESY, Notkestieg 1, 2000 Hamburg-52.

<sup>§</sup> Present address, Nuclear Physics Laboratory, Oxford, OX1-3RH.

## INTRODUCTION

A deck of 367 punched cards and a library of 16 magnetic tapes are both available to supplement Herndon et al., LBL-1065 Rev. This printed supplement documents those cards and tapes and also reproduces some computer printout of partial wave amplitudes at four representative energies.

### Convention on Scaling Errors

We quote here a paragraph from Section IV.E of the main text:

"An error hyperellipsoid may be defined by a hypersurface in  $\vec{A}$  space labelled by  $\Delta\chi^2 = 1$ , i. e. by  $L = L^{\max} e^{-1/2}$ . To plot error ellipses on our Argand plots we project this hypersurface on the complex plane representing a single  $T_\alpha$ . However, the probability that a result will be within this ellipse is only 40%. In order to increase this probability we have conservatively doubled our estimated error, thereby raising the  $\chi^2$  contour to 4, and enclosing 87% of the probability.<sup>11</sup> In summary, all the errors plotted or tabulated in this paper and in our previous publications<sup>11,20,22</sup> are twice those calculated by the program RUMBLE,<sup>11</sup> which uses Eq. (4.23)."

Accordingly, the cards with the data on amplitudes and errors (Sect. I of this Supplement) are not the original cards punched by RUMBLE, but have had their errors expanded by two. On the other hand the reproductions of RUMBLE printout in Section II of this Supplement have their errors unscaled.

## I. ARGAND AMPLITUDES ON PUNCHED CARDS

We have prepared a deck of 367 punched cards, which is available from A. H. Rosenfeld on the Particle Data Group at LBL or M. Neveu, Saclay. The cards are listed below, and there should be enough comment cards that they can be understood with only the following remarks:

At each energy there are listed 28 waves (complex numbers occupying two words, i. e. two columns of printout); but of course at the lower energies some of these amplitudes are written as 0,0.

To read the data cards use the following formats:

Amplitude cards: 8F10.5

Error Matrix cards: 9F8.X [They were written 3(2F8.5, F8.2).]

The phases of the Argand amplitudes have been rotated by a K-matrix fit and correspond to our published Argand plots (Fig. 13 of the document of which this is a supplement) or Fig. 2 of Rosenfeld et al., LBL-2633 submitted to Phys. Rev. Letters.



\* ARGAND PLOT AMPLITUDES GIVEN AS T-REAL AND T-IMAG.. ERRORS ARE GIVEN AS  
 \* ERROR T-REAL, ERROR T-IMAG. AND CORR. ANGLE. IF A WAVE WAS NOT USED IN FIT  
 \* AT A GIVEN ENERGY, T AND ERROR ARE PRINTED ZERO. LIST OF ORDER OF WAVES AS  
 \* FOLLOWS.  
 \* DELTA - PP11,SD11,OS13,OO13,FP15,OO15,FF15,PP31,SO31,OS33,PP33,OO33,FF35,FF37  
 \* RHO 3/2 - OS13,FP15,OS33,FP35,FF37  
 \* RHO 1/2 - SS11,PP11,PP13,SS31,PP31  
 \* EPSILON - PS11,SP11,OP13,FD15

● ARGAND PLOT 1970		SAMPLE		DELTA				
-.21661	-.11124	.04326	-.04658	.14334	-.09130	-.12584	.09006	
.11377	.08405	.11645	-.00765	-.09652	-.10779	-.11538	.06531	
-.03288	-.19034	.02910	.14647	.02030	-.07872	.04677	-.11954	
				I----- RHO 3/2 -----				
.13066	-.10624	.22412	-.00474	I -.03911	-.16026	.15576	-.06952	
----- RHO 3/2 -----				I----- RHO 1/2 -----				
-.02147	-.20708	-.07883	.26012	.18138	.13496	I .40659	.03748	
----- RHO 1/2 -----				I-----				
-.22656	-.09667	-.46791	.04626	-.19741	-.17905	-.00442	-.01767	
		----- EPSILON -----						
.18003	.25602	-.12859	-.18639	-.27740	.06450	.20785	.09370	
* ERRORS 1970		SAMPLE		DELTA				
.04030	.04409	60.93	.04265	.04389	64.36	.02687	.02957	58.78
.02908	.03090	58.43	.02518	.02171	96.69	.03088	.02310	-51.09
.02813	.02363	93.49	.02704	.02755	-68.98	.03139	.03116	109.99
.01886	.02023	-105.73	.01597	.02261	51.92	.02229	.01966	-53.96
				I----- RHO 3/2 -----				
.01509	.01990	48.50	.01208	.01742	56.80	I .02651	.02460	100.43
----- RHO 3/2 -----				I-----				
.01713	.02539	54.91	.01927	.01695	-116.88	.01114	.01650	-100.28
				I----- RHO 1/2 -----				
.01195	.01000	106.92	I .02979	.03062	66.76	.04338	.03353	79.75
----- RHO 1/2 -----				I-----				
.01184	.02013	58.26	.03440	.02617	-126.36	.03138	.02758	-120.73
		----- EPSILON -----						
.03746	.03846	114.85	.04290	.03956	102.71	.02416	.02866	51.84
.02258	.02021	87.36						

Sample

● ARGAND PLOT 1310		SAMPLE		DELTA				
.03015	.04695	0.00000	0.00000	-.09601	.00520	-.02225	.00644	
0.00000	0.00000	0.00000	0.00000	0.00000	0.00000	.02221	.00701	
0.00000	0.00000	-.02694	-.03345	0.00000	0.00000	0.00000	0.00000	
0.00000	0.00000	0.00000	0.00000	.03028	.01847	0.00000	0.00000	
0.00000	0.00000	0.00000	0.00000	0.00000	0.00000	0.00000	0.00000	
-.00394	.01144	0.00000	0.00000	0.00000	0.00000	.02975	.01061	
-.02718	-.11173	-.00414	.01668	.06801	.00708	0.00000	0.00000	
* ERRORS 1310		SAMPLE		DELTA				
.02829	.00859	90.82	0.00000	0.00000	-90.00	.01867	.02292	119.75
.00980	.01048	116.00	0.00000	0.00000	-90.00	0.00000	0.00000	-90.00
0.00000	0.00000	-90.00	.02980	.02428	99.10	0.00000	0.00000	-90.00
.01863	.00978	96.71	0.00000	0.00000	-90.00	0.00000	0.00000	-90.00
0.00000	0.00000	-90.00	0.00000	0.00000	-90.00	.01433	.01583	118.22
0.00000	0.00000	-90.00	0.00000	0.00000	-90.00	0.00000	0.00000	-90.00
0.00000	0.00000	-90.00	0.00000	0.00000	-90.00	.01756	.01310	103.36
0.00000	0.00000	-90.00	0.00000	0.00000	-90.00	.02058	.02317	115.72
.01896	.01145	104.68	.02428	.01681	-126.25	.02854	.01631	-132.16
0.00000	0.00000	-90.00						

● ARGAND PLOT 1340		SAMPLE		DELTA				
.04814	.07498	0.00000	0.00000	-.06789	-.03484	-.01987	.00218	
0.00000	0.00000	0.00000	0.00000	0.00000	0.00000	.03581	.01135	
0.00000	0.00000	-.03753	-.04661	0.00000	0.00000	0.00000	0.00000	

0.00000	0.00000	0.00000	0.00000	.05376	.04320	0.00000	0.00000	
0.00000	0.00000	0.00000	0.00000	0.00000	0.00000	0.00000	0.00000	
-.00879	.02573	0.00000	0.00000	0.00000	0.00000	.04499	.01603	
-.03713	-.12982	.03122	.02345	.03733	.01964	0.00000	0.00000	
* ERRORS	1340							
.05600	.01176	88.85	0.00000	0.00000	-90.00	.04254	.03140	78.43
.01984	.01141	92.66	0.00000	0.00000	-90.00	0.00000	0.00000	-90.00
0.00000	0.00000	-90.00	.04719	.04501	88.20	0.00000	0.00000	-90.00
.03581	.03110	84.53	0.00000	0.00000	-90.00	0.00000	0.00000	-90.00
0.00000	0.00000	-90.00	0.00000	0.00000	-90.00	.03378	.02335	83.34
0.00000	0.00000	-90.00	0.00000	0.00000	-90.00	0.00000	0.00000	-90.00
0.00000	0.00000	-90.00	0.00000	0.00000	-90.00	.03269	.04478	122.10
0.00000	0.00000	-90.00	0.00000	0.00000	-90.00	.05064	.03272	-126.25
.01934	.01189	105.49	.02212	.01430	78.80	.03274	.02433	80.56
0.00000	0.00000	-90.00						
ARGAND PLOT	1370							
.11675	.10240	0.00000	0.00000	-.12585	-.01075	-.06735	.02978	
0.00000	0.00000	0.00000	0.00000	0.00000	0.00000	.06580	.00171	
0.00000	0.00000	-.07599	-.05348	0.00000	0.00000	0.00000	0.00000	
0.00000	0.00000	0.00000	0.00000	.10188	.04293	0.00000	0.00000	
0.00000	0.00000	0.00000	0.00000	0.00000	0.00000	0.00000	0.00000	
-.00378	.03539	0.00000	0.00000	0.00000	0.00000	.07933	.00494	
-.08927	-.15983	-.00034	.04627	.08640	.00249	0.00000	0.00000	
* ERRORS	1370							
.06545	.01766	87.74	0.00000	0.00000	-90.00	.04115	.03835	71.00
.02388	.02412	-67.93	0.00000	0.00000	-90.00	0.00000	0.00000	-90.00
0.00000	0.00000	-90.00	.05662	.05617	74.68	0.00000	0.00000	-90.00
.04379	.04265	68.60	0.00000	0.00000	-90.00	0.00000	0.00000	-90.00
0.00000	0.00000	-90.00	0.00000	0.00000	-90.00	.04042	.02929	75.21
0.00000	0.00000	-90.00	0.00000	0.00000	-90.00	0.00000	0.00000	-90.00
0.00000	0.00000	-90.00	0.00000	0.00000	-90.00	.05521	.10430	-92.40
0.00000	0.00000	-90.00	0.00000	0.00000	-90.00	.04275	.07779	-98.92
.02052	.01581	108.55	.02817	.02042	-122.80	.03076	.03109	66.79
0.00000	0.00000	-90.00						
ARGAND PLOT	1400							
.16803	.19127	0.00000	0.00000	-.21239	.05294	-.08066	.02561	
0.00000	0.00000	0.00000	0.00000	0.00000	0.00000	.05998	-.03885	
0.00000	0.00000	-.08730	-.00104	0.00000	0.00000	0.00000	0.00000	
0.00000	0.00000	0.00000	0.00000	.12532	.02780	0.00000	0.00000	
0.00000	0.00000	0.00000	0.00000	0.00000	0.00000	0.00000	0.00000	
-.02488	.04835	0.00000	0.00000	0.00000	0.00000	.07165	-.04284	
-.17621	-.13271	-.03391	.03791	.15651	-.02063	0.00000	0.00000	
* ERRORS	1400							
.03494	.01198	91.70	0.00000	0.00000	-90.00	.01979	.01719	72.54
.01185	.01473	59.47	0.00000	0.00000	-90.00	0.00000	0.00000	-90.00
0.00000	0.00000	-90.00	.02135	.02368	-75.24	0.00000	0.00000	-90.00
.00920	.01284	56.59	0.00000	0.00000	-90.00	0.00000	0.00000	-90.00
0.00000	0.00000	-90.00	0.00000	0.00000	-90.00	.01028	.01455	52.98
0.00000	0.00000	-90.00	0.00000	0.00000	-90.00	0.00000	0.00000	-90.00
0.00000	0.00000	-90.00	0.00000	0.00000	-90.00	.01520	.01532	113.02
0.00000	0.00000	-90.00	0.00000	0.00000	-90.00	.02343	.01906	95.06
.02682	.01437	82.74	.02191	.01847	-130.25	.01351	.01302	106.31
0.00000	0.00000	-90.00						
ARGAND PLOT	1440							
.12099	.27036	0.00000	0.00000	-.14913	-.04019	-.07995	-.04157	
0.00000	0.00000	0.00000	0.00000	0.00000	0.00000	.07776	-.06811	
0.00000	0.00000	-.11996	.00197	0.00000	0.00000	0.00000	0.00000	
0.00000	0.00000	0.00000	0.00000	.19352	.05078	0.00000	0.00000	
0.00000	0.00000	0.00000	0.00000	0.00000	0.00000	.06260	.00376	
.00722	.06557	0.00000	0.00000	.01747	.04981	.03192	-.04398	
-.20080	-.19531	.06947	.03968	.13159	-.06141	0.00000	0.00000	
* ERRORS	1440							

.04755	.01658	88.53	0.00000	0.00000	-90.00	.02828	.01704	85.12
.01845	.01326	75.10	0.00000	0.00000	-90.00	0.00000	0.00000	-90.00
0.00000	0.00000	-90.00	.01961	.02436	-92.38	0.00000	0.00000	-90.00
.01194	.01135	-66.39	0.00000	0.00000	-90.00	0.00000	0.00000	-90.00
0.00000	0.00000	-90.00	0.00000	0.00000	-90.00	.01790	.01270	-53.91
0.00000	0.00000	-90.00	0.00000	0.00000	-90.00	0.00000	0.00000	-90.00
0.00000	0.00000	-90.00	.02884	.01752	-51.05	.01876	.02624	48.75
0.00000	0.00000	-90.00	.02378	.01606	95.01	.02062	.02198	-85.09
.03354	.02391	75.33	.03115	.02890	-125.02	.01523	.02336	50.31
0.00000	0.00000	-90.00						
* ARGAND PLOT 1470								
.10548	.27132	0.00000	0.00000		-.13970	-.10738	-.12227	-.09012
0.00000	0.00000	0.00000	0.00000		0.00000	0.00000	.09890	-.09113
0.00000	0.00000	-.14055	.01022		0.00000	0.00000	0.00000	0.00000
0.00000	0.00000	0.00000	0.00000		.25687	.08725	0.00000	0.00000
0.00000	0.00000	0.00000	0.00000		0.00000	0.00000	.12594	-.01055
.03872	.03999	0.00000	0.00000		-.02673	.08635	.05863	-.08846
-.25013	-.21894	.09611	.00351		.11715	.00273	0.00000	0.00000
* ERRORS 1470								
.05445	.02406	85.04	0.00000	0.00000	-90.00	.04080	.02540	89.92
.02432	.02034	71.58	0.00000	0.00000	-90.00	0.00000	0.00000	-90.00
0.00000	0.00000	-90.00	.03136	.03455	-97.81	0.00000	0.00000	-90.00
.02179	.01970	-63.96	0.00000	0.00000	-90.00	0.00000	0.00000	-90.00
0.00000	0.00000	-90.00	0.00000	0.00000	-90.00	.02963	.01567	-54.00
0.00000	0.00000	-90.00	0.00000	0.00000	-90.00	0.00000	0.00000	-90.00
0.00000	0.00000	-90.00	.03604	.02488	-59.61	.02831	.04668	48.41
0.00000	0.00000	-90.00	.03349	.03335	111.71	.02598	.03409	61.05
.03809	.03861	67.19	.03607	.03436	-114.59	.02519	.02569	-68.22
0.00000	0.00000	-90.00						
* ARGAND PLOT 1490								
.10519	.31658	0.00000	0.00000		-.07107	-.12001	-.12369	-.12266
0.00000	0.00000	.05246	.00691		0.00000	0.00000	.07598	-.09227
.06489	-.06192	-.15640	.02815		0.00000	0.00000	-.05814	.01342
0.00000	0.00000	0.00000	0.00000		.25763	.13853	0.00000	0.00000
0.00000	0.00000	0.00000	0.00000		0.00000	0.00000	.10554	.05029
.03558	.03064	0.00000	0.00000		-.00098	.09442	.01794	-.07604
-.20844	-.21947	.07667	.07821		.16547	-.08143	0.00000	0.00000
* ERRORS 1490								
.03989	.02018	84.97	0.00000	0.00000	-90.00	.02433	.01919	105.32
.02524	.01443	84.13	0.00000	0.00000	-90.00	.01705	.01695	67.78
0.00000	0.00000	-90.00	.01706	.02182	-99.98	.01603	.01815	-85.71
.00831	.01706	-82.65	0.00000	0.00000	-90.00	.00921	.01639	-84.77
0.00000	0.00000	-90.00	0.00000	0.00000	-90.00	.01249	.02362	45.54
0.00000	0.00000	-90.00	0.00000	0.00000	-90.00	0.00000	0.00000	-90.00
0.00000	0.00000	-90.00	.01691	.04047	49.51	.02292	.03682	51.36
0.00000	0.00000	-90.00	.01611	.01662	114.20	.01774	.01901	127.19
.03167	.02400	76.20	.02582	.03612	-87.94	.01577	.02404	47.77
0.00000	0.00000	-90.00						
* ARGAND PLOT 1520								
.08814	.31749	0.00000	0.00000		.02614	-.12007	-.04175	-.22555
0.00000	0.00000	.09959	-.02370		0.00000	0.00000	.10278	-.03839
.12026	-.12233	-.18089	-.01008		-.13004	.06205	-.07974	.03501
0.00000	0.00000	0.00000	0.00000		.11431	.31531	0.00000	0.00000
0.00000	0.00000	0.00000	0.00000		0.00000	0.00000	.08652	.04624
-.00671	.07939	.00936	.05988		-.01096	.10257	.02626	-.05493
-.21749	-.20063	-.00106	.10760		.11788	-.00045	0.00000	0.00000
* ERRORS 1520								
.05196	.02546	82.22	0.00000	0.00000	-90.00	.03010	.03294	116.49
.03398	.02153	100.66	0.00000	0.00000	-90.00	.02214	.02391	120.61
0.00000	0.00000	-90.00	.02942	.03655	-87.75	.02893	.02666	-115.89
.01878	.02498	-74.95	.02560	.02621	-111.75	.01740	.02798	-89.11
0.00000	0.00000	-90.00	0.00000	0.00000	-90.00	.04091	.01718	87.94

0.00000	0.00000	-90.00	0.00000	0.00000	-90.00	0.00000	0.00000	-90.00
0.00000	0.00000	-90.00	.04014	.02446	78.64	.04744	.02841	88.16
.02452	.01704	77.33	.03139	.02360	90.94	.03468	.03119	98.22
.03834	.03229	72.45	.03616	.03317	-63.47	.02310	.02769	51.74
0.00000	0.00000	-90.00						
ARGAND PLOT 1540								
.02486	.35062	0.00000	0.00000	.07013	-.10673	.02615	-.24486	
0.00000	0.00000	.11157	-.03969	0.00000	0.00000	.07755	-.04309	
.12137	-.12770	-.19945	-.01483	-.11809	.09058	-.09403	.00998	
0.00000	0.00000	0.00000	0.00000	.07495	.32461	0.00000	0.00000	
0.00000	0.00000	0.00000	0.00000	0.00000	0.00000	.09347	.08530	
-.02209	.09701	.02524	.06468	-.04418	.14459	.03190	-.08597	
-.17237	-.22257	.02439	.12058	.10625	-.01866	0.00000	0.00000	
* ERRORS 1540								
.05261	.02329	85.42	0.00000	0.00000	-90.00	.02687	.03108	118.21
.03136	.01946	100.63	0.00000	0.00000	-90.00	.01893	.02331	125.59
0.00000	0.00000	-90.00	.03164	.02838	-122.39	.03112	.02345	-132.04
.01523	.02683	-83.93	.02922	.01924	-132.69	.01714	.02399	-97.42
0.00000	0.00000	-90.00	0.00000	0.00000	-90.00	.03372	.01634	84.48
0.00000	0.00000	-90.00	0.00000	0.00000	-90.00	0.00000	0.00000	-90.00
0.00000	0.00000	-90.00	.03297	.02405	74.31	.04219	.02804	81.91
.02081	.01698	73.22	.02987	.02253	96.29	.03207	.02726	94.43
.03751	.03104	75.12	.03383	.03882	-76.40	.03044	.02343	-50.37
0.00000	0.00000	-90.00						
ARGAND PLOT 1650								
-.15112	.21659	-.00709	.06468	-.00853	-.05156	.22910	.02816	
-.10738	-.15333	.19364	.34374	.04178	.04061	-.08158	.04038	
-.04870	.40219	-.15457	-.14529	-.20691	-.25167	-.06798	-.06597	
0.00000	0.00000	0.00000	0.00000	-.07429	.24593	-.12059	-.19120	
-.19711	.00952	0.00000	0.00000	0.00000	0.00000	-.07625	.04532	
-.15742	.00088	.05010	.02362	-.16056	-.13129	-.10297	-.04868	
.02947	-.30647	.15345	.10670	.09046	.04056	-.21566	-.19230	
* ERRORS 1650								
.03762	.03953	64.88	.03602	.04721	51.11	.02929	.03115	63.52
.02465	.03360	-93.57	.01760	.03147	45.43	.02108	.02025	-66.77
.02573	.01943	-58.43	.03089	.03984	55.20	.02400	.03245	61.33
.02482	.02708	-70.44	.01438	.02110	-73.57	.02611	.02182	-61.67
0.00000	0.00000	-90.00	0.00000	0.00000	-90.00	.03289	.02245	86.20
.02073	.02153	-69.08	.03097	.02172	-132.52	0.00000	0.00000	-90.00
0.00000	0.00000	-90.00	.04430	.03104	79.65	.03560	.04080	-90.46
.02400	.02360	90.51	.03382	.03653	-72.73	.03498	.03931	-100.20
.03882	.03774	-56.42	.03922	.05171	-100.17	.02964	.03288	-70.58
.01709	.01067	99.07						
ARGAND PLOT 1690								
-.08489	.18307	-.02238	.16665	-.09056	-.12180	.16570	.05700	
.16888	-.22537	.00658	.44363	.01655	.09718	.12809	.04231	
-.14058	.35522	-.11230	-.18380	-.05388	-.35115	-.02345	-.08539	
0.00000	0.00000	0.00000	0.00000	-.08668	.19216	.09863	-.27591	
-.18941	.00531	0.00000	0.00000	0.00000	0.00000	-.11464	.02235	
-.30850	-.14934	.06758	.08888	-.03325	-.15387	-.17284	-.14926	
.05215	-.14788	-.03819	.22711	.17779	.16379	.03454	-.29009	
* ERRORS 1690								
.04333	.04554	65.47	.06348	.03851	84.92	.04198	.02980	89.10
.03285	.03054	70.46	.02781	.02566	109.44	.02132	.02638	63.33
.02515	.02477	67.90	.04180	.03940	90.73	.06043	.02995	86.29
.02929	.03942	51.63	.01780	.03358	57.09	.03051	.03390	64.36
0.00000	0.00000	-90.00	0.00000	0.00000	-90.00	.03409	.02342	92.27
.02784	.01842	87.13	.02998	.03214	121.79	0.00000	0.00000	-90.00
0.00000	0.00000	-90.00	.04816	.03771	104.58	.03510	.04067	-76.30
.02892	.02686	95.87	.05098	.04014	54.95	.03165	.04251	-78.06
.04311	.05643	55.52	.04466	.04890	62.30	.03405	.02779	-47.71
.01663	.02016	-103.11						

ARGAND PLOT 1730								
-.00005	.24160	-.10063	.14288	-.07007	-.15862	.10669	.06252	
.24543	-.15595	-.20575	.22366	.00968	.09860	.00900	.01740	
-.10415	.22108	-.05136	-.18941	-.13573	-.30813	-.09718	-.08572	
-.08468	-.11672	-.08538	-.07882	-.01971	.03540	.19903	-.15386	
-.18280	-.30104	.16180	-.00817	0.00000	0.00000	-.07676	-.18522	
-.15746	-.17313	.08936	.21162	-.04929	-.06711	-.08826	-.18192	
-.04747	-.15861	-.11704	.18617	.14296	.17743	.17824	-.20596	
* ERRORS 1730								
.05879	.04580	90.79	.06050	.04886	-130.74	.03556	.03420	109.52
.03321	.03552	116.91	.02957	.03123	-100.59	.02651	.03210	118.56
.02992	.02834	109.80	.04025	.03407	101.98	.03688	.03509	109.93
.02535	.02739	64.55	.01801	.01871	66.86	.02577	.02457	68.93
.02196	.02064	69.96	.01030	.02239	49.98	.03254	.03323	-109.22
.02682	.02403	-117.95	.02100	.03058	-90.95	.01661	.02005	-105.72
0.00000	0.00000	-90.60	.05062	.05116	-68.42	.04947	.04439	-45.00
.03113	.03444	-79.42	.03242	.03836	-87.82	.03678	.03615	-62.27
.05033	.05865	121.84	.06375	.05051	-131.61	.03584	.03276	76.81
.02429	.01840	-54.80						
ARGAND PLOT 1770								
-.13279	.22967	-.12947	.07669	-.06249	-.18260	.09483	.07932	
.26894	-.04480	-.13477	.12642	.02676	.12913	-.06187	.01171	
-.17261	.17188	-.04994	-.11401	-.14915	-.28006	-.12817	-.05042	
-.05580	-.10307	-.08156	-.14962	.08547	.00541	.16251	-.15162	
-.21052	.04866	.23464	.05088	.03382	.00823	-.11202	-.25698	
-.13480	-.13766	.12878	.30710	-.05154	-.14381	-.04698	-.10894	
-.07287	-.29152	-.22007	.14768	.13426	.23229	.15460	-.12015	
* ERRORS 1770								
.05820	.04520	89.75	.05134	.05893	131.34	.03581	.03604	66.60
.03883	.03734	72.20	.03087	.02735	-117.02	.03086	.03120	66.73
.03152	.03495	57.30	.04074	.04289	57.45	.04141	.03898	106.41
.02675	.03336	-83.56	.02922	.01755	-58.70	.02762	.02870	-68.98
.03013	.02119	-50.42	.02479	.01664	-57.60	.03560	.03680	-90.86
.02744	.02725	112.10	.03519	.02553	-127.32	.01773	.01879	-110.99
.01669	.02262	-100.88	.05736	.04414	-58.13	.04971	.05058	-68.60
.03299	.03456	-69.93	.03737	.04615	-64.24	.04460	.04620	-110.25
.04595	.05800	49.96	.04351	.05994	125.81	.03381	.03379	-67.44
.02588	.02788	-83.04						
ARGAND PLOT 1810								
-.14405	.24915	-.19923	.04710	-.01080	-.16473	.01701	.16797	
.21959	.03616	-.15010	-.02129	-.07268	.05478	-.04059	-.06066	
-.19339	.04540	.08214	-.07853	.06095	-.28103	-.07940	-.09003	
-.05228	-.12356	-.04992	-.21853	.17451	.03540	.15847	-.09828	
-.17627	-.09590	.14920	.23123	.08187	-.03491	.14802	-.22006	
-.07111	-.06560	-.12926	.38061	.10512	-.16424	-.07230	-.08073	
.11502	-.32300	-.26338	-.00697	-.00048	.25396	.24548	-.05756	
* ERRORS 1810								
.07238	.05040	89.38	.06132	.06101	-112.80	.04475	.04142	78.61
.04281	.04475	50.50	.03391	.03573	-107.94	.03408	.03462	66.18
.03747	.03748	112.62	.04180	.03800	90.48	.04285	.03429	-128.86
.02780	.02976	61.40	.01524	.01185	71.48	.02525	.03544	48.84
.02453	.02886	57.72	.01659	.02848	52.72	.04059	.03793	-129.05
.02862	.03127	116.91	.02468	.03479	-85.43	.02349	.01944	-62.14
.01657	.01887	-99.68	.07404	.04447	93.88	.05867	.06243	62.50
.03887	.03608	70.42	.04135	.03600	73.79	.04698	.04508	-64.98
.06280	.05305	75.51	.06033	.05756	-114.49	.03918	.04058	65.27
.03126	.02698	-45.00						
ARGAND PLOT 1850								
-.24323	.06512	-.14718	-.07105	.10781	-.22141	-.00928	.12350	
.18669	.09951	.02404	-.03045	-.00089	.03689	-.00211	-.00440	
-.22505	-.08427	.09530	.01300	-.01529	-.26941	-.05228	-.11872	
.03172	-.12899	.13639	-.19045	.06212	.04797	.10849	-.10016	

-.19086	-.13597	.10135	.26873	.15022	-.05875	.14696	-.20819
-.22708	-.09997	-.33642	.28158	-.02647	-.10855	-.09773	-.10520
.27436	-.14530	-.30019	-.06798	-.14822	.26960	.20105	-.01966

ERRORS 1850

.05238	.04141	91.00	.05009	.04637	-128.11	.03263	.03267	67.38
.03597	.03417	-53.17	.02893	.02617	-124.19	.03054	.02382	-55.67
.02965	.02710	83.01	.03125	.02973	-131.33	.02027	.03328	127.73
.02363	.02201	-122.91	.01110	.01792	-76.27	.02259	.02150	-64.15
.01998	.02115	63.71	.01272	.02328	47.76	.02848	.02722	70.51
.02435	.01924	77.79	.02460	.01917	-123.04	.01454	.02067	-98.13
.00758	.00896	65.02	.02610	.03705	-95.02	.03317	.03582	-106.27
.04638	.04961	61.31	.03984	.05645	133.26	.03474	.03057	-56.60
.02660	.03000	-90.50	0.00000	0.00000	-90.00	0.00000	0.00000	-90.00
0.00000	0.00000	-90.00						

ARGAND PLOT 1890

-.22483	.08196	-.06234	.03891	.12695	-.19540	-.10763	.09746
.17604	.12230	.13430	.07089	-.07400	-.10490	-.05755	.02460
-.15670	-.16618	.10551	.07628	.08002	-.17201	.02126	-.13846
.06685	-.14422	.24964	-.09974	.01354	.04328	.13587	-.13181
-.09544	-.18303	-.01909	.28136	.20771	.02933	.28057	-.14656
-.17718	-.16106	-.45383	.15683	.02868	-.14265	-.02097	-.10337
.31805	-.05166	-.23092	-.20628	-.27261	.20518	.22289	.07680

ERRORS 1890

.04688	.04396	72.29	.04530	.04621	-73.12	.03171	.03068	71.27
.03418	.03281	86.73	.02699	.02495	-129.71	.02728	.02607	70.83
.02886	.02668	-49.97	.02410	.02448	65.30	.02368	.02247	-114.56
.01833	.01716	-119.07	.01817	.01697	70.36	.01775	.01820	65.89
.01919	.01440	88.77	.01900	.01020	84.30	.03288	.02342	87.39
.02626	.01665	85.17	.01508	.02061	-83.94	.01460	.01274	-62.72
.00848	.01191	126.64	.04871	.02844	93.98	.04252	.03919	98.17
.03656	.01398	91.86	.02628	.02229	-61.23	.02803	.02645	-62.66
.04827	.03947	99.25	.03947	.04044	-111.49	.02822	.02924	65.68
.02443	.02395	-58.88						

ARGAND PLOT 1930

-.22196	.01927	-.04955	-.04820	.17838	-.18371	-.10155	.09634
.12472	.11966	.08999	.01337	-.06748	-.11710	-.11309	.08480
-.06292	-.19639	.02464	.13467	.05353	-.09448	.04054	-.14927
.10877	-.14384	.26057	-.06480	-.01595	-.07390	.16804	-.04962
-.06355	-.22334	-.03399	.29876	.20080	.11035	.33869	-.07035
-.22304	-.09145	-.46052	.10532	-.21709	-.16745	-.04471	-.05594
.29598	.15228	-.25937	-.20122	-.23408	.14338	.21446	.06771

ERRORS 1930

.03934	.04567	60.86	.04167	.04462	-80.18	.02593	.03179	53.85
.03010	.03301	48.81	.02349	.02486	127.64	.02264	.02738	59.78
.02528	.02457	-62.52	.03061	.04121	45.55	.03265	.03727	-98.24
.02538	.02404	-62.73	.02429	.02304	69.07	.02439	.02957	51.10
.02026	.02300	61.69	.02152	.01457	77.98	.03114	.02322	87.92
.02754	.01560	88.60	.02081	.02803	-98.11	.01426	.01922	-78.85
.01739	.01227	-131.69	.04540	.02743	87.02	.04075	.03578	106.25
.02918	.01299	83.27	.03675	.02789	-122.10	.03561	.04231	-97.01
.03703	.04260	120.14	.04221	.03568	-132.40	.02816	.02911	64.18
.02143	.02253	118.78						

ARGAND PLOT 1970

-.21661	-.11124	.04326	-.04658	.14334	-.09130	-.12584	.09006
.11377	.08405	.11645	-.00765	-.09652	-.10779	-.11538	.06531
-.03288	-.19034	.02910	.14647	.02030	-.07872	.04677	-.11954
.13066	-.10624	.22412	-.00474	-.03911	-.16026	.15576	-.06952
-.02147	-.20708	-.07883	.26012	.18138	.13496	.40659	.03748
-.22656	-.09667	-.46791	.04626	-.19741	-.17905	-.00442	-.01767
.18003	.25602	-.12859	-.18609	-.27740	.06450	.20785	.09370

ERRORS 1970

.04030	.04409	60.93	.04265	.04389	64.36	.02687	.02957	58.78
--------	--------	-------	--------	--------	-------	--------	--------	-------

.02908	.03090	58.43	.02518	.02171	96.69	.03088	.02310	-51.09
.02813	.02363	93.49	.02704	.02755	-68.98	.03139	.03116	109.99
.01886	.02023	-105.73	.01597	.02261	51.92	.02229	.01966	-53.96
.01509	.01990	48.50	.01208	.01742	56.80	.02651	.02460	100.43
.01713	.02539	54.91	.01927	.01695	-116.88	.01114	.01650	-100.28
.01195	.01000	106.92	.02979	.03062	66.76	.04338	.03353	79.75
.01184	.02013	58.26	.03440	.02617	-126.36	.03138	.02758	-120.73
.03746	.03846	114.85	.04290	.03956	102.71	.02416	.02866	51.84
.02258	.02021	87.36						

## II. SOLUTIONS AT FOUR ENERGIES

On the following pages are reproductions of RUMBLE printout for four representative energies. These are single-energy fits, whose overall phase is undetermined, so the phase of  $\Delta\pi(\text{PP}_{11})$  is arbitrarily set to zero.

The printout contains:

- 1st: Amplitudes and error, annotated. \*
- 2nd: An error matrix dimensioned equal to the number of waves used in the fit.
- 3rd: A  $60 \times 60$  error matrix. However, this involves repeating the amplitudes and error table in order to specify the numbers of waves and to give the the diagonal elements. Further, because of the size of the  $60 \times 60$  matrix, the format is different. See annotated example on page 2.4.

\* An explanation of the columns headed  $\frac{2}{3}$  SIGMA INEL and  $\frac{4}{3}$  SIGMA INEL:

These are merely sums of the  $\sigma$  (charge channel) at right. The first three of these channels are neutral ( $n\pi^0\pi^0$ ,  $n\pi^-\pi^+$ ,  $pn^-\pi^0$ ) and must come from  $\pi^-p$ . The last two ( $p\pi^+\pi^0$ ,  $n\pi^+\pi^+$ ) came from  $\pi^+p$ . So the output gives fit predictions for:

I	3 neutral modes	2 charge <sup>++</sup> modes
1/2	$\pi^-p \rightarrow N_{1/2}^* \rightarrow N\pi\pi$ , $\frac{2}{3} \sigma_{1/2}$	0
3/2	$\pi^+p \rightarrow N_{3/2}^* \rightarrow N\pi\pi$ , $\frac{1}{3} \sigma_{3/2}$	$\pi^+p \rightarrow \Delta \rightarrow N\pi\pi$ , $\sigma_{3/2}$

The leftmost  $I = 1/2$  column being a sum of  $2/3 \sigma_{1/2}$  for three modes is then labelled  $\frac{2}{3} \sigma_{1/2}$ .

The leftmost  $I = 3/2$  column similarly must be labelled  $\frac{4}{3} \sigma_{3/2}$ .

We are sorry if the notation on the summed columns is confusing, but it arises because they are just sums of the more physical cross sections for the individual charge channels.



SOLN B 1490 MeV

WAVE	Fitting Param RE A	$\delta(A)$ E (HE)	$\frac{1}{\sqrt{\delta(A)}}$ D (RE)	$\delta(A)$ IM A	$\delta$ E (IM)	$\frac{1}{\sqrt{\delta(A)}}$ D (IB)	PHASE REVERSE	E	RE I	IM T	E (AMP)	E (ANG)	[**2	E (T**2)	WAVE
P33 PP11	1.00	.03	.02	0.00	.09	.04	0	4	.3336	0.0000	.0101	.0207	.111304	.006844	1
P33 DS13	-.09	.01	.30	.02	.01	.00	168	6	-.1363	.0296	.0104	.0137	.019450	.003002	2
P33 DU13	-1.98	.09	.07	1.00	.17	.10	153	4	-.1554	.0787	.0081	.0126	.030323	.002704	3
P33 DU15	-.24	.10	.29	-.60	.12	.11	-.64	10	.0231	-.0476	.0087	.0091	.002799	.001302	4
P33 PP31	-.20	.04	.33	-.32	.03	.02	-.122	5	-.0636	-.1012	.0086	.0111	.014292	.002194	5
P33 DS31	-.48	.11	.09	-1.02	.10	.08	-.115	6	-.0383	-.0811	.0083	.0089	.008052	.001552	6
P33 DS33	-.02	.01	.30	.11	.00	.00	.98	4	-.0226	.1573	.0041	.0097	.025257	.001307	7
P33 DU33	-.07	.11	.08	.76	.05	.05	.95	8	-.0056	.0594	.0045	.0085	.003561	.000563	8
PH HMJ DS13	1.01	.08	.24	-1.71	.05	.04	-.43	2	.2127	-.2008	.0063	.0118	.085536	.003700	9
PH HH1 SS11	.69	.13	.17	-.72	.15	.08	-.46	11	.0810	-.0843	.0086	.0215	.013665	.002084	10
PH HH1 PP11	1.41	.52	.16	-.84	.59	.38	-.31	23	.0403	-.0251	.0115	.0192	.002209	.001210	11
PH HH1 SS31	.76	.07	.15	.26	.05	.06	.19	6	.0843	.0307	.0073	.0096	.008924	.001439	12
PH HH1 PP31	-2.31	.32	.22	-1.42	.32	.27	-1.48	7	-.0665	-.0410	.0088	.0095	.006100	.001456	13
EN S14 PS11	-1.95	.08	.16	.71	.13	.07	.155	3	-.2740	.1286	.0115	.0184	.091612	.007107	14
EN S19 SP11	2.81	.52	.36	-1.37	.37	.31	-.26	7	.0984	-.0481	.0171	.0142	.011990	.004026	15
EN S19 DP13	-.71	.28	.21	.30	.16	.16	-.98	3	-.0251	-.1827	.0110	.0094	.034001	.004169	16

\* See Appendix 1. of Herndon's Thesis UCL 544, reproduced here as 44 2.17 @ 2.18, 2.19, 2.20.

L+J	SIGMA-TOTAL (mb)	CHANNEL-1 $\pi^+\pi^+$	CHANNEL-2 $\pi^+\pi^+$	CHANNEL-3 $\pi^+\pi^+$	CHANNEL-4 $\pi^+\pi^+$	CHANNEL-5 $\pi^+\pi^+$
P1	4.849	1.278	2.642	.424	.445	.061
O3	0.444	1.062	3.287	3.055	1.221	.219
U5	.145	.034	.080	.031	0.000	0.000
S1	1.145	.074	.253	.263	.429	.027
TOTAL	14.083	2.447	6.263	3.773	2.095	.307

Seldom Used!

Sum of Channels at right

L+J	ETASQUARE	$\frac{2}{3}$ SIGMA-TOTAL (mb)	CH130	$\frac{2}{3}\sigma(\pi^+\pi^+)$	$\frac{2}{3}\sigma(\pi^+\pi^+)$	$\frac{2}{3}\sigma(\pi^+\pi^+)$	$\frac{2}{3}\sigma(\pi^+\pi^+)$	$\frac{2}{3}\sigma(\pi^+\pi^+)$	These are fitted predictions for actual $\sigma$ (mb) for $\pi^+\pi^+ \rightarrow \pi^+\pi^+$ or $\pi^+\pi^+ \rightarrow \pi^+\pi^+$
P11	0.03609	4.178	1.06	1.207	2.386	.385	0.000	0.000	0.000
U13	.196987	6.422	.128	1.077	3.365	2.480	0.000	0.000	0.000
U15	.988805	1.145	.048	.034	.080	.031	0.000	0.000	0.000
S11	.897371	1.442	.068	.070	.215	.197	0.000	0.000	0.000
TOTAL THIS ISPIN (1/2)		11.048		2.388	6.446	3.024	0.000	0.000	0.000
P31	.922349	.659	.072	.007	.096	.061	.445	.061	.061
S31	.930053	.673	.062	.003	.093	.052	.429	.027	.027
U33	.888320	1.225	.089	.024	.274	.146	1.221	.219	.219
TOTAL THIS ISPIN (3/2)		3.108		.034	.463	.300	2.095	.307	.307

16x16 ERROR MATRIX (AMP(I) AMP(J) PHA(I) AMP(J) / AMP(I) PHA(J) PHA(I) PHA(J)) . RAD = .008186 HYPERVOLUME = 1.6531E-67

I	2	3	4	5	6	7	8	9	10	11	12	13	14	15	16
1	A6	A2	U1	A4	A0	U3	O1	1	O4	U0	O1	O0	F2	E1	20
2	O5	A4	C5	C1	1	O1	1	E2	A1	OC	U	O	O5	24	30
3	AA	2C	U4	AA	A	A	UH	C	OB	A	1	AA	0	0A	B4
4	24	C2	O	24	0	O1	1	A1	A3	O1	O	O1	00	04	32
5	O1	O4	A2	U	U	O0	O0	A	O	O	O	1	O	O	00
6	U	A	A	B	O	O	O	O	O	O	O	O	O	O	1A
7	U	A	A	B	O	O	O	O	O	O	O	O	O	O	1A
8	O	A	A	B	O	O	O	O	O	O	O	O	O	O	1A
9	O	A	A	B	O	O	O	O	O	O	O	O	O	O	1A
10	O	A	A	B	O	O	O	O	O	O	O	O	O	O	1A
11	O	A	A	B	O	O	O	O	O	O	O	O	O	O	1A
12	O	A	A	B	O	O	O	O	O	O	O	O	O	O	1A
13	O	A	A	B	O	O	O	O	O	O	O	O	O	O	1A
14	O	A	A	B	O	O	O	O	O	O	O	O	O	O	1A
15	O	A	A	B	O	O	O	O	O	O	O	O	O	O	1A
16	O	A	A	B	O	O	O	O	O	O	O	O	O	O	1A

RUMBLE NOTES: Key for Error Matrix.

SYMBOL (BLANK)	RANGE	SYMBOL	RANGE
.	-.01 TO .01	.	-.01 TO -.03
0	.01 TO .03	A	-.03 TO -.05
1	.03 TO .05	B	-.05 TO -.15
2	.05 TO .15	C	-.15 TO -.25
3	.15 TO .25	D	-.25 TO -.35
4	.25 TO .35	E	-.35 TO -.45
5	.35 TO .45	F	-.45 TO -.55
6	.45 TO .55	G	-.55 TO -.65
7	.55 TO .65	H	-.65 TO -.75
8	.65 TO .75	I	-.75 TO -.85
9	.75 TO .85	J	-.85 TO -.95
0	.85 TO .95	K	-.95 TO -1.05
1	.95 TO 1.05	L	-1.05 TO -5.00
2	1.05 TO 5.00	M	-5.00 AND BELOW
3	5.00 AND ABOVE		

Whole Matrix is symmetric. Each box is not. Each box reads

$$\frac{\langle \delta T_i \delta T_j \rangle}{|\delta T_i| |\delta T_j|} \quad \frac{\langle \delta \phi_i \delta T_j \rangle}{|\delta \phi_i| |\delta T_j|}$$

$$\frac{\langle \delta T_i \delta \phi_j \rangle}{|\delta T_i| |\delta \phi_j|} \quad \frac{\langle \delta \phi_i \delta \phi_j \rangle}{|\delta \phi_i| |\delta \phi_j|}$$

where T (complex)  $\equiv T e^{i\phi}$ .

Dis require normalized diagonal, read  $\delta T$ ,  $\delta \phi$  above.

This page same format as annotated 16-wave format on page 2.3 except that here all 60 waves are defined.

SOLN B 1490 MeV repeated with 60-waves Defined,

WAVE	RE A	E(RE)	D(RB)	IM A	E(IM)	D(IB)	PHASE	E	RE T	IM T	E(AMP)	E(ANG)	T**2	E(T**2)	WAVE
P33 PP11	1.00	-.04	.02	0.00	.11	.04	0	6	.3355	0.0000	.0128	.0373	.112580	.008736	1
P33 SD11	.00	.24	.12	0.00	.31	.15	0	999	.0000	0.0000	.0184	.0241	.000000	.000339	2
P33 DS13	-.10	.01	.00	.01	.01	.00	175	8	-.1421	.0117	.0134	.0207	.020336	.004010	3
P33 PP13	.00	.07	.03	0.00	.09	.03	0	999	.0000	0.0000	.0220	.0275	.000000	.000486	4
P33 DD13	-2.06	.15	.07	.68	.25	.11	162	6	-.1622	.0532	.0126	.0190	.029140	.004474	5
P33 PF13	.00	.57	.33	0.00	.65	.44	0	999	.0000	0.0000	.0113	.0128	.000000	.000128	6
P33 FP15	.00	.03	.01	0.00	.04	.02	0	999	.0000	0.0000	.0114	.0146	.000000	.000131	7
P33 DD15	.40	.17	.09	-.49	.19	.12	-51	19	.0314	-.0385	.0122	.0161	.002472	.001368	8
P33 FF15	.00	.51	.28	0.00	.76	.42	0	999	.0000	0.0000	.0100	.0149	.000000	.000101	9
P33 FF17	.00	.42	.30	0.00	.62	.45	0	999	.0000	0.0000	.0083	.0123	.000000	.000069	10
P33 PP31	-.17	.05	.03	-.36	.03	.02	-116	7	-.0551	-.1152	.0108	.0165	.016314	.002363	11
P33 SD31	-.28	.17	.09	-1.07	.15	.08	-105	9	-.0224	-.0858	.0121	.0136	.007864	.002297	12
P33 DS33	-.03	.01	.00	.10	.01	.00	105	6	-.0412	.1521	.0105	.0164	.024834	.003427	13
P33 PP33	.00	.05	.02	0.00	.05	.02	0	999	.0000	0.0000	.0185	.0167	.000000	.000344	14
P33 DD33	-.18	.17	.08	.73	.11	.05	104	13	-.0141	.0574	.0081	.0134	.003493	.001017	15
P33 PF33	.00	.37	.27	0.00	.35	.23	0	999	.0000	0.0000	.0074	.0070	.000000	.000055	16
P33 FP35	.00	.03	.02	0.00	.02	.01	0	999	.0000	0.0000	.0079	.0063	.000000	.000062	17
P33 DD35	.00	.14	.08	0.00	.11	.06	0	999	.0000	0.0000	.0108	.0086	.000000	.000117	18
P33 FF35	.00	.48	.25	0.00	.33	.18	0	999	.0000	0.0000	.0097	.0066	.000000	.000094	19
P33 FF37	.00	.39	.27	0.00	.33	.19	0	999	.0000	0.0000	.0079	.0066	.000000	.000063	20
RH3 PP11	.00	.68	.27	0.00	.98	.36	0	999	.0000	0.0000	.0255	.0282	.000000	.000649	21
RH3 SD11	.00	2.20	1.14	0.00	3.09	1.44	0	999	.0000	0.0000	.0179	.0251	.000000	.000322	22
RH3 DS13	2.06	.12	.04	-1.35	.15	.04	-33	4	.2432	-.1590	.0095	.0208	.084419	.005582	23
RH3 PP13	.00	1.11	.31	0.00	1.12	.35	0	999	.0000	0.0000	.0318	.0322	.000000	.001013	24
RH3 DD13	.00	2.66	.76	0.00	2.73	.83	0	999	.0000	0.0000	.0215	.0222	.000000	.000464	25
RH3 PF13	.00	4.31	2.59	0.00	5.69	3.10	0	999	.0000	0.0000	.0106	.0140	.000000	.000113	26
RH3 FP15	.00	.38	.15	0.00	.50	.17	0	999	.0000	0.0000	.0111	.0143	.000000	.000123	27
RH3 DD15	.00	2.60	.84	0.00	2.85	.96	0	999	.0000	0.0000	.0211	.0231	.000000	.000444	28
RH3 FF15	.00	7.42	2.21	0.00	8.03	2.34	0	999	.0000	0.0000	.0183	.0198	.000000	.000335	29
RH3 FF17	.00	5.72	2.34	0.00	5.17	2.21	0	999	.0000	0.0000	.0141	.0127	.000000	.000199	30
RH3 PP31	.00	.68	.23	0.00	.68	.26	0	999	.0000	0.0000	.0197	.0197	.000000	.000389	31
RH3 SD31	.00	1.71	.79	0.00	1.50	.78	0	999	.0000	0.0000	.0141	.0124	.000000	.000200	32
RH3 DS33	.00	1.10	.03	0.00	.11	.04	0	999	.0000	0.0000	.0120	.0128	.000000	.000343	33
RH3 PP33	.00	.85	.21	0.00	.71	.21	0	999	.0000	0.0000	.0246	.0206	.000000	.000607	34
RH3 DD33	.00	1.80	.53	0.00	1.48	.50	0	999	.0000	0.0000	.0148	.0122	.000000	.000221	35
RH3 PF33	.00	3.28	1.91	0.00	3.23	1.67	0	999	.0000	0.0000	.0083	.0081	.000000	.000068	36
RH3 FP35	.00	.23	.12	0.00	.26	.11	0	999	.0000	0.0000	.0067	.0075	.000000	.000045	37
RH3 DD35	.00	2.10	.57	0.00	1.53	.63	0	999	.0000	0.0000	.0173	.0126	.000000	.000298	38
RH3 FF35	.00	4.84	1.54	0.00	4.50	1.50	0	999	.0000	0.0000	.0122	.0114	.000000	.000149	39
RH3 FF37	.00	3.02	1.57	0.00	4.10	1.76	0	999	.0000	0.0000	.0076	.0104	.000000	.000058	40
RH1 SS11	.45	-.21	-.07	-.29	.28	.09	-17	18	.1125	-.0341	.0171	.0372	.013813	.004300	41
RH1 PP11	.00	1.04	.34	0.00	1.17	.40	0	999	.0000	0.0000	.0299	.0337	.000000	.000897	42
RH1 PP13	.00	.68	.21	0.00	.81	.27	0	999	.0000	0.0000	.0196	.0233	.000000	.000384	43
RH1 DD13	.00	2.63	.82	0.00	3.26	.96	0	999	.0000	0.0000	.0214	.0265	.000000	.000458	44
RH1 DD15	.00	1.69	.62	0.00	1.88	.77	0	999	.0000	0.0000	.0137	.0153	.000000	.000189	45
RH1 FF15	.00	6.15	2.17	0.00	7.09	2.54	0	999	.0000	0.0000	.0152	.0175	.000000	.000230	46
RH1 FF17	.00	4.03	1.81	0.00	3.79	2.20	0	999	.0000	0.0000	.0100	.0094	.000000	.000099	47
RH1 SS31	.75	.13	.05	.35	.17	.06	25	12	.0886	.0412	.0151	.0200	.009543	.003176	48
RH1 PP31	-1.87	.79	.22	-1.83	.86	.26	-136	17	-.0544	-.0531	.0258	.0223	.005784	.004591	49
RH1 PP33	.00	.48	.15	0.00	.50	.18	0	999	.0000	0.0000	.0140	.0145	.000000	.000196	50
RH1 DD33	.00	1.88	.55	0.00	1.95	.54	0	999	.0000	0.0000	.0155	.0161	.000000	.000240	51
RH1 DD35	.00	1.36	.44	0.00	1.13	.52	0	999	.0000	0.0000	.0112	.0094	.000000	.000126	52
RH1 FF35	.00	4.03	1.55	0.00	4.73	1.53	0	999	.0000	0.0000	.0102	.0119	.000000	.000103	53
RH1 FF37	.00	2.39	1.26	0.00	3.18	1.43	0	999	.0000	0.0000	.0060	.0080	.000000	.000037	54
SIG PS11	-1.96	.12	.06	.81	.22	.07	158	6	-.2776	.1142	.0171	.0316	.090104	.010571	55
SIG SP11	2.19	.79	.36	-.44	.58	.31	-9	12	.0984	-.0156	.0279	.0206	.009917	.006332	56
SIG DP13	-.25	.42	.21	-5.50	.44	.15	-93	4	-.0090	-.1942	.0157	.0145	.037783	.006345	57
SIG PD13	.00	1.97	.93	0.00	1.46	.70	0	999	.0000	0.0000	.0199	.0147	.000000	.000397	58
SIG FD15	.00	1.70	.72	0.00	1.44	.48	0	999	.0000	0.0000	.0172	.0145	.000000	.000294	59
SIG DF15	.00	3.84	2.51	0.00	2.34	1.77	0	999	.0000	0.0000	.0120	.0073	.000000	.000143	60



40 00 10000000.,00.,0,000,000 01,A01BA0E6,000 A20013DF50 .,
0,.,00 0000..A000 .,.,11,0. 00 01..0 .A10,. 001 . 0,0
41 A,.10000 C0,00,0000 B1A30.,010AA1 00,0.+2AA, A0 10., 1B01A
.101C C0.0C00 0 .A0,0BBBA200,0.DA0.,.0 .5.AA 0.1, 000 .B2,...

60x60
Error
Matrix
Page 2

2.5

SOLN B 1490 MeV

Diagonal Elements of 60 x 60 Error Matrix

Table with columns: E, ERROR, Re, Im, Conrd Comp, Re, Im, Con. Cal, I (RUMBLE), Re, Im, C.C. It lists diagonal elements for various error components.

Table with columns: T, THMATRIX, and numerical values. It lists diagonal elements for the THMATRIX.

repeated from Amplitude list.

2.6

SOLN B 1520 MeV

Table with columns: WAVE, RE A, E (RE), D (RB), IM A, E (IM), D (IB), PHASE, E, RE T, IM T, E (AMP), E (ANG), T\*\*2, E (T\*\*2), WAVE. Rows include P33 PP11, P33 OS13, P33 OD13, P33 OD15, P33 PP31, P33 SO31, P33 OS33, P33 PP33, P33 OD33, RH3 OS13, RH1 SS11, RH1 PP11, RH1 FP13, RH1 SS31, RH1 PP31, SIG PS11, SIG SP11, SIG OP13.

Table with columns: L, J, SIGMA-TOTAL, CHANNEL- 1, 2, 3, 4, 5. Rows include P1, O3, O5, S1, P3, TOTAL.

Table with columns: L, I, J, ETASQUAKE, SIGMA-TOTAL, CHISQ, 1, 2, 3, 4, 5. Rows include P11, O13, O15, S11, P13, TOTAL THIS ISPIN, P31, S31, O33, P33.

SOLN B 1520 MeV

ERROR MATRIX ( AMP(I) AMP(J) PHA(I) PHA(J) / AMP(I) PHA(J) PHA(I) PHA(J) ). RAD = .011882 HYPERVOLUME = 4.9727E-70

Error matrix table with columns 1-18 and rows 1-18. Contains numerical values for error correlations.

18x18 Error Matrix









SOLN B 1690 MeV

WAVE	RE A	E (KE)	D(RB)	IM A	E (IM)	D(IR)	PHASE	T	RE T	IM T	E (AMP)	E (ANG)	I**2	E(I**2)	WAVE
P33 PP11	1.00	.10	.07	0.00	.13	.11	0	7	.2018	0.0000	.0128	.0263	.000736	.008841	1
P33 S011	2.06	.25	.19	-.64	.42	.33	-17	11	.1606	-.0498	.0199	.0322	.002026	.007049	2
P33 OS13	-.14	.03	.12	-.25	.04	.03	119	6	-.0724	.1334	.0197	.0166	.001301	.006539	3
P33 O013	-.23	.18	.14	-.23	.04	.20	-96	5	-.0180	-.1743	.0194	.0140	.001702	.007161	4
P33 FP15	-1.35	.06	.04	-.29	.08	.06	-168	3	-.2755	-.0584	.0115	.0168	.001306	.006604	5
P33 O015	5.12	.17	.10	-.247	.26	.16	-26	3	.3997	-.1926	.0089	.0226	.000881	.007993	6
P33 FE15	2.63	.37	.30	-1.81	.56	.45	-35	10	.0912	-.0559	.0100	.0180	.001733	.007198	7
P33 OP31	-.78	.10	.08	-.68	.11	.10	-97	8	-.0153	-.1340	.0209	.0197	.002806	.006066	8
P33 SO31	4.88	.19	.19	-.79	.40	.27	-3	5	.3814	-.0219	.0149	.0310	.003930	.011598	9
P33 OS33	-.23	.03	.02	-.34	.03	.02	124	5	-.1195	.1792	.0151	.0197	.002041	.006739	10
P33 PP33	-1.43	.08	.05	-.95	.12	.07	146	5	-.2959	.1966	.0162	.0232	.002216	.005383	11
P33 O033	-.87	.20	.14	-.74	.27	.21	140	14	-.0676	.0572	.0139	.0218	.001789	.007661	12
RH3 OS13	1.93	.11	.08	-.02	.16	.11	-1	5	.2108	-.0072	.0117	.0171	.001487	.005192	13
RH3 FP15	-4.31	.30	.23	-.86	.45	.35	175	3	-.2918	.6266	.0192	.0140	.003869	.005485	14
RH3 OS33	.80	.14	.09	1.60	.15	.11	64	5	-.0845	.1696	.0152	.0160	.001386	.005977	15
RH1 SS11	.64	.17	.14	-.89	.26	.19	54	12	-.0685	.0946	.0225	.0246	.003638	.005779	16
RH1 PP11	-.19	.69	.53	11.75	.55	.42	91	4	-.0057	.3427	.0170	.0215	.001743	.007483	17
RH1 PP13	1.08	.43	.30	-3.18	.47	.37	-62	7	.0522	-.0967	.0143	.0135	.002274	.003485	18
RH1 SS31	-1.19	.19	.14	-.90	.24	.20	143	8	-.1256	.0949	.0227	.0233	.003402	.007685	19
RH1 PP31	-2.04	.76	.61	7.14	.50	.52	106	6	-.0627	.2196	.0151	.0237	.002176	.007108	20
SIG PS11	-1.93	.30	.24	-.18	.34	.24	175	10	-.1561	.0149	.0234	.0282	.003483	.007807	21
SIG SP11	7.52	.75	.64	-2.06	.87	.75	-15	7	.2221	-.0639	.0211	.0267	.003335	.007169	22
SIG OP13	2.50	.53	.40	-7.79	.52	.42	-72	4	.0738	-.2332	.0145	.0165	.002046	.007223	23
SIG FO15	-23.10	.99	.72	7.57	.68	.91	162	2	-.2777	.0907	.0109	.0079	.001360	.006478	24

L,J	SIGMA-TOTAL	CHANNEL-	1	2	3	4	5
P1	3.846		.217	.601	1.830	1.153	.639
S1	4.807		.190	1.574	.237	2.522	.284
O3	7.136		.671	2.011	1.257	3.346	.221
F5	7.002		1.418	3.775	1.889	0.000	0.000
O6	5.844		1.378	3.253	1.243	0.000	0.000
P3	5.243		.748	.770	.677	3.317	.432
TOTAL	33.958		3.782	11.985	7.173	10.742	.976

L,I,J	ETASQUARE	SIGMA-TOTAL	CHISQ	1	2	3	4	5
P11	.093310	2.243 +- .095	0.0	.206	.753	1.085	0.000	0.000
S11	.573354	1.056 +- .122	0.0	.267	.019	.169	0.000	0.000
O13	.433734	2.777 +- .140	1.9	.630	1.554	.593	0.000	0.000
F15	.045906	7.082 +- .172	1.1	1.418	3.775	1.889	0.000	0.000
O15	.212598	5.844 +- .239	0.0	1.378	3.253	1.283	0.000	0.000
P13	.950104	.247 +- .063	0.0	0.000	.082	.165	0.000	0.000
TOTAL THIS ISPIN		19.249		3.830	10.236	5.184	0.000	0.000
P31	.676621	1.600 +- .068	0.0	.004	.260	.139	1.138	.037
S31	.241808	3.752 +- .182	.5	.032	.567	.347	2.522	.284
O33	.559917	4.356 +- .192	7.5	.025	.677	.388	3.346	.221
P33	.492135	4.990 +- .215	2.1	.048	.730	.464	3.317	.432
TOTAL THIS ISPIN		14.705		.108	2.240	1.338	10.742	.976

ERROR MATRIX ( AMP(I) AMP(J) PHA(I) PHA(J) / AMP(I) PHA(J) PHA(I) PHA(J) ) . . . . . HYPERVOLUME = 2.9577E-09

Table with 24 columns and 24 rows, containing numerical data for an error matrix. The columns are labeled 1 through 24, and the rows are labeled 1 through 24. The data consists of various alphanumeric characters and numbers, representing the matrix elements.

24x24  
Error  
Matrix

28

SOLN B 1690 MeV

WAVE	RE A	E(RE)	D(FR)	IM A	E(IM)	D(IØ)	PHASE	E	RE T	IM T	E(AMP)	E(ANG)	T**2	E(T**2)	WAVE
P33 PP11	1.00	.13	.07	0.00	.16	.10	0	9	.2018	0.0000	.0254	-.0325	-.040736	.010920	1
P33 SD11	2.06	.27	.19	-1.64	.49	.33	-17	13	-.1606	-.0498	-.0226	-.0272	-.028266	.008107	2
P33 OS13	-.114	-.04	-.02	-.225	-.05	-.03	119	8	-.0724	-.1334	-.0267	-.0209	-.023031	.008822	3
P33 PP13	-.00	.12	.06	0.00	.15	.08	0	999	.0000	0.0000	.0245	-.0296	.000000	.000598	4
P33 OD13	-.223	.22	.14	-2.23	.29	.20	-96	6	-.0180	-.1743	-.0232	-.0172	-.030702	.008650	5
P33 PF13	-.00	.51	.38	0.00	.78	.55	0	999	.0000	0.0000	-.0159	-.0241	-.000000	.000252	6
P33 FP15	-1.35	.07	.04	-.29	.10	.06	-168	4	-.2755	-.0584	-.0148	-.0197	-.079376	.008548	7
P33 DD15	5.12	.21	.16	-2.47	.34	.16	-26	4	.3997	-.1926	.0132	-.0286	.196851	.011855	8
P33 FF15	2.63	.52	.30	-1.81	.72	.45	-35	13	.0812	-.0559	.0158	-.0229	-.009730	.003368	9
P33 FF17	-.00	.46	.24	0.00	.64	.38	0	999	.0000	0.0000	-.0142	-.0199	-.000000	.000201	10
P33 PP31	-.038	.14	.08	-.68	.14	.10	-97	12	-.0155	-.1340	-.0273	-.0284	-.018206	.008127	11
P33 SD31	4.88	.23	.19	-.28	.47	.27	-3	6	-.3814	-.0219	.0179	-.0370	.145930	.013996	12
P33 OS31	-.23	.04	.02	-.34	.05	.02	124	7	-.1195	-.1792	-.0227	-.0274	-.046411	.010290	13
P33 PP33	-1.43	.14	.05	-.95	.18	.07	146	7	-.2959	-.1966	-.0217	-.0413	-.126216	.015902	14
P33 OD33	-.87	.26	.14	-.74	.35	.21	140	18	-.0676	-.0572	-.0199	-.0272	-.007839	.003918	15
P33 FF33	.00	.48	.36	0.00	.76	.47	0	999	.0000	0.0000	.0148	-.0216	.000000	.000219	16
P33 FP35	.00	.08	.05	0.00	.10	.06	0	999	.0000	0.0000	.0158	-.0185	.000000	.000250	17
P33 OD35	-.00	.24	.11	0.00	.35	.17	0	999	.0000	0.0000	.0188	-.0271	.000000	.000352	18
P33 FF35	.00	.48	.30	0.00	.69	.40	0	999	.0000	0.0000	.0148	-.0213	.000000	.000220	19
P33 FF37	.00	.44	.25	0.00	.62	.40	0	999	.0000	0.0000	.0136	-.0189	.000000	.000186	20
RH3 PP11	.00	.91	.49	0.00	1.00	.54	0	999	.0000	0.0000	.0282	-.0310	.000000	.000795	21
RH3 SD11	.00	2.56	1.50	0.00	2.85	1.49	0	999	.0000	0.0000	-.0287	-.0318	.000000	.000823	22
RH3 OS13	1.98	.14	.08	-.02	.19	.11	-1	6	.2108	-.0022	.0148	-.0204	.044457	.006459	23
RH3 PP13	.00	.70	.41	0.00	.61	.37	0	999	.0000	0.0000	.0217	-.0189	.000000	.000472	24
RH3 OD13	.00	1.99	1.08	0.00	2.13	1.25	0	999	.0000	0.0000	.0224	-.0239	.000000	.000500	25
RH3 PF13	.06	3.78	2.48	0.00	4.04	2.81	0	999	-.0060	0.0000	.0171	-.0183	.000000	.000293	26
RH3 FP15	-9.41	.37	.23	.86	.55	.35	175	3	-.2918	-.0266	-.0115	-.0171	-.085869	.006879	27
RH3 DD15	.00	1.62	.93	0.00	1.53	.92	0	999	.0000	0.0000	.0181	-.0171	.000000	.000329	28
RH3 FF15	.00	4.07	2.26	0.00	4.25	2.62	0	999	.0000	0.0000	.0185	-.0193	.000000	.000341	29
RH3 FF17	.00	3.34	2.13	0.00	3.12	1.99	0	999	.0000	0.0000	.0151	-.0141	.000000	.000229	30
RH3 PP31	.00	.97	.53	0.00	1.06	.59	0	999	.0000	0.0000	.0298	-.0326	.000000	.000891	31
RH3 SD31	.00	2.47	1.54	0.00	2.76	1.71	0	999	.0000	0.0000	.0275	-.0306	.000000	.000756	32
RH3 OS31	.80	.18	.09	1.60	.19	.11	64	6	.0845	-.1696	.0194	-.0207	-.035886	.007714	33
RH3 PP33	.00	.92	.43	0.00	.73	.42	0	999	.0000	0.0000	.0283	-.0276	.000000	.000831	34
RH3 OD33	.00	2.24	1.17	0.00	2.05	1.12	0	999	.0000	0.0000	.0249	-.0228	.000000	.000621	35
RH3 FF33	.00	3.84	2.62	0.00	3.83	2.63	0	999	.0000	0.0000	.0172	-.0172	.000000	.000297	36
RH3 FP35	.00	.43	.28	0.00	.50	.33	0	999	.0000	0.0000	.0133	-.0160	.000000	.000177	37
RH3 DD35	.00	1.90	1.03	0.00	1.61	.96	0	999	.0000	0.0000	.0211	-.0179	.000000	.000445	38
RH3 FF35	.00	4.42	2.49	0.00	3.83	2.35	0	999	.0000	0.0000	.0199	-.0172	.000000	.000394	39
RH3 FF37	.00	4.02	2.42	0.00	3.15	2.09	0	999	.0000	0.0000	.0180	-.0141	.000000	.000325	40
RH1 SS11	.64	.22	.14	.89	.32	.19	54	16	.0685	-.0946	-.0264	-.0317	.013638	.006866	41
RH1 PP11	-.13	.93	.53	11.05	.68	.42	91	5	-.0057	-.3427	-.0211	-.0288	.117483	.014894	42
RH1 PP13	1.68	.59	.36	-3.18	.73	.37	-62	10	.0522	-.0987	.0221	-.0191	.012474	.005418	43
RH1 OD13	.00	1.62	.97	0.00	1.44	.84	0	999	.0000	0.0000	.0181	-.0184	.000000	.000329	44
RH1 DD15	.00	1.19	.80	0.00	1.49	.85	0	999	.0000	0.0000	.0133	-.0167	.000000	.000177	45
RH1 FF15	.00	3.03	1.94	0.00	3.25	1.92	0	999	.0000	0.0000	.0137	-.0147	.000000	.000188	46
RH1 FF17	.00	2.48	1.72	0.00	2.86	1.74	0	999	.0000	0.0000	.0112	-.0130	.000000	.000126	47
RH1 SS31	-1.19	.25	.14	.90	.31	.20	143	11	-.1256	-.0949	.0307	-.0297	.024802	.010604	48
RH1 PP31	-2.04	1.00	.61	7.14	.69	.52	106	8	-.0627	-.2196	.0198	-.0318	.052176	.009435	49
RH1 PP33	.00	.70	.38	0.00	.69	.39	0	999	.0000	0.0000	.0214	-.0211	.000000	.000457	50
RH1 OD33	.00	1.87	1.10	0.00	1.57	.86	0	999	.0000	0.0000	.0208	-.0174	.000000	.000433	51
RH1 DD35	.00	1.46	.87	0.00	1.25	.83	0	999	.0000	0.0000	.0163	-.0138	.000000	.000264	52
RH1 FF35	.00	3.69	2.27	0.00	2.86	1.97	0	999	.0000	0.0000	.0165	-.0128	.000000	.000274	53
RH1 FF37	.00	3.04	1.91	0.00	2.65	1.75	0	999	.0000	0.0000	.0136	-.0119	.000000	.000185	54
SIG PS11	-1.93	.36	.24	.18	.43	.24	175	13	-.1561	-.0149	-.0281	-.0355	.024600	.009589	55
SIG SP11	7.52	.96	.64	-2.06	1.13	.75	-15	9	.2221	-.0609	.0266	-.0349	.053035	.012936	56
SIG OP13	2.50	.68	.40	-7.79	.66	.42	-72	5	.0738	-.2302	.0180	-.0212	.058446	.009027	57
SIG PD13	.00	1.86	1.09	0.00	2.22	1.35	0	999	.0000	0.0000	-.0223	-.0266	.000000	.000497	58
SIG FD15	-23.19	1.03	.72	7.57	.81	.91	162	2	-.2777	.0907	.0124	-.0095	.085360	.007424	59
SIG DF15	.00	2.86	2.04	0.00	3.82	2.44	0	999	.0000	0.0000	.0147	-.0197	.000000	.000217	60

ERROR MATRIX ( AMP(I) AMP(J) ) ( AMP(I) PHA(IJ) )

SOLN B 1690 MeV

RAO = .015143 HYPERVOLUME = 4.2287-219

1 ---  
J ---

2.10

1 2 3 4 5 6 7 8 9 10 11 12 13 14 15 16 17 18 19 20 21 22 23 24 25 26 27 28 29 30 31 32 33 34 35 36 37 38 39

1 +0R11R11A010A0A C010002AL,131001001 0,00,0.F .,0101,0 C10A1  
110A 2A001B1 1, .0000K1C0,180 .001 00.01A0 A 0A2100, 00CAAA0

2 7+10R11A1A A001 0.A00A,0U 0 .,00 01 00B00. 0, .100 00A1000  
2RCA30RA10 ,C .100.1AA01010000.00.000.000H,00,0 1A1 0.0000.

3 R1+1C100 ,01 .00A0,003010,00A .,A00.0000.2,2 A00,00 ,000,A.  
000010CA0 A 01 ,0111.00CA00 0A0,1 0,000C1 00A00.1 ,00C, 1,0011

4 101+AR111B000F, .A0,0A00.0U10000001 0.000 ACA1,0.0, .00,00.1,7  
1,02.,20A2 00, CA,02A B.0A80,0A00, CA ., . 1A0 000.00 A00000

5 1B0A+ABA100.0.,,1100,ABAU,000.1000',00000,B ., .00000.00000 20  
A 00A1,0R0000.0,0000001.A1CAAB.00 .0., . 0 10000 00,., .000 000

6 B11BA+ 0A10, 1000AC.,.1.,.1A A.0,1,0. .00C1, 0,0 0000 ,0,00  
0 101,AB2A0, .0000.0.001,00, .0. ., .000000.0,1 1,.1000A.

7 A101B +.B2100 ,01A1 200,0,B0A .,A100 000CA21.0000A000, .0021BA  
.00,A.,A0.,00C0., .0000 0000 0,A0,AD ,.000.10,1,00. .,0,010A

8 0A01A0 .+A0 0A0C,CA10 00AA10DA.00.21 0100. .A10A000100 000A000  
00.,0 00000A10A1, ,2A01100.0.1A00 ,. .,202A2. .10,00000002.00

9 1A 11ABA+0A0 C ,01B0AA.01,0020,0 ,00. 0.A00,A,01000.0000,0  
0AA1. .AA2B010AA0 .0 01A,010001 ., .10, C.A.000.1 00 ,0 0 0.00

10 0 B01200+0,0.000A001A.0.0000200.00010000011A010 .0 0.0010A0  
0 ,1,00A4200 0000.0 00CA000000.00,0000 1.001 0B.0 11 000,0 0

11 AA,0001 A0+B A000,1000A101,000,01A01000A1011A1, .20A0,01 002 A  
0AA10AB01A01AA1B01A0A0000000. C00A00A,100A0A, .040.0, .01 0 0

12 0000.,000,B+A,20B0A1A.1A .00,0A000,0001CA0A A0.F21.00001,A,  
0A0.00B,100A,GR01A,0.0A100000A01A01A.001A10000031A000 .0,10

13 A11A0 0A 0 A+ 00000 0000000.0000F 01 .0020100001A00. 0.000 ,  
0AA0000C11BR00R.2. 20.A00A 010,00201.002 00A00000002 11000000B11

14 1 .,1 00.A, +A0 0 00,00 0A000.0702.10, 0A0AA00.4A00, A00000  
01. .0A0,00A10B 2C0020A1 000002000 0,001010. .,2,A10,00B,1,0

15 0 .,0,0 0020A+.A1 0011A0000,0,1R00CA00,00B A00C0,201.01,A,0  
1A011AB.1A0AA00B200000000,00,00120.0000,1A.0,0,3100000,A, .00

16 000A,00,00000.+00A0 A.U, 0.,000A,0A0,0000.0 00A0.0 0.0  
0000000000100A10AA00,0A000000,C 1011,AB001A0 011.0000.0, .

17 1.001010000000 A0+02B1AA. 00A003A,010A0B10A1,0.010A, B0 0010,  
00,710, 01RC,A,1U10-UA, ,00A0, A00A0101A2C 002A00A1 0000. .

18 0AA,1AA01A,C00100+A1B,000010,0,1R10.040.0 A000000 020001A010  
,AA000, A00001, .4 2A1. .001100A2,000A0A,ANBA00001A0C1.01C0.

19 0000011R01A0 AZA+0.0, .A0 .,0100.001.00.00 .,0180.02 ,000A  
,AA, .,A, .100 ADA1210.01.0010000.000 0111 010,0A.0000 ., .0

20 00,00. 00001 000B10+.0000,01.0A1,0001, .0000A0,00010000,00000  
0,0,0.01000A 10.1020. .000,0,00.01A00 ,0A,A 0100. .,201.A0.

21 2A00, 2 A10A000 1B. +A011A0 A12A,AA0.AC 1 200 11AA 0,0AA01.0  
00.00011A0,0.0A,000 2B,020A,B100 01. .A,001,.B10 100A00,0000

22 A,00A.00AA0.0,1AA,00A+, D1010002 .0 .,A 0A, .10 0A,A00 010.0  
,.0010 A0000100. 000000100001A1,000010.00.01010. .,A.,000A 1 .

23 003.B100. .A1001.A0,00 +00GA00000,00 1 . 00B1A0000000 0BA00  
000.0.A10 .,0. 0 0,0001,0,00, .,00 100AA0 0 1,71 C.02,A. .0

24 . 00A.,A001A0 0A0.0.01,0+10021,0000.000, .1A2A01AA C, .10.  
.013000 ,00 C 10002A0001A00180.11 0,0200.,10 000,000A,20A

25 10100,0A1.0 0 0, 0A01001+A002,0A0,1 00,0A0C.A,00000,000000  
,.01A,100A0 0,000 0000A,00A, .100A0001000.00A0,00A1 0000 0A

26 0 01, .,1,01.0 0 000,A100A+000200 .02. C.0000A01.00A0.0. .0,0  
0 A 1.000 00.00.010000A.100102.1000 0,01 A0B. .20,00A01010000

27 1 ,000000,0000001 000A000+001,1,1 ,0, .,AB0.001,00.A00.20A81  
1 AA. C00000,00 .0B1000 .,A1 0, 0. 1A.A000 1010. 0 0,0

28 00000A000000.A0.A0.1 1A2000+10A000A 00.0A000A50.000100 0101  
A00, 10A 0,0, .00,00,211 A, 11811000A0,00A.AC00A100A. 100001

29 0 000 AA200,00,00,00, .,A0012001+A 0. .0 1A0,1B10A 0A0 0 00. 0  
B01 A0A. .00,00,00,00 0B00001,0 AA.000 A 001A100A.1. .0 .,01000

30 1,A0.A. .0200000000000100, 210A+.A.,00 A,0A00 .5A,01, .,0 .00  
10R00A 0000 0.010,.,A0.202030010 1 10100101,20 00,010,0000

31 0. .01. .0,0,A,0,03,1A200,00,A .+A100000800 00. .0188.100, A0110  
1001 0 10 2BA.B.3A1A10A.,0.0A03B112. .B0, .1. 0010A00A1A00C100

32 0 .000A000000.10A101A200A0100AA+00C100,0 0A,00010A0A1.010A0.  
,0AB00A,00B2102001A 000A 0000A1B1A0A01 AA.A0 A100.1,110A00

33 10A10,1.,.10FRRA,B0, .00,0. .00+01,0A,0B0, 0 A000A 100A  
1000 ., .,A.0A3.RG1A0000A00A000AA.10A0A 01 01, .,01. A0 0A0 000

34 .00 0102 0A0 70,01.0A.0U, .1B ,100+10,10,00B0AA,A03A10. 00000  
.100001 A.0A,4A0 01000,1.U, .00102001,0.0100 001A. 0. .B00.0

35 0 00, .01,00,0001000A00010 A.00C11+A021A0 .00A.0.100A00 0.  
1 A ., .0000,A1B,CA0100A000000A, 3A00, 000.1A00A0.0, .A0A00.0.

36 ,0. .00 0010120A0.000 .2, 0001,0A+AAB20. .0, .1002R.0 00000  
00.0,001. 10 0002 0A1 0. .0000100 011010100000.1.A. ., .0 A01.0

37 01000.000100 .A0A011. 1U .00 000,0A+11B0100100A.3,C.AA 0000  
100.0000.0,00 03.,01A ,.0A001B,00101A,000, 0.010100.00. .10

38 0 000.01.000.10 04.,A. 00 ,0 00A12A1+200,00, .0.1A5A,00AA.0  
100000,0.C0111.A1A1 1,0A 00A01B1A,110A A0, .0031010A 0.A.1

39 ,000000 0A1000,00C.0, .000-.1AB, 01B12+, .,0.0CA12B1000100.  
01.0,0,0 .A00000B,A10 0,0C 00AA1 A0.010000,00,11000A .0,0



WAVE	RE A	E (RE)	D (RE)	IM A	E (IM)	D (IM)	PHASE	E	RE T	IM T	E (AMP)	E (ANG)	T**2	E (T**2)	WAVE
P33 PP11	1.00	.09	.07	0.00	.10	.09	0	6	.2393	0.0000	.0212	.0249	.057263	.010613	1
P33 SD11	.56	.19	.16	-.12	.17	.16	-12	18	.0719	-.0152	.0233	.0226	.005395	.003958	2
P33 OS13	-.42	.03	.03	.31	.04	.03	143	4	-.1862	.1461	.0149	.0165	.054319	.007152	3
P33 OD13	1.04	.13	.11	-.42	.13	.11	-22	7	.1345	-.0547	.0165	.0170	.021083	.005060	4
P33 FP15	-.52	.05	.05	-.73	.05	.05	-125	4	-.1235	-.1752	.0125	.0136	.045943	.005498	5
P33 UD15	-.79	.10	.08	-.88	.11	.10	-132	5	-.1019	-.1120	.0145	.0126	.023063	.004607	6
P33 FF15	.48	.21	.18	1.77	.20	.17	75	6	.0236	.1239	.0141	.0137	.018485	.003826	7
P33 PP31	.26	.05	.04	-.01	.05	.04	-3	12	.0625	-.0034	.0117	.0126	.003920	.001604	8
P33 SD31	.70	.11	.08	1.63	.08	.08	67	4	.0903	.2098	.0099	.0145	.052160	.004599	9
P33 OS33	-.16	.02	.02	-.24	.02	.02	-124	4	-.0730	-.1078	.0083	.0096	.016955	.002223	10
P33 PP33	-.56	.03	.03	.56	.04	.03	135	3	-.1341	.1342	.0083	.0103	.036000	.003207	11
P33 OD33	-.32	.07	.05	.95	.08	.06	119	4	-.0674	.1228	.0089	.0095	.019620	.002973	12
P33 FF35	-1.60	.10	.08	1.61	.14	.10	135	3	-.1122	.1126	.0084	.0085	.025259	.002751	13
P33 FF37	-3.84	.07	.05	.12	.14	.10	178	2	-.2687	.0082	.0050	.0101	.072241	.002728	14
RH3 OS13	.01	.07	.07	-.29	.11	.08	-87	15	.0021	-.0453	.0165	.0118	.002060	.001771	15
RH3 FP15	-2.51	.12	.12	1.12	.19	.16	156	4	-.1728	.0773	.0090	.0129	.035830	.003474	16
RH3 US33	.17	.07	.05	1.31	.05	.04	83	3	.0267	.2054	.0077	.0104	.042890	.003239	17
RH3 FP35	1.65	.12	.09	-3.73	.09	.06	-66	2	.1143	-.2578	.0057	.0088	.079511	.003259	18
RH3 FF37	-11.60	.31	.24	-6.19	.35	.30	-152	2	-.1851	-.0987	.0042	.0062	.044021	.001769	19
RH1 SS11	-2.00	.09	.08	.27	.16	.13	172	4	-.3138	.0416	.0147	.0245	.010196	.009512	20
RH1 PP11	1.01	.28	.23	3.07	.31	.26	62	5	.1113	.2120	.0208	.0201	.057315	.010371	21
RH1 PP13	6.94	.10	.12	.12	.27	.24	1	2	.4801	.0081	.0070	.0185	.230585	.006733	22
RH1 SS31	-.44	.09	.07	.79	.07	.06	121	6	-.0758	.1242	.0103	.0154	.021157	.003092	23
RH1 PP31	-1.23	.21	.17	1.51	.19	.15	99	8	-.0157	.1043	.0128	.0147	.011116	.002870	24
SIG PS11	-3.91	.22	.20	-.67	.28	.26	-169	4	-.3165	-.0604	.0193	.0249	.103886	.012815	25
SIG SP11	3.32	.54	.56	6.19	.42	.44	62	5	.1463	.2729	.0173	.0245	.095877	.011020	26
SIG OP13	7.40	.31	.29	-2.25	.37	.36	-17	3	.3264	-.0994	.0128	.0169	.116416	.008886	27
SIG FD15	-7.79	.52	.50	-6.32	.51	.52	-141	3	-.1831	-.1485	.0123	.0119	.055602	.005948	28

L, J	SIGMA-TOTAL	CHANNEL-	1	2	3	4	5
P1	1.821		.323	.884	.502	.107	.005
S1	2.439		.209	.629	.748	.785	.068
O3	4.706		.621	1.670	.491	1.825	.694
F5	7.130		.566	2.725	.444	3.294	.100
D5	.455		.102	.253	.101	0.000	0.000
P3	2.983		.010	1.305	1.958	.020	.691
F7	6.985		.043	1.065	.617	4.778	.383
TOTAL	27.414		1.872	8.530	4.860	11.409	.742

L, I, J	ETASQUARE	SIGMA-TOTAL	CHISQ	1	2	3	4	5
P11	-.015442	1.671 +- .062	1.5	.339	.897	.435	0.000	0.000
S11	.209131	1.301 +- .061	4.5	.212	.646	.444	0.000	0.000
D13	.349344	2.141 +- .091	12.2	.607	1.321	.213	0.000	0.000
F15	.472905	2.502 +- .099	2.0	.589	1.453	.559	0.000	0.000
D15	.917747	.455 +- .086	0.0	.102	.253	.101	0.000	0.000
P13	.377661	3.035 +- .085	8.4	0.000	1.012	2.023	0.000	0.000
TOTAL THIS ISPIN		11.206		1.849	5.582	3.775	0.000	0.000
P31	.954321	.150 +- .034	0.0	.001	.024	.013	.107	.005
S31	.654297	1.138 +- .066	2.7	.008	.175	.102	.785	.068
O33	.611200	2.559 +- .079	37.6	.010	.406	.224	1.825	.094
P33	.856001	.948 +- .082	0.0	.010	.138	.089	.620	.091
F35	.541367	4.528 +- .164	0.0	.011	.734	.389	3.294	.100
F37	.476971	6.885 +- .170	0.0	.043	1.065	.617	4.778	.383
TOTAL THIS ISPIN		16.208		.082	2.540	1.434	11.409	.742

SOLN B 1890 MeV

ERROR MATRIX ( AMP(I) AMP(J) PHA(I) PHA(J) / AMP(I) PHA(J) PHA(I) PHA(J) ), KAD = .011051 HYPERVOLUME = 2.6994-110

I	J	1	2	3	4	5	6	7	8	9	10	11	12	13	14	15	16	17	18	19	20	21	22	23	24	25	26	27	28
1	1	+	1	00	AA	AA	AC	0,	0,	0	00	01	00	0,	0,	0	0	0	0	0	0	00	10	0	0	E1	0,	10	1A
1	2	+	1	AA	1	1	01	A1	A1	05	01	00	00	01	01	03	0	0	0	0	0	00	00	0	0	00	00	00	A
2	1	0A	+	10	00	0,	0	0	0	00	00	00	00	0.	0	00	0	0	0	0	0A	01	00	00	0	0	00	0	00
2	2	0A	+	10	00	0,	0	0	0	00	00	00	00	0.	0	00	0	0	0	0	0A	01	00	00	0	0	00	0	00
3	1	10	+	0J	AJ	A.	0	0	00	0	01	01	00	0,	0	01	01	00	0	0	00	0	0	0	00	0	0	0	00
3	2	0A	+	10	00	0,	0	0	00	00	00	00	00	0.	0	00	0	0	0	0	0A	01	00	00	0	0	00	0	00
3	3	10	+	0J	AJ	A.	0	0	00	0	01	01	00	0,	0	01	01	00	0	0	00	0	0	0	00	0	0	0	00
4	1	A,	0J	A	+	0	0A	0J	0	0	00	0	0	0	0	0	0	0	0	0	0	0	0	0	0	0	0	0	00
4	2	A,	0J	A	+	0	0A	0J	0	0	00	0	0	0	0	0	0	0	0	0	0	0	0	0	0	0	0	0	00
5	1	A0	A0	A	0	+	00	C,	00	00	00	00	00	0	0	0	0	0	0	0	00	00	00	00	0	0	00	00	B2
5	2	AA	?	?	?	?	?	?	?	?	?	?	?	?	?	?	?	?	?	?	?	?	?	?	?	?	?	?	C
6	1	A0	0	0	0A	00	+	1	0,	0,	0,	0,	0,	0,	0,	0,	0,	0,	0,	0,	0,	0,	0,	0,	0,	0,	0,	0,	00
6	2	01	10	11	A3	00	1+	B1	0,	0,	0,	0,	0,	0,	0,	0,	0,	0,	0,	0,	0,	0,	0,	0,	0,	0,	0,	0,	00
7	1	0A	00	0,	01	CA	0B	+	0	00	0,	01	00	0,	01	A2	2	00	02	0	0	00	00	0	0	0	0	0	00
7	2	0A	00	0,	01	CA	0B	+	0	00	0,	01	00	0,	01	A2	2	00	02	0	0	00	00	0	0	0	0	0	00
8	1	0	0	0	0	0	0	0	0	0	0	0	0	0	0	0	0	0	0	0	0	0	0	0	0	0	0	0	00
8	2	00	00	00	00	00	00	00	00	00	00	00	00	00	00	00	00	00	00	00	00	00	00	00	00	00	00	00	00
9	1	00	00	00	00	00	00	00	00	00	00	00	00	00	00	00	00	00	00	00	00	00	00	00	00	00	00	00	00
9	2	00	00	00	00	00	00	00	00	00	00	00	00	00	00	00	00	00	00	00	00	00	00	00	00	00	00	00	00
10	1	0	0	0	0	0	0	0	0	0	0	0	0	0	0	0	0	0	0	0	0	0	0	0	0	0	0	0	00
10	2	00	00	00	00	00	00	00	00	00	00	00	00	00	00	00	00	00	00	00	00	00	00	00	00	00	00	00	00
11	1	00	00	00	00	00	00	00	00	00	00	00	00	00	00	00	00	00	00	00	00	00	00	00	00	00	00	00	00
11	2	00	00	00	00	00	00	00	00	00	00	00	00	00	00	00	00	00	00	00	00	00	00	00	00	00	00	00	00
12	1	00	00	00	00	00	00	00	00	00	00	00	00	00	00	00	00	00	00	00	00	00	00	00	00	00	00	00	00
12	2	00	00	00	00	00	00	00	00	00	00	00	00	00	00	00	00	00	00	00	00	00	00	00	00	00	00	00	00
13	1	0	00	00	0	0	0	0A	0C	0A	0B	0	A	0B	0B	0	0	0	0	0	0	00	00	0	0	0	0	0	00
13	2	01	00	00	01	00	01	02	0C	02	03	03	03	03	03	03	03	03	03	03	03	03	03	03	03	03	03	03	03
14	1	00	00	00	00	00	00	00	00	00	00	00	00	00	00	00	00	00	00	00	00	00	00	00	00	00	00	00	00
14	2	00	00	00	00	00	00	00	00	00	00	00	00	00	00	00	00	00	00	00	00	00	00	00	00	00	00	00	00
15	1	00	00	00	00	00	00	00	00	00	00	00	00	00	00	00	00	00	00	00	00	00	00	00	00	00	00	00	00
15	2	00	00	00	00	00	00	00	00	00	00	00	00	00	00	00	00	00	00	00	00	00	00	00	00	00	00	00	00
16	1	0	0	0	0	0	0	0	0	0	0	0	0	0	0	0	0	0	0	0	0	0	0	0	0	0	0	0	00
16	2	00	00	00	00	00	00	00	00	00	00	00	00	00	00	00	00	00	00	00	00	00	00	00	00	00	00	00	00
17	1	0	0	0	0	0	0	0	0	0	0	0	0	0	0	0	0	0	0	0	0	0	0	0	0	0	0	0	00
17	2	00	00	00	00	00	00	00	00	00	00	00	00	00	00	00	00	00	00	00	00	00	00	00	00	00	00	00	00
18	1	00	00	00	00	00	00	00	00	00	00	00	00	00	00	00	00	00	00	00	00	00	00	00	00	00	00	00	00
18	2	00	00	00	00	00	00	00	00	00	00	00	00	00	00	00	00	00	00	00	00	00	00	00	00	00	00	00	00
19	1	0	0	0	0	0	0	0	0	0	0	0	0	0	0	0	0	0	0	0	0	0	0	0	0	0	0	0	00
19	2	00	00	00	00	00	00	00	00	00	00	00	00	00	00	00	00	00	00	00	00	00	00	00	00	00	00	00	00
20	1	00	00	00	00	00	00	00	00	00	00	00	00	00	00	00	00	00	00	00	00	00	00	00	00	00	00	00	00
20	2	00	00	00	00	00	00	00	00	00	00	00	00	00	00	00	00	00	00	00	00	00	00	00	00	00	00	00	00
21	1	00	00	00	00	00	00	00	00	00	00	00	00	00	00	00	00	00	00	00	00	00	00	00	00	00	00	00	00
21	2	00	00	00	00	00	00	00	00	00	00	00	00	00	00	00	00	00	00	00	00	00	00	00	00	00	00	00	00
22	1	00	00	00	00	00	00	00	00	00	00	00	00	00	00	00	00	00	00	00	00	00	00	00	00	00	00	00	00
22	2	00	00	00	00	00	00	00	00	00	00	00	00	00	00	00	00	00	00	00	00	00	00	00	00	00	00	00	00
23	1	00	00	00	00	00	00	00	00	00	00	00	00	00	00	00	00	00	00	00	00	00	00	00	00	00	00	00	00
23	2	00	00	00	00	00	00	00	00	00	00	00	00	00	00	00	00	00	00	00	00	00	00	00	00	00	00	00	00
24	1	0	0	0	0	0	0	0	0	0	0	0	0	0	0	0	0	0	0	0	0	0	0	0	0	0	0	0	00
24	2	00	00	00	00	00	00	00	00	00	00	00	00	00	00	00	00	00	00	00	00	00	00	00	00	00	00	00	00
25	1	E0	00	00	1	10	0	0	0	00	00	00	00	0	0	0	0	0	0	0	0	0	0	0	0	0	0	0	00
25	2	10	01	00	00	00	00	00	00	00	00	00	00	00	00	00	00	00	00	00	00	00	00	00	00	00	00	00	00
26	1	0	0A	0	0	0	0	0	0	0	0	0	0	0	0	0	0	0	0	0	0	0	0	0	0	0	0	0	00
26	2	00	00	00	00	00	00	00	00	00	00	00	00	00	00	00	00	00	00	00	00	00	00	00	00	00	00	00	00
27	1	10	00	00	00	00	00	00	00	00	00	00	00	00	00	00	00	00	00	00	00	00	00	00	00	00	00	00	00
27	2	00	00	00	00	00	00	00	00	00	00	00	00	00	00	00	00	00	00	00	00	00	00	00	00	00	00	00	00
28	1	1	00	00	10	00	00	00	00	00	00	00	00	00	00	00	00	00	00	00	00	00	00	00	00	00	00	00	00
28	2	AA	00	00	00	00	00	00	00	00	00	00	00	00	00	00	00	00	00	00	00	00	00	00	00	00	00	00	00

2.13

28x28

Error Matrix

WAVE	RF A	I (FC)	O (SB)	IM A	C (IM)	O (IB)	PHASE	E	RE T	IM T	E (AMP)	F (ANG)	T**2	E (T**2)	WAVE
P33 PP11	1.34	.13	.07	0.00	.11	.09	0	6	.2393	0.0000	.0241	.0270	.057263	.012137	1
P33 PP11	.56	.20	.16	-.12	.19	.16	-12	20	.0719	-.0152	.0256	.0254	.005395	.004412	2
P33 PP13	-.42	.04	.03	.31	.04	.03	143	5	-.1862	.1401	.0164	.0188	.054319	.007947	3
P33 PP13	.00	.08	.06	0.00	.10	.07	0	999	.0000	0.0000	.0185	.0229	.000000	.000341	4
P33 DP13	1.04	.14	.11	-.42	.15	.11	-22	8	.1345	-.0547	.0182	.0195	.021083	.005624	5
P33 FF13	.00	.26	.20	0.00	.24	.21	0	999	.0000	0.0000	.0182	.0168	.000000	.000331	6
P33 FF15	-.52	.06	.05	-.73	.06	.05	-125	4	-.1235	-.1752	.0138	.0156	.045943	.006084	7
P33 DP15	-.79	.11	.08	-.83	.14	.10	-132	6	-.1019	-.1126	.0169	.0159	.023063	.005421	8
P33 FF15	.48	.23	.18	1.77	.22	.17	75	7	.0336	.1239	.0157	.0159	.016485	.004265	9
P33 FF17	.00	.19	.12	0.00	.22	.18	0	999	.0000	0.0000	.0130	.0152	.000000	.000170	10
P33 PP11	.20	.06	.04	-.01	.06	.04	-3	13	.0625	-.0034	.0139	.0145	.003923	.001938	11
P33 DP11	.70	.12	.08	1.63	.09	.08	67	4	.0903	.2098	.0109	.0168	.052160	.005091	12
P33 DP13	-.16	.02	.02	-.24	.02	.02	-124	5	-.0730	-.1078	.0099	.0116	.016955	.002666	13
P33 DP33	-.56	.04	.03	.56	.05	.03	135	4	-.1341	.1342	.0108	.0127	.036000	.004197	14
P33 DP33	-.52	.09	.05	.95	.09	.06	119	5	-.0674	.1228	.0111	.0111	.019620	.003218	15
P33 DP33	.00	.14	.10	0.00	.16	.12	0	999	.0000	0.0000	.0096	.0111	.000000	.000092	16
P33 DP35	.00	.04	.03	0.00	.04	.03	0	999	.0000	0.0000	.0091	.0094	.000000	.000083	17
P33 DP35	.00	.06	.04	0.00	.09	.06	0	999	.0000	0.0000	.0083	.0116	.010000	.000064	18
P33 FF15	-1.60	.12	.08	1.61	.15	.10	135	3	-.1122	.1126	.0101	.0094	.025259	.003318	19
P33 FF17	-3.84	.09	.05	.12	.17	.10	178	2	-.2687	.0082	.0062	.0117	.072241	.003364	20
RH3 PP11	.00	.31	.23	0.00	.44	.31	0	999	.0000	0.0000	.0213	.0306	.000000	.000453	21
RH3 DP11	.00	.73	.50	0.00	.80	.63	0	999	.0000	0.0000	.0237	.0259	.000000	.000561	22
RH3 DP13	.01	.08	.07	-.29	.12	.08	-87	16	.0021	-.0453	.0190	.0129	.002060	.002092	23
RH3 FF13	.00	.31	.20	0.00	.37	.22	0	999	.0000	0.0000	.0217	.0254	.000000	.000470	24
RH3 DP13	.00	.50	.38	0.00	.75	.54	0	999	.0000	0.0000	.0160	.0242	.000000	.000257	25
RH3 FF13	.00	.39	.26	0.00	1.16	.92	0	999	.0000	0.0000	.0142	.0186	.000000	.000202	26
RH3 PP15	-2.50	.13	.12	1.12	.26	.16	156	5	-.1728	.0773	.0103	.0176	.035830	.003991	27
RH3 DP15	.00	.54	.38	0.00	.57	.41	0	999	.0000	0.0000	.0187	.0183	.000000	.000350	28
RH3 FF15	.00	.30	.22	0.00	1.18	.87	0	999	.0000	0.0000	.0128	.0189	.000000	.000165	29
RH3 FF17	.00	.84	.57	0.00	1.01	.67	0	999	.0000	0.0000	.0134	.0162	.000000	.000181	30
RH3 PP31	.00	.24	.16	0.00	.22	.14	0	999	.0000	0.0000	.0165	.0153	.000000	.000271	31
RH3 DP31	.00	.56	.39	0.00	.41	.30	0	999	.0000	0.0000	.0181	.0134	.000000	.000327	32
RH3 DP33	.17	.08	.05	1.31	.06	.04	93	4	.0267	.2054	.0091	.0129	.042890	.003865	33
RH3 DP33	.00	.19	.11	0.00	.19	.11	0	999	.0000	0.0000	.0130	.0128	.000000	.000168	34
RH3 DP33	.00	.34	.23	0.00	.34	.22	0	999	.0000	0.0000	.0110	.0112	.000000	.000121	35
RH3 FF33	.00	.65	.50	0.00	.57	.43	0	999	.0000	0.0000	.0104	.0091	.000000	.000108	36
RH3 FF35	1.65	.15	.09	-3.73	.12	.06	-66	2	.1143	-.2578	.0774	.0111	.079511	.004217	37
RH3 DP35	.00	.34	.17	0.00	.28	.18	0	999	.0000	0.0000	.0109	.0091	.000000	.000119	38
RH3 FF35	.00	.52	.37	0.00	.60	.37	0	999	.0000	0.0000	.0082	.0096	.000000	.000068	39
RH3 FF37	-11.60	.41	.24	-6.19	.45	.30	-152	2	-.1851	-.0987	.0058	.0079	.044021	.002454	40
RH1 SS11	-2.00	.11	.08	.27	.20	.13	172	6	-.3138	.0416	.0181	.0307	.100196	.011775	41
RH1 PP11	1.61	.40	.23	3.07	.36	.26	62	7	.1113	.2120	.0237	.0287	.057315	.011931	42
RH1 DP13	6.94	.12	.12	.12	.34	.24	1	3	.4801	.0081	.0082	.0236	.230585	.007949	43
RH1 DP13	.00	.48	.32	0.00	.65	.46	0	999	.0000	0.0000	.0157	.0211	.000000	.000246	44
RH1 DP15	.00	.40	.23	0.00	.52	.38	0	999	.0000	0.0000	.0128	.0168	.000000	.000165	45
RH1 FF15	.00	.72	.52	0.00	.99	.70	0	999	.0000	0.0000	.0115	.0158	.000000	.000133	46
RH1 FF17	.00	.63	.40	0.00	.88	.63	0	999	.0000	0.0000	.0101	.0140	.000000	.000103	47
RH1 DP31	-.44	.12	.07	.79	.09	.06	121	8	-.0758	.1242	.0124	.0197	.021157	.003772	48
RH1 PP31	-.23	.20	.17	1.51	.24	.15	99	11	-.0157	.1043	.0165	.0201	.011116	.003763	49
RH1 PP33	.00	.19	.11	0.00	.17	.10	0	999	.0000	0.0000	.0130	.0116	.000000	.000169	50
RH1 DP33	.00	.38	.25	0.00	.33	.22	0	999	.0000	0.0000	.0123	.0106	.000000	.000152	51
RH1 DP35	.00	.35	.21	0.00	.22	.16	0	999	.0000	0.0000	.0113	.0071	.000000	.000127	52
RH1 FF35	.00	.55	.40	0.00	.52	.34	0	999	.0000	0.0000	.0087	.0082	.000000	.000076	53
RH1 FF37	.00	.48	.32	0.00	.40	.28	0	999	.0000	0.0000	.0077	.0065	.000000	.000059	54
SIG PS11	-3.51	.24	.20	-.67	.32	.26	-169	5	-.3165	-.0604	.0214	.0291	.103816	.014275	55
SIG DP11	3.32	.65	.56	6.19	.50	.44	62	6	.1463	.2720	.0201	.0299	.095877	.012870	56
SIG DP13	7.40	.34	.29	-2.25	.43	.36	-17	3	.3264	-.0994	.0138	.0199	.116476	.009591	57
SIG DP13	.00	1.01	.72	0.00	.95	.73	0	999	.0000	0.0000	.0237	.0223	.000000	.000563	58
SIG DP15	-7.79	.58	.50	-6.32	.56	.52	-141	3	-.1831	-.1485	.0136	.0132	.055602	.006583	59
SIG DP15	.00	1.20	1.00	0.00	1.35	.98	0	999	.0000	0.0000	.0158	.0177	.000000	.000249	60







APPENDIX I (reproduced from D. J. Herndon, Thesis, LBL-544, 1972).

In this Appendix, we wish to review another property of the variance matrix, E, and the second derivative matrix, D, where D is  $E^{-1}$ . E (or D) is positive definite. This is necessary to ensure a maximum in the likelihood, L, rather than a saddle point or a minimum.

Defining the origin of the parameter space to be at the maximum, we can write

$$\mathcal{F} = \ln L = \ln L_0 - 1/2 \chi^2, \quad (\text{A.1})$$

and near the origin we can expand  $\chi^2$  as

$$\chi^2 = \underline{A}^\dagger \cdot D \cdot \underline{A}. \quad (\text{A.2})$$

The surface, enclosing the origin, defined by  $1 = \underline{A}^\dagger \cdot D \cdot \underline{A}$  is known as the error ellipsoid. This surface intercepts each axis at the points  $A_i^{\text{int}} = (D_{ii})^{-1/2}$ . (A.3)

This is sketched, in two dimensions, in Fig. A.1. It can be shown\* that the planes defining the circumscribed box intercept the axes at the points  $A_i^{\text{max}}$ , given by

$$A_i^{\text{max}} = (E_{ii})^{1/2} \equiv \delta A_i. \quad (\text{A.4})$$

(The plane  $A_1 = A_1^{\text{max}} = \delta A_1$  is the dashed line of Fig. A.1). In A.4 we have written

$$E = \begin{pmatrix} \delta A_1 \delta A_1 & \delta A_1 \delta A_2 c_{12} & \dots & \delta A_1 \delta A_n c_{1n} \\ \delta A_1 \delta A_2 c_{12} & \delta A_2 \delta A_2 & \dots & \delta A_2 \delta A_n c_{2n} \\ \vdots & \vdots & \ddots & \vdots \\ \delta A_1 \delta A_n c_{1n} & \delta A_2 \delta A_n c_{2n} & \dots & \delta A_n \delta A_n \end{pmatrix} \quad (\text{A.5})$$

\* Rosenfeld, A.H. and Solmitz, F.T. Lawrence Berkeley Laboratory Group A Memo 753 (unpublished, 1972).

and  $|c_{ij}| < 1$  and are the correlation coefficients. Now (as is evident from Fig. A.1)

$$(D_{ii})^{-1/2} \leq \delta A_i \tag{A.6}$$

and the equality holds if and only if  $c_{ij} = 0$  for all  $j \neq i$ . Thus one can get a measure of how strong the correlations are by comparing  $(D_{ii})^{-1/2}$  with  $\delta A_i$ .

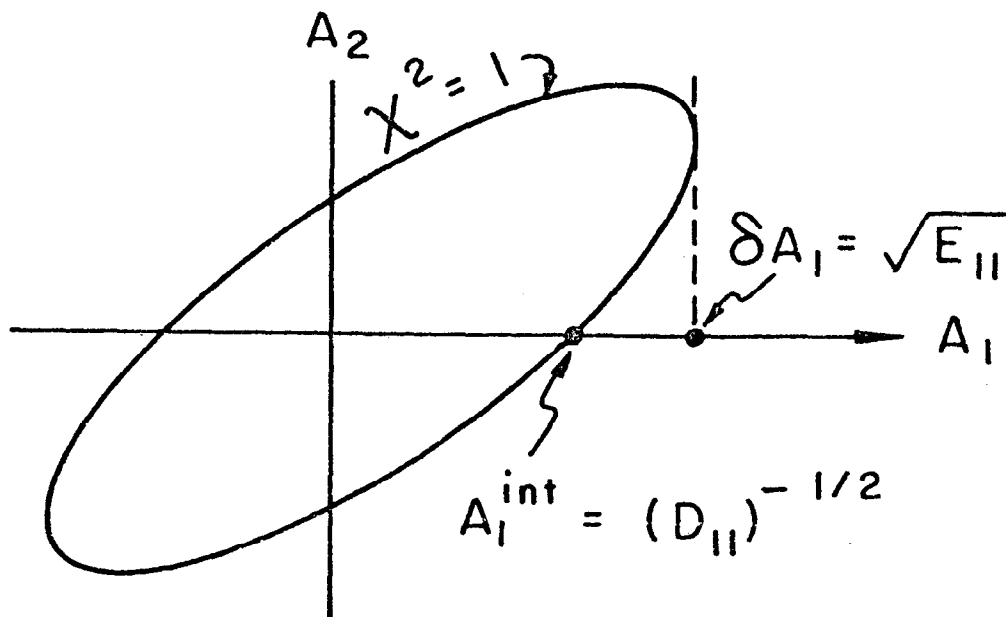
In Table AI we compare  $\delta A_i$  and  $(D_{ii})^{-1/2}$  for all the waves at a typical energy,  $\sqrt{s} = 1690$  MeV. Note that there are three entries for  $(D_{ii})^{-1/2}/\delta A_i$ , which exceed 1.0, one of them by 20%! This difficulty presumably has to do with invalid approximations in the inversion of D. Remember that we fit in a space of two, too many variables; i. e., we use the real and imaginary part of all amplitudes, even though the overall amplitude and phase are undetermined. Therefore, D is singular, and we have to subtract two eigenvalues -- see Eq. 14 of Miller's thesis, Ref. 4. Apparently approximations in this procedure can introduce errors at the 10-20% level.

2.19

TABLE AI. Comparison of  $\delta A_i$  and  $(D_{ii})^{-1/2}$  for all the waves at a typical energy,  $\sqrt{s} = 1690$  MeV.

		Re			Im		
		$\delta A_i$	$(D_{ii})^{-1/2}$	$(D_{ii})^{-1/2}/\delta A_i$	$\delta A_i$	$(D_{ii})^{-1/2}$	$(D_{ii})^{-1/2}/\delta A_i$
P <sub>33</sub>	PP <sub>11</sub>	0.0755	0.0630	0.834	0.0734	0.0528	0.719
	DS <sub>13</sub>	0.0206	0.0162	0.786	0.0208	0.0144	0.692
	DD <sub>13</sub>	0.1520	0.1281	0.843	0.1223	0.1036	0.847
	FP <sub>15</sub>	0.0589	0.0382	0.649	0.0392	0.0288	0.735
	DD <sub>15</sub>	0.1916	0.1021	0.533	0.1269	0.1269	0.551
	PP <sub>31</sub>	0.0913	0.0745	0.816	0.0642	0.0533	0.830
	SD <sub>31</sub>	0.2283	0.1944	0.852	0.1589	0.1346	0.847
	DS <sub>33</sub>	0.0264	0.0194	0.735	0.0189	0.0134	0.709
	PP <sub>33</sub>	0.1006	0.0689	0.685	0.0295	0.0327	> 1
	FF <sub>33</sub> FF <sub>35</sub> FF <sub>37</sub>						
RH <sub>3</sub>	DS <sub>13</sub>	0.0973	0.0767	0.788	0.0882	0.0647	0.734
	FP <sub>15</sub>	0.3184	0.2347	0.737	0.1910	0.1493	0.782
	DS <sub>33</sub>	0.980	0.0742	0.757	0.0979	0.0701	0.716
	FP <sub>35</sub> FF <sub>37</sub>						
RH <sub>1</sub>	SS <sub>11</sub>	0.1111	0.0976	0.878	0.1356	0.0974	0.718
	PP <sub>13</sub>	0.3066	0.2297	0.749	0.2924	0.2474	0.846
	SS <sub>31</sub>	0.1549	0.1198	0.773	0.1414	0.1037	0.733
	PP <sub>31</sub>	0.5790	0.4471	0.772	0.4885	0.4268	0.874
SIG	PS <sub>11</sub>	0.2106	0.1559	0.740	0.1927	0.1675	0.869
	SP <sub>11</sub>	0.6360	0.5678	0.893	0.4441	0.4621	> 1
	DP <sub>13</sub>	0.3282	0.2855	0.870	0.3741	0.3107	0.831
	FD <sub>15</sub>	0.4801	0.5859	> 1	0.6085	0.5367	0.882

2.20



XBL727-3577

Fig. A. 1.

### III. DATA TAPES OF ALL THE $N_{\pi\pi}$ EVENTS

All 160,000  $N_{\pi\pi}$  events are available on 16 BCD data summary tapes, but from two different sources:

- 1) The  $\pi^+p$  events at or above  $\sqrt{s} = 1810$  MeV are available from Prof. Anne Kernan, University of California, Riverside, CA.
- 2) The rest of the events may be requested from LBL (Rosenfeld) or SLAC (Leith) or Saclay (Mme. M. Neveu).

The tapes consist of 132-character BCD records, two such records per event. Each record was written with an 11F11.8 format. Each event consists of 21 words including the center-of-mass 4-vectors ( $P_x, P_y, P_z, E$ ) for each of the five particles in the following order,

words 1-4 : beam pion

5-8 : target proton

9-12: outgoing baryon

13-16: outgoing pion of same charge as beam

17-20: remaining outgoing pion

21: "mark number" M, specifying the final state:

$M = 2$  for  $n\pi^-\pi_0^+$        $M = 4$  for  $p\pi^+\pi^0$

$M = 3$  for  $p\pi^-\pi^0$        $M = 5$  for  $n\pi^+\pi^+$  [see 1), above].

The tape numbers and  $\sqrt{s}$  bins (1 file/bin) are:

1.	DST131	1310 1340 1370 1400
2.	DST144	1440 1470
3.	DST149	1490
4.	DST152	1520

5.	DST154	1540	
6.	DST165	1650	
7.	DST169	1690	
8.	DST173	1730	
9.	DST177	1770	
10.	DST181-	1810	} $\pi^-$ only
		1850	
11.	DST189-	1890	
12.	DST193-	1930	
13.	DST197-	1970	
14.	DST181+	1810	} $\pi^+$ only
		1850	
15.	DST189+	1890	
16.	DST193+	1930	
		1970	